UNIVERSIDAD DE CHILE
FACULTAD DE CIENCIAS FÍSICAS Y MATEMÁTICAS
DEPARTAMENTO DE ASTRONOMÍA

DYNAMICALLY SELF-CONSISTENT ORBITAL ELEMENTS FOR BINARIES WITH JOINT SPECTROSCOPIC AND ASTROMETRIC DATA

TESIS PARA OPTAR AL GRADO DE
MAGÍSTER EN CIENCIAS, MENCIÓN ASTRONOMÍA

JENNIFER ESTER ANGUITA AGÜERO

PROFESOR GUÍA:
RENÉ MÉNDEZ BUSSARD

MIEMBROS DE LA COMISIÓN:
EDGARDO COSTA HECHENLEITNER
NIDIA MORRELL ZABALETA
SEBASTIÁN LÓPEZ MORALES

Este trabajo ha sido parcialmente financiado por:
FONDECYT/ANID grant No. 1190038

SANTIAGO DE CHILE
2023

RESUMEN DE LA TESIS PARA OPTAR
AL GRADO DE MAGÍSTER EN CIENCIAS,
MENCIÓN ASTRONOMÍA
POR: **JENNIFER ESTER ANGUITA AGÜERO**
FECHA: 2023
PROF. GUÍA: RENÉ A. MÉNDEZ

ELEMENTOS ORBITALES DINÁMICAMENTE AUTOCONSISTENTES PARA ESTRELLAS BINARIAS CON DATOS ESPECTROSCÓPICOS Y ASTROMÉTRICOS CONJUNTOS

La masa es el parámetro fundamental que determina la estructura y evolución de una estrella. Sin embargo, medir la masa de las estrellas no es una tarea fácil, por lo que el número de estrellas con masas bien conocidas es bastante limitado.

Las Binarias Espectroscópicas (SB), que son el objeto de este trabajo de tesis, proporcionan actualmente el enfoque más eficaz y directo para determinar masas estelares. Con este fin, hemos estado realizando observaciones interferométricas (Speckle) y espectroscópicas de alta resolución (Echelle) de un gran número de sistemas SB para determinar sus parámetros orbitales y sus curvas de velocidad radial. Mediante algoritmos tipo Markov Chain Monte Carlo (MCMC) desarrollados por nuestro grupo, combinamos los datos astrométricos y espectroscópicos y derivamos una solución conjunta a partir de la cual se obtienen las órbitas y las masas.

Se distinguen dos tipos de SB: las binarias espectroscópicas de doble línea ($SB2$), en cuyos espectros se pueden observar las líneas espectrales de ambas componentes, y las binarias espectroscópicas de una sola línea ($SB1$, que son las más numerosas), en las que sólo se observan las líneas de la componente primaria. En el caso de las $SB2$, la curva de velocidad radial junto con la órbita astrométrica permiten determinar directamente las masas de los componentes individuales, así como sus paralajes orbitales. En el caso de las $SB1$, es imposible determinar directamente las masas individuales, pero nuestro algoritmo MCMC permite hacer estimaciones razonables para ellas.

En el capítulo 2 presentamos el esquema utilizado, y los resultados obtenidos, para un grupo de sistemas $SB2$ (Anguita-Aguero et al., 2022), y en el capítulo 3 lo análogo para un grupo de sistemas $SB1$ (Anguita-Aguero et al., 2023). En la actualidad, las binarias australes están siendo observadas sistemáticamente principalmente por nuestro equipo, lo que hace que nuestro estudio Speckle/Echelle sea único.

RESUMEN DE LA TESIS PARA OPTAR
AL GRADO DE MAGÍSTER EN CIENCIAS,
MENCIÓN ASTRONOMÍA
POR: **JENNIFER ESTER ANGUITA AGÜERO**
FECHA: 2023
PROF. GUÍA: RENÉ A. MÉNDEZ

DYNAMICALLY SELF-CONSISTENT ORBITAL ELEMENTS FOR BINARIES WITH JOINT SPECTROSCOPIC AND ASTROMETRIC DATA

Mass is the fundamental parameter that determines the structure and evolution of a star. Measuring the masses of the stars is however not an easy task, so the number of stars with well-known masses is quite limited.

Spectroscopic Binaries (SB), which are the the subject of this thesis work, currently provide the most effective and direct approach to determine stellar masses. To this end, we have been securing interferometric (Speckle) and high-resolution spectroscopic observations (Echelle) of a large number of SB systems to determine their orbital parameters and radial velocity (RV) curves. By means of Markov Chain Monte Carlo (MCMC) algorithms developed by our group, we combine the astrometric and spectroscopic data and derive a joint solution from which the orbits and the masses are obtained.

Two types of SB are distinguished: double-line spectroscopic binaries ($SB2$), in whose spectra, the spectral lines of both components can be observed, and single-line spectroscopic binaries ($SB1$, which are the most numerous), for which only the lines of the primary component are easily recognized. In the case of $SB2$, the RV curve together with the astrometric orbit allows the masses of the individual components to be determined *directly*, as well as orbital parallaxes. In the case of $SB1$s, it is impossible to directly determine the individual masses, but our MCMC algorithm permits to make reasonable estimates for them.

In chapter 2 we present the scheme used, and the results obtained, for a group of $SB2$s (Anguita-Aguero et al., 2022), and in chapter 3 the analog for a group of $SB1$s (Anguita-Aguero et al., 2023). We note that southern binaries are currently being monitored systematically mainly by our team, which makes our Speckle/Echelle survey unique.

La vida
es sin llorar.

En todo amar y servir.

A.M.D.G

Agradecimientos

En primer lugar, agradezco a Dios por el don de la vida y las bendiciones que me da cada día. Sé que no puedes evitar que tropiece, pero no me has dejado caer. Eres mi luz y mi salvación. Bajo tu amparo y el de nuestra Madre Santísima confío mi ser.

Quisiera dedicar este capítulo en mi vida a mi familia por su incondicional apoyo e infinito amor. Gracias por confiar en mí más que yo misma y por no cuestionar mis acciones ni mis decisiones, por acompañarme en todas mis locuras y no permitir que me rinda. A mi madre Herta por estar siempre a mi lado, por ser mi fiel compañera y el pilar fundamental de mi vida. A mi padre Sergio por enseñarme a vivir la vida sin mirar atrás, a seguir adelante a pesar de los tropiezos y a tener la fuerza para enfrentar los obstáculos. A mi hermana Tamara por ser mi heroína y mi ejemplo a seguir. Me has enseñado lo importante que es luchar por nuestros sueños y que a pesar de los mil problemas que tengamos en frente solo debemos avanzar, valdrá la pena.

Agradezco también de manera especial a mi profesor guía, René Méndez. René confió en mí y sin dudar me abrió las puertas de su equipo, en un momento académico y de mi vida particularmente difícil. Sin usted no hubiese podido avanzar ni mucho menos llegar a este punto. Estoy muy contenta por los logros que hemos obtenido y todo lo que aprendí en estos años, es un gran científico y profesional. Ha sido un verdadero honor trabajar con usted y con el profesor Edgardo Costa, a quien le agradezco por su colaboración y liderazgo en este exitoso proyecto del que tengo el privilegio de ser parte.

A mis tíos y tías, primos y primas, sobrinos y sobrinas, a mi querida comunidad de San Ignacio de Loyola, a mis bebés Julieta y Benjamín y ahijados-hijos Maximiliano y Máximo, muchísimas gracias. A quienes me acompañan desde un plano superior, en especial a mi pita María, este logro también es para ti, sé que estarías feliz de ver donde he llegado y en lo que me he convertido, te extraño mucho, pero sé que estas en cada paso que doy.

A mis amigos y amigas de toda la vida; Pamela, Yasmira, Iris, Bruno, Gabriela, Diego y Roxana. Gracias por aguantarme todos estos años y ser tan incondicionales. También agradezco a los amigos que me dejo mi paso por Concepción y la gloriosa UdeC; Paula, Gonzalo, Elizabeth, Rubén, Víctor, Javiera, Claudio, Camila y a EDA. Gracias por cada momento vivido con ustedes y por ser mi refugio lejos de casa. Gracias también a quienes hicieron de mi estadía en UChile una linda experiencia a pesar de todo, Víctor, Antonia y Sebastián.

No puedo dejar de mencionar a los amigos/as que he encontrado en este nuevo camino, Astro-pintoras y colegas en la divulgación. He aprendido mucho de ustedes, son una gran inspiración. Gracias a Cazadoras de Estrellas por ayudarme a darme cuenta de que las mujeres somos capaces de todo y que nada ni nadie nos puede limitar. Finalmente, agradezco a mi comunidad de Astronomía Rapidita, por su fidelidad e inmenso cariño. Sin duda lo mejor que me dejó la pandemia fue el haber descubierto mi verdadera vocación, **la educación y comunicación científica**.

Table of Content

Table Index

Figure Index

Chapter 1

Introduction

In astronomy, a binary or multiple stellar system is a system consisting of a small number of stars that interact gravitationally, so that they orbit around a common center of mass. Depending on the observation technique used, there can be several types of binary systems such as Visual Binaries, Astrometric Binaries, and Spectroscopic Binaries (SB). A visual binary is one in which the relative position of both components is observable. The positional or astrometric observations measure the position of the fainter (secondary) component relative to the brighter (primary) component as position measurements of the projection of the real (relative) orbit -motion of the system in which both objects are assumed to behave as point masses with the primary component at the center- on the plane of the sky relative to the observer (reference plane), denoted as the apparent orbit.

These orbits and the motion of stars in binary systems, are described by the following orbital parameters:

- ***Period (P)***: The rotation period of the system (measured in years).
- ***Time of periastron passage (T)***: Instant at which the minimum true distance between the components occurs, measured in years and fraction of a year due to the periodicity of the system.
- ***Semi-major axis (a)***: Maximum distance between stars (measured in true elliptical orbit, in arcseconds). Mathematically, it is half the longest diameter of the ellipse.
- ***Eccentricity (e)***: Measures the greater or lesser flattening of the ellipse. It is equal to the quotient between the distance from the center of each focus, and its semi-major axis.
- ***Longitude of the ascending node (Ω)***: The position angle from a reference direction to the ascending node (point at which the real orbit of the object passes through the reference plane). Varies from 0° to 360°.
- ***Argument of periapsis (ω)***: The angle from the node to the periastron in the real orbit, following the direction of motion (ranging from 0° to 360°).
- ***Inclination (i)***: The angle (ranging from 0^o to 180^o) formed between the orbital plane (where the real orbit exists) and the observation plane (where the apparent orbit exists).

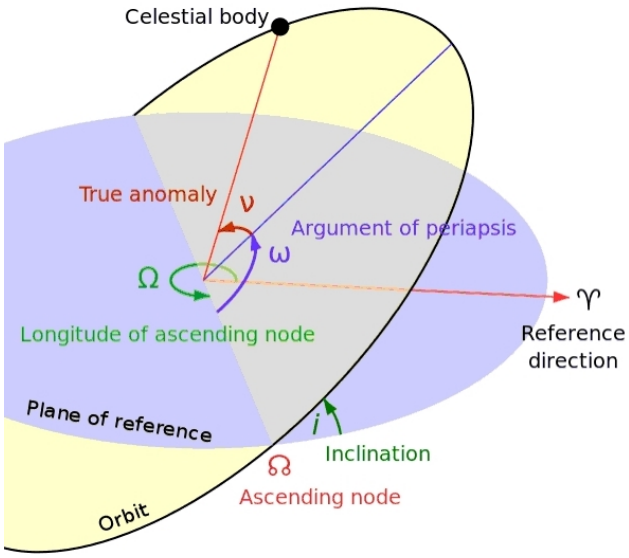

Figure 1.1: Orbital elements describing the orientation of the orbit in space.

Some of these parameters are represented graphically in Figure 1.1[1], specifically, the geometric parameters (i, Ω, and ω), which describe the orientation of the orbit in space, necessary to project the real orbit into the apparent orbit. The angle ν, describes the position of the secondary star with respect to the primary star relative to the periastron.

SB provide a very effective platform to test our understanding of stellar astrophysics because, as said, they make it possible to determine an elusive parameter which rules the structure and evolution of stars: their mass. As indicated by the well-known Vogt-Russell theorem (Kahler, 1972), the most important parameter determining the internal structure and evolution of a star of a given chemical composition is its initial mass. This theoretical prediction is however not easy to test, because the number of stars with well-known individual masses is limited. According to the most comprehensive catalog for Visual Binary Stars, only 317 (from 3579) systems have uncertainties less than 1 % from which good mass estimates can be obtained; this in spite of the fact that in the Solar Neighborhood roughly one-half of solar-type stars belong to binary systems (e.g. Fuhrmann et al. (2017)), so in principle it should be possible to determine precise masses for a very large number of stars, but unfortunately, most of them are either unresolved or do not have high-precision orbital elements.

Among the different types of binary systems, SB are specially important, because combining interferometric and spectroscopic observations for these systems it is possible to derive a complete characterization of their orbital parameters and also the masses and other astrophysical parameters of the individual components. In our case, this is done by means of Markov Chain Monte Carlo (MCMC) algorithms, which combine the orbital data derived from the interferometry and the Radial Velocity (RV) data derived from the spectroscopy, yielding a joint solution from which the orbits and the masses are obtained.

[1] Image by Lasunncty, CC-BY-SA-3.0

A starting point for systematic surveys to determine stellar masses are all-sky catalogs of confirmed or suspected visual binaries, such as the Hipparcos catalog (Lindegren et al., 1997), as well as the more recent Gaia discoveries (e.g. Brandt (2021)); or catalogs of spectroscopic binaries, such as the Geneva-Copenhagen spectroscopic survey (Nordström et al., 2004). With the above motivation, in 2014 we started a systematic campaign to complete and/or improve the observation of southern binaries included in these catalogs, using the Speckle camera HRCam on the SOAR 4.1m telescope. Subsequently, in 2019 we initiated a complementary program to target fainter and/or spatially compact systems -beyond the capability of our SOAR set-up- with the ZORRO Speckle Camera on the Gemini South 8.1m telescope. About the same epoch, we also started a high-resolution spectroscopic program to determine RV curves for the above samples, which has been carried out principally with the FEROS Echelle spectrograph on the ESO/MPG 2.2m telescope. Additionally, we have also included some recent observations using the FIDEOS Echelle spectrograph on the 1m telescope at the ESO/La Silla Observatory.

We note that, for the present thesis work, we have used historical astrometric and spectroscopic data, which has been supplemented with our own observations. Southern binaries are currently being monitored systematically mainly by our team, which makes our Speckle survey unique.

Two groups of SB are distinguished: double-line spectroscopic binaries (SB2), in whose spectra, the spectral lines of both components can be observed, and single-line spectroscopic binaries (SB1), for which only the lines of the primary component are easily recognized. SB2 are certainly the most interesting systems because in their case a joint treatment of the astrometric and RV data allows one to determine directly the individual component masses, e.g. Anguita-Aguero et al. (2022) and Mendez et al. (2017), as well as a orbital parallaxes, providing an independent assessment of Gaia's trigonometric parallaxes (e.g. Mason (2015)). Unfortunately, and despite sustained efforts to monitor SB2s (e.g. Halbwachs et al. (2020)), the number of systems for which both a RV curve and a precise astrometric orbit are available, is still rather small (only 219 systems in the Sixth Catalog of Orbits of Visual Binary Stars have a combined solution and 73 in the 9th Catalog of Spectroscopic Binary Orbits (Pourbaix et al., 2004)). That is why our work is importantly contributing to alleviate this situation.

In the case of SB1s -which are the majority (67 %) of the systems included in the 9th Catalog of Spectroscopic Binary Orbits- usually only the mass function can be obtained directly (Struve & Huang, 1958). For this reason, in the past this latter group has not been fully exploited. Now, thanks to a newly developed Bayesian methodology based on the MCMC algorithm No-U-Turn sampler (NUTs, Videla et al. (2022)) created to address the orbital parameters inference problem in SB1 systems, including an estimation of the individual component masses, this situation is rapidly changing. Our work is also contributing to this end (Anguita-Aguero et al., 2023).

One of the main relationships reflecting the dependency on mass of the star's properties is the mass-luminosity relation (MLR). Improving the observational MLR is not a simple task, because it involves determining not only precise masses but also another elusive parameter, the distance. The advent of the Gaia satellite (Luri et al., 2018), a European space mission, whose objective is to build the largest and most precise three-dimensional map of our Galaxy providing astrometry, photometry, and spectroscopy of nearly 2000 million stars, has dramatically improved the precision of stellar distances within the solar neighborhood. Up to a distance of 250 pc, well beyond what it is usually adopted as the "radius" of the solar neighborhood, a parallax determined by Gaia has an uncertainty under 1 %, which by current standards would have basically solved the distance dilemma in the MLR. Despite this promising scenario, much remains to be done to increase the number of stars with well-known masses because of the relative lack of high-precision orbits and RV curves for binary systems.

Complementarity with Gaia is also a strong reason to study nearby binaries now, because Gaia faces observational difficulties resolving binary systems close to its angular resolution. Currently, a single sweep of Gaia's star mapper can detect stars 0.3/0.7 [arcsec] (along/cross scan) apart (Ziegler et al., 2018a), which implies that probably Gaia will never resolve some of the objects included in our studies. As was the case of Hipparcos parallaxes, Gaia parallaxes will probably be biased due to the orbital motion of the binary. Although by the end of its mission it is expected that Gaia will have a final resolution of about 0.1 arcsec.

This thesis deals with two principal problems, the first one is to increase the number of stars in the solar neighborhood with well-defined masses, and the second one is related to the need to develop a methodology to study objects that have been under-explored for stellar mass estimation because they don't provide empirical data for the secondary component, but are more numerous. These issues have been addressed in two recent papers, Anguita-Aguero et al. (2022) and Anguita-Aguero et al. (2023), respectively. These papers are presented in Chapters 2 and 3. In them, technical aspects and other details are fully described. Finally,in Chapter 4 we present the summary and the main conclusions from our study.

Chapter 2

Orbital elements and individual component masses from joint spectroscopic and astrometric data of double-line spectroscopic binaries

2.1. Introduction

Binary stars are powerful laboratories to test various aspects of stellar astrophysics, because they enable us to access a key but elusive parameter which dictates the structure and evolution of stars: their mass. In combination with Kepler's laws, the observation of binary systems allows to determine directly the masses of stars. Indeed, the most fundamental parameter determining the internal structure and evolutionary path of stars of a given chemical composition is their initial mass as shown by the well-known Vogt-Russell theorem (Kahler (1972), Kippenhahn et al. (2012), for a general review see Massey & Meyer (2001); and the textbooks by Iben (2012) for details of the physical models). This theoretical prediction is, however, not straightforward to test due to the limited number of stars with well-known individual masses.

Kepler's laws give us the way to determine directly the mass of a stellar system by studying the motion of stars that are bound by their mutual gravitational attraction, i.e., binary stars (Pourbaix, 1994). Considering that roughly half of solar-type stars in the Solar Neighborhood belong to binary systems (Raghavan et al., 2010, Duchêne & Kraus, 2013, Fuhrmann et al., 2017), in principle, it is possible to determine precise masses for a very large number of stars. Gravitational microlensing might eventually become another potentially very precise method for mass determination (Ghosh et al., 2004, Gould, 2014), but so far, it has been restricted to a few cases (Bennett et al., 2020, Wyrzykowski & Mandel, 2020). Circumstelar disks around young stars (Pegues et al., 2021) are also becoming a viable and promising method. In the case of microlensing events, the mass of the lens can be determined only in limited cases, because it requires a knowledge of both the source and lens distances, as well as their relative proper motions. The second method relies on the existence of a purely Keplerian disk[2], i.e., in a steady-state configuration, and not subject to magnetohydrodynamical effects, which enables a purely dynamical mass determination. In the case of visual binary stars, the subject of this paper, a mass determination requires a determination of the so-called orbital elements

[2] Usually found only on young stars.

that completely define the projected orbit in terms of the true intrinsic orbital parameters.

One of the main relationships reflecting the dependency on mass of the star's properties is the mass-luminosity relation (MLR), first discovered empirically in the early 20th century, and later explained on theoretical grounds (Eddington, 1924). Improving the observational MLR is not a simple task, because it involves determining not only precise masses but also another elusive parameter, distance, by means of trigonometric parallaxes. To complicate things further, the observational MLR has a statistical dispersion that cannot be explained exclusively by observational errors in the luminosity or mass; there seems to be an intrinsic dispersion caused by differences in age and/or chemical composition from star to star. Currently, the best MLRs for main-sequence stars are those of Torres et al. (2010) and Benedict et al. (2016), but neither of them include low-metallicity stars (e.g., only one with $[Fe/H] < -0.25$ in Torres et al. (2010)). Other studies, using long-baseline optical interferometry of binary systems, have begun to address metallicity (e.g. Boyajian et al. (2012a,b), Feiden & Chaboyer (2012), but have reached only as low as about $[Fe/H] = -0.5$. For a recent study of the effects of metallicity on the MLR for $M < 0.7 M_{\odot}$ see Mann et al. (2019). Our own speckle survey, described below, is focusing, in part, precisely on low-metallicity objects, following the pioneer study of Horch et al. (2015b, 2019a).

The recent advent of the Gaia satellite (Luri et al., 2018) has dramatically improved the precision of stellar distances within the solar neighborhood. Up to a distance of 250 pc, well beyond what it is usually adopted as the "radius" of the solar neighborhood, a parallax determined by Gaia has an uncertainty under 1 %, which by current standards would have basically solved the distance dilemma in the MLR. Despite this promising scenario, much remains to be done to increase the number of stars with well-known masses because of the relative lack of high-precision orbits for binary systems. On the other hand, the Gaia satellite faces observational difficulties at resolving systems close to its angular resolution limit. It is well known that the Hipparcos parallaxes were indeed biased due to the orbital motion of the binary (i.e., the parallax and orbit signal are blended), as shown by Söderhjelm (1999a) (see, in particular, Section 3.1, and Table 2), and it is likely that Gaia will suffer from a similar problem[3].

A good starting point for systematic surveys to determine stellar masses are all-sky catalogs that include identification of confirmed or suspected visual binaries, such as the Hipparcos catalog (Lindegren et al., 1997), as well as the more recent Gaia discoveries (Kervella et al., 2019, El-Badry et al., 2021, Brandt, 2021); or spectroscopic binaries, such as the Geneva-Copenhagen spectroscopic survey (Nordström et al., 2004). To this end, in 2014, we initiated a systematic campaign to complete or improve the observation of southern binaries mainly from the above catalogs (Mendez et al., 2018), using the high-speed speckle camera HRCam at the Southern Astrophysical Research (SOAR) 4.1m telescope (Tokovinin & Cantarutti, 2008, Tokovinin, 2018a); several publications have resulted from this effort, including Gomez et al. (2016), Mendez et al. (2017), Claveria et al. (2019), Docobo et al. (2019), Mendez et al. (2021), Villegas et al. (2021), Gómez et al. (2021). Considering that metal-poor binary systems are typically farther away and therefore fainter and/or more compact spatially, making them difficult objects for optical interferometry with 4 m or smaller telescopes, in 2019, we

[3] For example, according to Tokovinin's multiple star catalog, HIP 64421 contains a binary with a 27 yr orbit. Its Hipparcos parallax is 8.6 mas, its dynamical parallax is 8.44 mas, and its Gaia DR2 parallax is 3 mas. However, Gaia does give a consistent parallax for the C component at 1.9 arcsec: 9.7 ± 0.3 mas, see https://www.ctio.noirlab.edu/~atokovin/stars/stars.php. There are other examples like this in the cited catalog.

also started a program focused on these very systems with the ZORRO Speckle Camera of the Gemini South (GS) 8.1 m telescope at Cerro Pachón[4]. We note that southern binaries are currently being monitored systematically only by our team, which makes our speckle survey unique. Complementarity with Gaia is a very strong reason to carry out a survey of nearby binaries now; during each observation, Gaia is not expected to resolve systems closer than about 0.4 arcsec, though over the mission, there will be a final resolution of 0.1 arcsec. This is shown graphically in Figure 1 from Ziegler et al. (2018b), where the current resolution of the second Gaia data release is shown to be around 1 arcsec, being a function of the magnitude difference between primary and secondary[5].

For many years, exoplanet searches excluded binary systems, but nowadays, more than 200 planets have been discovered in them[6], representing a multiplicity rate of about 23 % for hosts to exoplanets across all spectral types (Fontanive & Bardalez Gagliuffi, 2021). Initially they were discovered serendipitously, like Gliese 86 Ab (Queloz et al., 2000) and γ Cep Ab (Hatzes et al., 2003) but, more recently, as part of dedicated imaging, transit and RV surveys (e.g., see Fontanive & Bardalez Gagliuffi (2021)). Given that the formation of stars in multiple systems is a frequent by-product of stellar formation, a current open question is to understand how the presence of a stellar companion can affect the planetary formation process. For years, planetary formation theories have been restricted to the case of a single-star environment to understand the formation of our own solar system (Mordasini et al., 2008). For the most frequent dynamical configuration observed for planet(s) in binaries (see classification by Dvorak 1982), the S-type circumprimary one with a planet orbiting one component of the binary, generally the most massive one, the models predict that the presence of a very close binary companion can truncate a protoplanetary disk, hence obstructing the formation of a planet by core accretion or ejecting the planet in unstable systems (Thebault & Haghighipour, 2015). Dedicated observing campaigns confirmed that short and intermediate-separation (≤ 300 au) binaries have a statistically lower chance of hosting planets or brown dwarf companions, and that wide binaries, on the contrary, have no influence on the architectures of planetary systems (Matson et al., 2018). This effect seems to also be corroborated by the study of young stars for which short-separation (≤ 100 au) binaries have a lower probability of hosting circumstellar dust in the innermost few au around each star, therefore having a depleted reservoir of solids for the formation of planets by core accretion (Duchêne, 2010).

Among different types of binary systems, spatially resolved double-line spectroscopic binaries with known RV curves are particularly important. If their RV curves can be combined with their astrometric orbits, it is possible to obtain a complete and unambiguous solution for the orbital elements, as well as individual component masses, with high precision (Mendez et al., 2017, 2021). With high-quality data in hand, it is also possible to derive parallax-free distances —the so-called orbital parallaxes— for these systems, which are derived from the ratio of the semi-major axes (Docobo et al., 2018b, Piccotti et al., 2020). Orbital parallaxes are completely independent of the trigonometric parallax and thus allow an assessment of Gaia's parallaxes (Pourbaix, 2000, Mason, 2015). Furthermore, increasing the sample of well-studied

[4] See https://www.gemini.edu/instrumentation/current-instruments/alopeke-zorro

[5] It is expected that, from the third Gaia data release on, the treatment of binary stars will be much improved by incorporating orbital motion (and its impact on the photocenter position of unresolved pairs) into the overall astrometric solution, thus significantly suppressing/alleviating the parallax bias; this, in turn, calls precisely for having good orbital elements for these binaries, which is one of the secondary goals of our project.

[6] As of November 3rd 2021, 217 planets are known in 154 binary systems (https://www.univie.ac.at/adg/schwarz/multiple.html.)

SB2s is important because, statistically, the mass-ratio distribution of these binaries—a parameter assumed to be frozen since their formation but observationally retrievable —has an important imprint from the initial mass function, as shown by, e.g., the simulations by Ducati et al. (2011). This traditional vision is, however, being somewhat challenged by more recent simulations that demonstrate that high-mass stars can capture lower-mass stars with luminosities far smaller than those of their host during the first few million years of star cluster evolution (Wall et al., 2019). Additionally, *N*-body simulations that incorporate magnetohydrodynamic effects have shown that dynamical interactions between stars in the presence of gas during cluster formation can modify the initial mass-ratio distribution toward binaries with a larger mass difference (Cournoyer-Cloutier et al., 2021).

Unfortunately, and despite sustained efforts to monitor SB2s (see e.g. Halbwachs et al. (2020) and their series of papers), the number of systems for which both an RV curve and a precise astrometric orbit are available is still rather small. In this paper, we contribute to alleviating this situation by determining combined orbits for 14 SB2 systems, some of which have been observed during our SOAR speckle survey of southern binary stars (Mendez et al., 2018) and for which there are complementary published data as well.

Methodologically, the most common procedure is to solve the astrometric visual orbit separately from the RV curve. In this approach, the amplitude ratio between the RV curves of the primary and secondary gives an estimation of the mass ratio, while the astrometric orbit gives the mass sum (assuming a parallax). This is most often done when the primary and secondary amplitudes are not well determined, e.g., when the spectral resolution prevents full deblending of the spectral lines of both components (see e.g., Tokovinin & Latham (2017)), or in the case of single-line spectroscopic binaries with a visual orbit (see, e.g., Docobo et al. (2018c)). In both cases, it is not possible to directly link the RV curve to the astrometric orbit in a self-consistent manner. On the other hand, if the visual orbit and velocity amplitudes are believed to be reliable, it is possible to determine a simultaneous solution and, in the process, determine the orbital parallax based solely on the orbital motion of the pair. Both scenarios are thoroughly explained, including graphical flowcharts, in (Villegas et al. (2021), Section 4.2), while in Appendix A of Mendez et al. (2017) they provide a detailed step-by-step flow of our calculations. In this work, well-measured RV curves and visual orbits are available for most systems, so by adopting the latter of these schemes, we were able to determine orbital parallaxes for the majority of our binaries.

2.2. Basic properties of the Binary Systems

To select the sample for the present work, we started by doing a cross-match between the Sixth Catalog of Orbits of Visual Binary Stars maintained by the US Naval Observatory (hereafter Orb6[7]) and the 9th Catalog of Spectroscopic Binary Orbits (hereafter SB9[8]; Pourbaix et al. (2004)). Orb6 is the most comprehensive catalog of binary systems with published orbital elements, and SB9 contains RV amplitudes for all binary systems for which it has been possible to fit an RV curve. Having identified those systems confirmed as SB2s in SB9, we pinpointed the binaries for which a combined astrometric/RV study of the orbit was not available in the literature by means of the notes and comments given in Orb6 and SB9. This led to an initial working list of 17 binary systems.

For the systems selected as indicated above, we retrieved their RV data from SB9 or

[7] Available at https://www.usno.navy.mil/USNO/astrometry/optical-IR-prod/wds/orb6
[8] Updated regularly, and available at https://sb9.astro.ulb.ac.be/

references provided therein, astrometric data from the US Naval Observatory Fourth Catalog of Interferometric Measurements of Binary Stars,[9] and historical astrometry included in the Washington Double Star Catalog (WDS) effort (Mason et al. (2001); kindly provided to us by Dr. Brian Mason from the US Naval Observatory). Finally, we included recent results obtained with the HRCam speckle camera at the SOAR 4.1 m telescope as part of our monitoring of southern binaries described in Mendez et al. (2017). Examination of the information collected showed that only 14 of the systems in our starting list had sufficient data to warrant further analysis. We must emphasize that, as a result of our selection process, our final sample is very heterogeneous, and it is not complete or representative in any astrophysical sense. From this point of view, the main contribution of this paper is the addition of new orbits and individual component masses for this type of binary. In our final list, we also included a few previously studied objects in order to test our procedures and compare results. When available, we added SOAR+HRCam astrometric measurements we secured after the publication of their last orbit determination to improve the solution.

Table 2.1 presents the basic properties available in the literature for the sample studied in this paper. The first three columns give the name in the WDS (and below it, its corresponding HD number), the discoverer designation code assigned in the WDS to each target used throughout the paper, and the sequential number in the Hipparcos catalog. The fourth column gives the apparent V magnitude for the system as listed in SIMBAD ($V_{\rm Simbad}$, Wenger et al. (2000)). The fifth and sixth columns present the V magnitude given on the Hipparcos catalog ($V_{\rm Hip}$) and its source, respectively. The seventh and eighth columns list the color ($(V-I)_{\rm Hip}$) and its source, respectively, also from the Hipparcos catalog. The ninth and tenth columns give the V magnitudes for the primary ($V_{\rm A}$) and secondary ($V_{\rm B}$) components, respectively, as listed in the WDS catalog. As a sanity test, the integrated apparent magnitude for the system $V_{\rm t}$ (from the WDS individual component photometry) is given in the eleventh column[10]. In the twelfth and thirteenth columns we report our own measured magnitude differences in the Strömgren y filter (Δy) and in the Cousins I filter ΔI ($\equiv I_{\rm B} - I_{\rm A}$ between secondary and primary), respectively. These measurements are part of our speckle binary program mentioned in the previous paragraph. Finally, in the last column, we report the spectral type and luminosity class for the primary and secondary, after the plus sign, when available, from WDS and SIMBAD, respectively.

Precise photometry is required to place the individual components in an HR diagram (Section 2.6). While there is an overall good agreement between SIMBAD, Hipparcos, and the combined ($V_{\rm t}$) magnitudes, the quality of the photometry presented in Table 2.1 is somewhat variable, as can be readily seen by comparing the fourth, fifth, and 11th columns of that table. Therefore, in order to increase our comparison basis, we have searched for additional photometry of our targets in more recent all-sky photometric surveys for bright stars, in particular, in the "The All Sky Automated Survey" (ASAS[11] Pojmanski (1997)), the "All-Sky Automated Survey for Supernovae" (ASAS-SN[12], Kochanek et al. (2017), Jayasinghe et al. (2019)) and "The AAVSO Photometric All-Sky Survey" (APASS[13], Henden et al. (2009), data release 10, November 2018). All three catalogs report V-band magnitudes. APASS includes

[9] The latest version, called int4, is available at https://www.usno.navy.mil/USNO/astrometry/optical-IR-prod/wds/int4/fourth-catalog-of-interferometric-measurements-of-binary-stars

[10] Computed as $V_t = -2.5 \times \log\left(10^{-0.4 \cdot V_A} + 10^{-0.4 \cdot V_B}\right)$

[11] http://www.astrouw.edu.pl/asas/?page=main

[12] http://www.astronomy.ohio-state.edu/asassn/index.shtml

[13] https://www.aavso.org/apass

Table 2.1: Object Identification and Basic Photometry

WDS name HD number	Discoverer designation	HIP number	$V_{\rm Simbad}$[a]	$V_{\rm Hip}$[b]	Source$_{V_{\rm Hip}}$[c]	$(V-I)_{\rm Hip}$[b]	Source$_{(V-I)_{\rm Hip}}$[d]	$V_{\rm A}$[e]	$V_{\rm B}$[e]	$V_{\rm t}$[b]	Δy[f]	ΔI[f]	Sp. Type WDS/Simbad
00352−0336 3196	HO212AB	2762	5.201 ± 0.009	5.2	G	0.64 ± 0.02	A	5.61	6.9	5.32	1.33 ± 0.06	1.17 ± 0.06	F8V/F7V+G4V
02128−0224 13612	TOK39Aa,Ab	10305	5.66 ± 0.01	5.65	H	0.63 ± 0	G	6.18	6.69	5.65	0.35 ± 0.40	—	F8V/F8V
04107−0452 26441	A2801	19508	7.35 ± 0.01	7.36	G	0.71 ± 0.00	H	8.3	8.3	7.55	0.80 ± 0.10	0.57 ± 0.28	G0/G3/5IV
04184+2135 27176	MCA14Aa,Ab	20087	5.631 ± 0.005	5.64	H	0.34 ± 0.03	C	5.6	8.1	5.50	—	—	F0V/F0V
07518−1354 64096	BU101	38382	—	5.16	G	0.67 ± 0.02	A	5.61	6.49	5.21	0.93 ± 0.16	0.83 ± 0.06	G1V/G0V
11560+3520 103613	CHR258	58184	6.74 ± 0.01	6.74	H	0.60 ± 0.01	L	7.0	9.1	6.85	—	—	F5/F5
14492+1013 130669	A2983	72479	—	8.42	H	0.91 ± 0.01	H	9.27	9.36	8.56	0.22 ± 0.26	0.43 ± 0.12	K2VK2V
15282−0921 137763	BAG25Aa,Ab	75718	6.883	6.89	G	0.86 ± 0.02	A	6.9	10.2	6.85	3.52 ± 0.19	2.28 ± 0.22	G9V/G9V
16584+3943 153527	COU1289	83064	8.09 ± 0.01	8.09	H	0.65 ± 0.01	H	8.4	8.4	7.65	—	—	G0/G0
18384−0312 172088	A88AB	91394	6.482 ± 0.010	6.49	G	0.64 ± 0.07	F	7.22	7.51	6.60	0.15 ± 0.20	0.0	F9V/F8V
20102+4357 191854	STT400	99376	—	7.41	H	0.73 ± 0.00	H	7.6	9.83	7.47	—	—	G3V/G4V+G8V
20205+4351 193793	IOT2Aa,Ab	100287	6.85	6.78	G	0.53 ± 0.00	H	6.85	—	—	—	—	WR+O/WC7p+O5
20527+4607 –	A750	103055	8.709 ± 0.015	8.65	H	0.83 ± 0.01	L	9.11	10.26	8.79	—	—	G8V/G8V
23485+2539 223323	DSG8	117415	7.070 ± 0.009	7.08	H	0.51 ± 0.01	L	7.8	7.9	7.10	—	—	F5V+F5.5V/F2IV−V

[a] From the SIMBAD database.

[b] From the Hipparcos mission, VizieR catalog I/239.

[c] G=ground-based, H=HIP.

[d] "A" for an observation of $V-I$ in the Cousins system, "F", "G", "H" and "I" when $V-I$ was derived from measurements in other bands/photoelectric systems; "L" when $V-I$ was derived from Hipparcos and Star Mapper photometry.

[e] From the WDS catalog.

[f] From our own HRCam@SOAR measurements in the Strömgren y-band or in the Cousins I-band, respectively. When more than one measurement, it is the average.When more than three measurements, we quote the standard deviation on the mean.

Sloan i'-band photometry, which unfortunately cannot be compared directly with I-band values from Hipparcos. To have an extra comparison source in the I bandpass, we used the "All-sky spectrally matched Tycho-2 stars" available at the CDS[14]. This catalog presents synthetic photometry in various bands, including V and I, from a spectral energy distribution (SED) fit to 2.4 million stars in the Tycho-2 catalog by Pickles & Depagne (2010) (PD2010 hereafter). In Table 2.2 we present the photometry obtained from the above catalogs, together with their quoted uncertainties. While the above surveys measure and report everything they detect, their photometry is not reliable at the bright end. Based on the description of the different surveys, the reliability limit for ASAS, ASAS-SN, and APASS is 8, 10, and 7 mag, respectively. Therefore, in Table 2.2 we indicate dubious values (up to 1 mag brighter than the bright magnitude limit for each survey) with an asterisk (*) and even brighter objects whose measurements should be considered very uncertain with a double asterisk (**). Since most of our targets are quite bright, the photometry from these surveys is unfortunately not very reliable for some of them. An important point to make here is that while many of our targets do have high-quality Gaia photometry, it is unfortunately not useful for our purposes due to the special bandpass adopted by the mission (Maíz Apellániz, 2017)[15], which does not agree with the bandpass in which we measure magnitude differences at SOAR or the passbands used in the WDS.

In Figure 2.1 we show a comparison of the V and I photometry presented in Tables 2.1 and 2.2. We chose to plot Hipparcos magnitudes in the abscissa because they are the largest and most homogeneous data set for our sample of targets. As can be seen in this figure, there is a relatively good correspondence in the V band between the photometry from Hipparcos and that from SIMBAD and also with the combined photometry $V_{\rm t}$ from WDS. The fit of $V_{\rm Sim}$ *vs.* $V_{\rm Hip}$ has an rms residual of 0.053 mag, while that of $V_{\rm t}$ *vs.* $V_{\rm Hip}$ is 0.17 mag. The larger rms for the latter can be explained mostly by one measurement: the $V_{\rm t}$ for COU1289 is too bright in comparison with $V_{\rm Hip}$ (which is the value adopted by SIMBAD too; see Table 2.1). This object is further discussed in Section 2.5. Based on our photometric comparisons, we will thus adopt 0.06 mag as an estimate of the uncertainty of the photometry in Section 2.4; see also Figures 2.5 and 2.6.

As can be seen in Figure 2.1, at the bright end ($V < 7.0$), the ASAS and APASS magnitudes exhibit larger photometric errors and scatter, consistent with their declared bright-end reliability. In the case of ASAS-SN, this problem extends down to the faintest data plotted with ASAS photometry ($V \sim 9$). The ASAS-SN V for object BAG25Aa,Ab is an extreme outlier, but we believe this is due to a miss-identification of another object near the target located at a distance of 5 arscec, because the binary is too bright for the survey (in contrast, the available measurements from the other surveys cluster around the one-to-one relationship). In the range $V > 7.0$ both ASAS and APASS exhibit good consistency within the errors, between each other, and with Hipparcos and SIMBAD.

[14] VizieR catalog VI/135

[15] See also https://www.cosmos.esa.int/web/gaia/edr3-passbands and Riello et al. (2021).

Table 2.2: Additional photometry from recent All-Sky Surveys

WDS name HD number	Discoverer designation	$V_{\rm ASAS}$	$V_{\rm ASAS\text{-}SN}$	$V_{\rm APASS}$	$i'_{\rm APASS}$	$V_{\rm PD2010}$	$I_{\rm PD2010}$
00352−0336 3196	HO212AB	5.772 ± 0.306 **	5.69 ± 0.644 **	6.157 ± 0.078 *	5.148 ± 0.012	5.203	4.58
02128−0224 13612	TOK39Aa,Ab	6.046 ± 0.194 **	—	6.084 ± 0.001 *	5.482 ± 0.001	5.663	5.06
04107−0452 26441	A2801	7.352 ± 0.34 *	—	7.403 ± 0.04	7.214 ± 0.069	7.385	6.65
04184+2135 27176	MCA14Aa,Ab	6.171 ± 0.319 **	6.24 ± 0.119 **	—	—	5.625	5.29
07518−1354 64096	BU101	5.91 ± 0.244 **	—	6.366 ± 0.049 *	5.333 ± 0.025	5.202	4.51
11560+3520 103613	CHR258	—	6.24 ± 0.119 **	—	—	6.729	6.12
14492+1013 130669	A2983	8.401 ± 0.032	8.96 ± 0.109 **	8.403 ± 0.058	7.772 ± 0.024	8.421	7.54
15282−0921 137763	BAG25Aa,Ab	6.883 ± 0.032 **	11.39 ± 1.084[a]	6.939 ± 0.111 *	—	6.864	5.99
16584+3943 153527	COU1289	—	8.52 ± 0.094 **	—	—	8.093	7.4
18384−0312 172088	A88AB	6.543 ± 0.052 **	—	6.862 ± 0.01 *	—	6.484	5.81
20102+4357 191854	STT400	—	7.92 ± 0.097 **	—	—	7.425	6.70
20205+4351 193793	IOT2Aa,Ab	—	7.67 ± 0.091 **	—	—	6.757	6.03
20527+4607 –	A750	—	8.98 ± 0.09 **	—	—	8.677	7.82
23485+2539 223323	DSG8	7.057 ± 0.028 *	7.54 ± 0.114 **	—	—	7.042	6.52

[a] Five arc sec away from the target, possible miss-identification.

For the I band, the comparison is restricted only to the PD2010 SED-fitted photometry (Pickles & Depagne, 2010) and the Sloan i' filter measurements from the APASS survey. As shown in Mendez et al. (2021), there is an offset of about 0.38 mag between APASS i' and I, which is depicted by the dotted-dashed line in the plot. After applying this offset, the APASS i'-band photometry is commensurable to that derived by Hipparcos and PD2010. In general, we appreciate a good correspondence between Hipparcos, PD2010, and APASS, with an overall rms of the one-to-one fit of 0.06 mag, i.e., similar to the one found for the V-band.

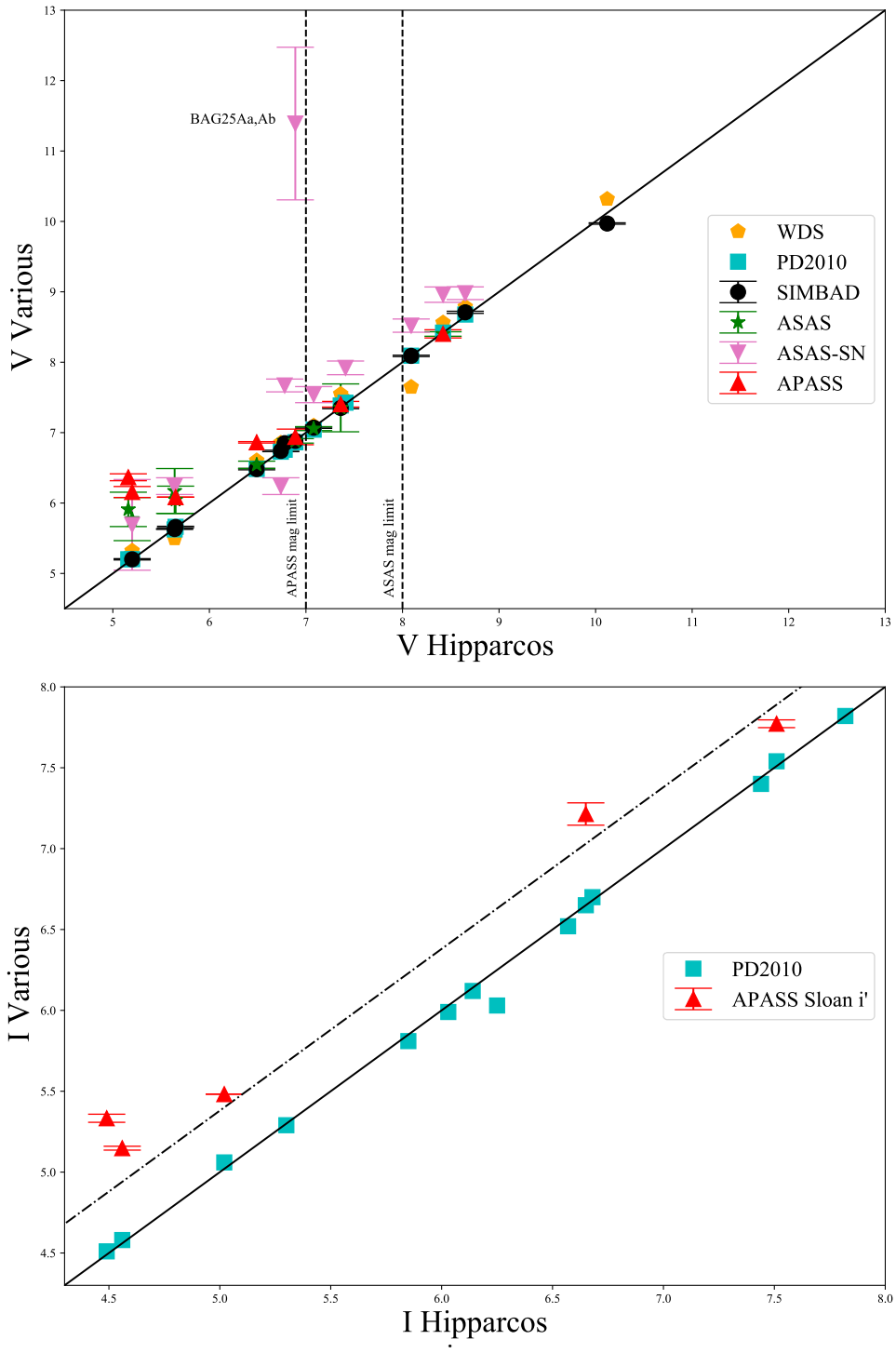

Figure 2.1: Comparison of Hipparcos V (top panel) and I-band magnitudes (bottom panel) with other photometric data presented in Tables 2.1 and 2.2. The dotted vertical lines in the top panel show the reliability bright limits of the APASS ($V = 7$) and ASAS ($V = 8$) surveys. In the whole magnitude range covered by these figures, *all* ASAS-SN photometry is unreliable (note their large declared error bars), but it was included for completeness. In both panels, the diagonal line depicts a one-to-one relationship. In the bottom panel, the diagonal dotted-dashed line shows the 0.38 mag offset between I and i' from APASS, found by Mendez et al. (2021, their Figure 1). The highly discrepant point for Bag25Aa,Ab from ASAS-SN in the top panel is probably due to a miss-identification of the target. See text for details.

2.2.1. Individual component magnitudes

To place our targets in an HR diagram (see Section 2.4), individual component magnitudes are needed. The I-band combined magnitude for each system was computed from $I_{\rm Hip} = V_{\rm Hip} - (V-I)_{\rm Hip}$, and the individual I component magnitudes are as follows: $I_{\rm A} = I_{\rm Hip} + 2.5 \times \log\left(1.0 + 10^{-0.4 \cdot \Delta I}\right)$ (primary) and $I_{\rm B} = I_{\rm A} + \Delta I$ (secondary). For the V-band we used the Hipparcos system magnitudes and the WDS magnitude differences - or our own value ΔV derived from our measured values of Δy quoted in Table 2.1, depending on the location of the binary on the HR diagram relative to the theoretical isochrones plotted (see Section 2.4).

From the data in Table 2.1, it can be seen that the Hipparcos photometry is in general in good agreement with the photometry for the system given in WDS ($V_{\rm t}$) and SIMBAD; as well as with that from other photometric surveys (see Table 2.2). Furthermore, if we define $\Delta V = V_{\rm B} - V_{\rm A}$, the mean difference $< \Delta V - \Delta y >= -0.13 \pm 0.32$ mag for seven objects in Table 2.1 is in agreement with Tokovinin et al. (2010) and Mendez et al. (2021), indicating that our SOAR magnitude differences seem reliable. This gives us some confidence on the photometry presented, but see the extended discussion about this for individual objects on Section 2.5, and Figures 2.5 and 2.6 in Section 2.4.

For one target, IOT2Aa,Ab, individual component magnitudes are not available in WDS, and, being a northern target, it was not observed at SOAR. Several other, mostly northern, targets in Table 2.1 also lack a measured ΔI; hence, we could not compute individual component magnitudes for them.

2.3. Orbital elements, orbital parallaxes, and individual components mass

As mentioned in Section 2.2, the astrometric data used in this work are a combination of published information from WDS with recent measurements made with the HRCam speckle camera [16] mounted on the SOAR 4.1 m telescope in the context of the program described in Mendez et al. (2017). Part of our data has not been published yet[17].

Regarding the uncertainty or equivalent weight of the historical data that we included in our orbit calculations, we adopted the value indicated in the WDS, when available, or errors typical for the observational procedure used (e.g., interferometric/digital imaging/photographic/micrometer). On the other hand, HRCam has been shown to deliver a precision of 1-3 mas in angular separation for objects brighter than $V \sim 12$ on a routine basis (Tokovinin, 2018a). In our HRCam@SOAR survey "calibration binaries", binaries with very well-known orbits (grades 1 or 2 in Orb6), are observed every night to calibrate our measurements, leading to systematic errors of less than 0.1° in position angle, and better than 0.2 % in scale, smaller than our internal precision[18]. The exact final precision of our measurements depends, however, on a number of factors, but in this paper, we will adopt an uncertainty of 3 mas as representative of all our HRCam data. As emphasized in Mendez et al. (2017), one should

[16] For up-to-date details of the instrument see https://www.ctio.noirlab.edu/~atokovin/speckle/

[17] In the site http://www.das.uchile.cl/~rmendez/B_Research/JAA-RAM-SB2/ we make available our input files, indicating the adopted uncertainty and quadrant flips, if any, for each data entry and the origin of the measurements in the last column, following the nomenclature in int4.

[18] One of these "astrometric standards", WDS07518−1354=BU101, is an SB2 and is included in this paper; see Section 2.5

bear in mind that the assignment of weights to each observational point is somewhat subjective (especially for older data) and plays an important role in the orbital solution. Slightly different orbital solutions from authors using the same astrometric data set are in some cases due to different weighting.

Orbits have been derived using our Markov Chain Monte Carlo (MCMC) code. In order to reduce the dimensions of the search space, we adopt the parameterization of Mendez et al. (2017) in which elements P, T, e, Ω, i, mass ratio $q = m_{\rm B}/m_{\rm A}$ and parallax ϖ are explored via MCMC, whereas a (semi-major axis), ω and $V_{\rm CoM}$ are calculated analytically via the exact least-squares solution given (P, T, e, Ω, i, q, ϖ). The details can be found in Mendez et al. (2017), where an MCMC algorithm is used to carry out joint estimation of orbital parameters and RV (see Mendez et al. (2017), Appendix A, for details of the least-squares estimate).

From a methodological standpoint, the only difference between the algorithm utilized here and that of Mendez et al. (2017) is that in the present work, we lift the restriction $q = m_{\rm B}/m_{\rm A} < 1$. This allows the algorithm to handle uncertainty about the primary and secondary stars; if the mass ratio q is greater than one, the algorithm simply calculates the parameters as if $m_{\rm B}$ was the primary (this "swap" leaves all the parameters other than ω, Ω untouched). While the value $m_{\rm B}/m_{\rm A}$ (i.e., q) reported in Table 2.4 is just a natural element of the parametrization adopted (hence a raw output of the MCMC algorithm), amplitudes $K_{\rm A}$, $K_{\rm B}$ in Table 2.3 are calculated as a function of the values of P, e, q, a, $\sin i$, ϖ of each MCMC sample.

Since the code incorporates the parallax of the system as an unknown parameter of the estimation process, it allows us to determine dynamically self-consistent orbital parallaxes, as originally suggested by Pourbaix (2000). Additionally, SB2s allow a calculation of individual component masses because the astrometric solution gives the mass sum, while the amplitudes of the RV curve give the mass ratio. Our code produces posterior probability distribution functions (PDFs) for all of the physical and geometrical parameters involved. These PDFs allow us to reliably estimate parameter uncertainties in the following way. It is customary to represent the uncertainties in terms of the dispersion σ, but this quantity is well defined only for orbits where the PDFs are "well behaved" (e.g., they are symmetrical), and it becomes meaningless for orbits that may exhibit long tails, as in the case of uncertain orbits. For this reason, we instead adopt the upper (third) quartile (Q75) and lower (first) quartile (Q25) of the distribution as a measure of the spread of the corresponding PDF and hence as a quantitative measure of the dispersion (uncertainty) of the corresponding parameter[19], which is consistent with the available data and the underlying Keplerian model.

We ran our MCMC routine with a chain length of 2 million samples and a burn-in period of $50,000$ iterations. The comparatively short burn-in time is explained on the grounds that the target parameters were initialized favorably; we fed the MCMC routine with approximate initial values from the optimization-based routine ORBIT developed by Tokovinin (1992)[20]. From the steadiness of the average value of the orbital parameters over time, we conclude that all of the solutions obtained are stable. It is worth noting that an added benefit of the large number of samples generated is that the resulting PDF histograms look rather smooth (see Figures 2.3 and 2.8) despite the fact that they are based directly on the MCMC samples, i.e., they are raw histograms rather than kernel-smoothed densities as in, e.g., Wand & Jones (1994).

[19] For a Gaussian function, one can convert from one to the other using the fact that $\sigma = (Q75 - Q25)/1.349$.
[20] The code and user manual can be downloaded from https://www.ctio.noirlab.edu/~atokovin/orbit/

The results from our MCMC code for the 14 SB2s selected as explained in Section 2.2 are given in Table 2.3. In the first two columns, we give the WDS name and the source of the previous orbital information, if available. In the following columns, we present the seven classical orbital elements, the RV for the center of mass of the system ($V_{\rm CoM}$) and the semi-amplitudes for the primary (K_1) and secondary (K_2). In the penultimate column, we indicate the grade of the orbit according to Orb6 (1: best, 5: worst) and SB9 (5: best, 1: worst), and in the last column, we give the reference to the most recently published astrometric orbit (from Orb6) or RV solution (from SB9). For each object in this table, two sets of values for the orbital elements are provided. The upper row gives the maximum-likelihood (ML) value. For an explanation of why this is the selected estimator, please see the discussion in Mendez et al. (2021; Section 3.1). The lower row gives the median derived from the posterior PDF of the MCMC simulations, as well as the upper ($Q75$) and lower ($Q25$) quartile of the distribution in the form of a superscript and subscript, respectively. As explained before, the quartiles give us an estimation of the uncertainty of our estimated parameters. A look at the results in this table indicates that our values generally coincide quite well with those from previous studies. In particular, it is well known that the argument of periapsis (ω) is well determined by RV measurements as long as the distinction between primary and secondary is unambiguous (difficult, e.g., for equal-mass binaries); the table shows that our values are indeed quite close to those from SB9, albeit with smaller uncertainties in our case. On the other hand, the longitude of the ascending node (Ω) can be well determined from astrometric observations alone, but it suffers from the same ambiguity in the case of equal- brightness binaries. From the table, we see that there is good correspondence between our values for Ω and those from Orb6 (but again, with smaller formal uncertainties in our case), except for five objects. As will be shown below, four of these objects have values of the mass ratio q quite close to 1, which probably explains this discrepancy.

In Figure 2.2 we show a subset of representative examples of orbital solutions from our simultaneous fit to the astrometric orbit (left panels) and the RV curve (right panels), and in Figure 2.3 we present the PDFs for the same three systems. Inspection of Table 2.3, and Figures 2.2 and 2.3 shows that well- determined orbits have an ML value that approximately coincides with the second quartile of the PDF, their interquartile range is relatively well constrained, and the PDFs have a Gaussian-like distribution. On the contrary, poor orbits show PDFs with long tails—and therefore large interquartile ranges—on which the ML value usually differs significantly from the second quartile, and the PDFs are tangled. The top panel of Figure 2.8) shows an extreme case in this respect: TOK39Aa,Ab. For completeness, in http://www.das.uchile.cl/~rmendez/B_Research/JAA-RAM-SB2/, we make available the orbital plots and the relevant PDFs for all the systems in our sample.

Table 2.3: Extended Orbital Elements for our SB2s

WDS name HD number	Source	P (yr)	T_0 (yr)	e	a (mas)	ω (°)	Ω (°)	i (°)	V_{CoM} (km/s)	K_1 (km/s)	K_2 (km/s)	Gr	Orbit Author
00352−0336	This paper	6.8975	1890.6130	0.7616	234.26	104.73	328.34	47.89	9.09	11.67	15.64		
3196		$6.8975^{+0.0005}_{-0.0006}$	$1890.6139^{+0.0091}_{-0.0085}$	$0.7615^{+0.0013}_{-0.0014}$	$234.07^{+0.74}_{-0.73}$	$104.70^{+0.18}_{-0.18}$	$328.39^{+0.22}_{-0.22}$	$47.83^{+0.24}_{-0.24}$	$9.08^{+0.03}_{-0.03}$	$11.68^{+0.51}_{-0.51}$	$15.59^{+0.17}_{-0.17}$		
	ORB6	6.89	2000.98	0.773	241	283.8	149.0	49.4	–	–	–	1	Mason(2005)
	SB9	6.9185-Fixed	1987.187 ± 0.011	0.77-Fixed	–	109.0 ± 3.1	–	–	8.83 ± 0.22	10.90 ± 0.59	16.44 ± 0.43	–	Duquennoy(1991a)
02128−0224	This paper	0.259516	1983.85112	0.6917	13.82	76.28	240.2	23.9	−5.95	19.01	19.65		
13612		$0.259516^{+0.000011}_{-0.000011}$	$1983.85112^{+0.00027}_{-0.00026}$	$0.6920^{+0.0027}_{-0.0027}$	$13.98^{+0.75}_{-0.64}$	$76.23^{+0.41}_{-0.41}$	$240.3^{+1.4}_{-1.3}$	$25.6^{+6.4}_{-7.8}$	$-5.95^{+0.02}_{-0.02}$	$19.01^{+0.04}_{-0.04}$	$19.74^{+0.40}_{-0.43}$		
	ORB6	–	–	–	–	–	–	–	–	–	–	–	–
	SB9	0.259515 ± 0.000012	1989.55859 ± 0.00015	0.689 ± 0.003	–	74.3 ± 0.5	–	–	-5.95 ± 0.07	19.08 ± 0.15	19.77 ± 0.15	–	Duquennoy(1991a)
04107−0452	This paper	20.6327	1931.498	0.8349	164.32	67.88	154.10	67.80	26.49	11.65	12.41		
26441		$20.6290^{+0.0077}_{-0.0076}$	$1931.513^{+0.031}_{-0.031}$	$0.8384^{+0.0011}_{-0.0011}$	$164.72^{+0.66}_{-0.66}$	$67.94^{+0.18}_{-0.18}$	$154.20^{+0.28}_{-0.28}$	$67.81^{+0.23}_{-0.24}$	$26.49^{+0.00}_{-0.00}$	$11.61^{+0.04}_{-0.04}$	$12.41^{+0.06}_{-0.06}$		
	ORB6	20.621 ± 0.005	2014.031 ± 0.003	0.8400 ± 0.0014	167.2 ± 2.1	68.6 ± 0.3	153.3 ± 0.6	69.0 ± 0.5		–	–	2	Tokovinin(2017)
	SB9	20.608 ± 0.011	1993.426 ± 0.011	0.8372 ± 0.0015	–	69.0 ± 0.4	–	–	26.55 ± 0.03	11.59 ± 0.06	12.51 ± 0.10	5	Griffin(2015)
04184+2135	This paper	11.3630	1955.100	0.1537	135.39	162.61	352.25	123.88	37.79	7.46	8.97		
27176		$11.3642^{+0.0071}_{-0.0071}$	$1955.100^{+0.031}_{-0.030}$	$0.1540^{+0.0016}_{-0.0016}$	$135.37^{+0.16}_{-0.16}$	$162.67^{+0.80}_{-0.80}$	$352.22^{+0.24}_{-0.24}$	$123.88^{+0.25}_{-0.25}$	$37.79^{+0.01}_{-0.01}$	$7.50^{+0.32}_{-0.32}$	$8.96^{+0.11}_{-0.11}$		
	ORB6	11.350 ± 0.021	1977.740 ± 0.056	0.1670 ± 0.0044	132.90 ± 0.95	$339. \pm 1.9$	350.70 ± 0.61	125.50 ± 0.73	–	–	–	2	Pourbaix(2000)
	SB9	11.323 ± 0.016	1989.075 ± 0.038	0.1711 ± 0.0028	–	159.1 ± 1.3	–	–	37.78 ± 0.12	7.32 ± 0.48	9.01 ± 0.16	–	Torres(1997)
07518−1354	This paper	23.3225	1892.630	0.7537	611.9	253.174	103.054	80.839	−21.37	9.76	9.75		
64096		$23.3207^{+0.0054}_{-0.0053}$	$1892.639^{+0.026}_{-0.027}$	$0.7538^{+0.0015}_{-0.0015}$	$612.0^{+1.7}_{-1.6}$	$253.185^{+0.080}_{-0.079}$	$103.044^{+0.059}_{-0.061}$	$80.835^{+0.045}_{-0.044}$	$-21.38^{+0.02}_{-0.02}$	$9.70^{+0.15}_{-0.15}$	$9.69^{+0.47}_{-0.46}$		
	ORB6	23.330 ± 0.010	1985.923 ± 0.011	0.7647 ± 0.0021	617.9 ± 2.4	253.64 ± 0.12	282.65 ± 0.09	80.82 ± 0.06	–	–	–	1	Tokovinin(2012a)
	SB9	22.701 ± 0.027	1985.914 ± 0.020	0.741 ± 0.007	–	253.1 ± 0.4	–	–	-21.34 ± 0.16	9.13 ± 0.63	9.69 ± 0.26	5	Pourbaix(2000)
11560+3520	This paper	13.553	1996.16	0.1010	127.7	316.3	279.5	145.4	−4.99	4.19	4.99		
103613		$13.566^{+0.057}_{-0.056}$	$1996.11^{+0.18}_{-0.19}$	$0.1008^{+0.0054}_{-0.0054}$	$127.6^{+2.0}_{-2.0}$	$315.3^{+4.0}_{-4.0}$	$279.9^{+1.3}_{-1.3}$	$146.1^{+3.7}_{-3.3}$	$-4.99^{+0.01}_{-0.01}$	$4.19^{+0.12}_{-0.12}$	$4.98^{+0.02}_{-0.02}$		
	ORB6	13.53	2010.54	0.165	143	9.90	302.5	135.1	–	–	–	3	Griffin(2013)
	SB9	13.66 ± 0.15	2009.46 ± 0.30	0.103 ± 0.011	–	309 ± 8	–	–	-4.97 ± 0.04	5.00 ± 0.06	4.25 ± 0.16	5	Griffin(2013a)
14492+1013	This paper	10.0052	1988.130	0.4994	125.174	162.22	319.48	44.44	−88.29	6.66	6.61		
130669		$10.0062^{+0.0041}_{-0.0042}$	$1988.130^{+0.014}_{-0.014}$	$0.4999^{+0.0022}_{-0.0021}$	$125.07^{+0.35}_{-0.35}$	$162.31^{+0.67}_{-0.68}$	$319.43^{+0.47}_{-0.47}$	$44.30^{+0.48}_{-0.48}$	$-88.29^{+0.01}_{-0.01}$	$6.65^{+0.06}_{-0.06}$	$6.61^{+0.09}_{-0.10}$		
	ORB6	10.010	2018.174	0.518	123	335.9	144.8	43.5	–	–	–	1	Docobo(2018a)
	SB9	9.91 ± 0.18	2008.127 ± 0.030	0.488 ± 0.009	–	163.0 ± 2.0	–	–	-88.27 ± 0.05	6.73 ± 0.07	6.76 ± 0.09	5	Griffin(2015)
15282−0921	This paper	2.4359	1980.4630	0.97525	104.3	254.898	272.47	54.3	7.16	37.45	55.65		
137763		$2.4359^{+0.0001}_{-0.0001}$	$1980.4629^{+0.0002}_{-0.0002}$	$0.97530^{+0.00011}_{-0.00011}$	$104.7^{+2.4}_{-2.4}$	$254.888^{+0.058}_{-0.059}$	$272.64^{+0.64}_{-0.64}$	$54.5^{+1.1}_{-1.2}$	$7.16^{+0.01}_{-0.01}$	$37.47^{+0.06}_{-0.06}$	$55.56^{+0.63}_{-0.63}$		
	ORB6	2.43623	2007.2603	0.976	107.4 ± 8.1	255.6	272.8 ± 2.1	55.4 ± 3.6	–	–	–	2	Tokovinin(2016)
	SB9	2.436175 ± 0.000047	1990.205532 ± 0.000041	0.9733 ± 0.0006	–	252.64 ± 0.73	–	–	7.47 ± 0.20	36.42 ± 0.38	52.90 ± 1.73	–	Halbwachs(2018)
16584+3943	This paper	16.023	1985.170	0.7732	75.40	336.04	245.46	109.38	33.54	10.46	11.90		
153527		$16.022^{+0.039}_{-0.039}$	$1985.171^{+0.040}_{-0.040}$	$0.7729^{+0.0019}_{-0.0019}$	$75.38^{+0.41}_{-0.42}$	$336.06^{+0.43}_{-0.43}$	$245.36^{+0.47}_{-0.46}$	$109.55^{+0.83}_{-0.82}$	$33.54^{+0.08}_{-0.08}$	$10.45^{+0.09}_{-0.09}$	$11.89^{+0.13}_{-0.13}$		
	ORB6	16.09	2001.07	0.753	75	154.3	63.2	113.0	–	–	–	2	Docobo(2013)
	SB9	16.153-Fixed	2001.1970 ± 0.0080	0.775 ± 0.003	–	337.0 ± 0.9	–	–	33.59 ± 0.16	10.40 ± 0.18	11.96 ± 0.23	5	Griffin(2003)
18384−0312	This paper	12.1422	1910.000	0.2454	145.35	257.88	352.99	123.90	−15.97	7.21	7.55		
172088		$12.1426^{+0.0044}_{-0.0044}$	$1909.996^{+0.039}_{-0.039}$	$0.2456^{+0.0019}_{-0.0019}$	$145.37^{+0.38}_{-0.39}$	$257.87^{+0.30}_{-0.30}$	$353.03^{+0.22}_{-0.22}$	$123.87^{+0.22}_{-0.22}$	$-15.97^{+0.00}_{-0.00}$	$7.20^{+0.03}_{-0.03}$	$7.55^{+0.03}_{-0.03}$		
	ORB6	12.135 ± 0.006	2007.18 ± 0.04	0.2567 ± 0.0029	146.1 ± 0.8	79.7 ± 1.5	173.4 ± 0.9	123.9 ± 5.0	–	–	–	1	Hartkopf(2013b)
	SB9	12.1342-Fixed	2007.185 ± 0.049	0.230 ± 0.006	–	258.9 ± 1.5	–	–	-15.95 ± 0.03	7.19 ± 0.06	7.51 ± 0.06	5	Griffin(2013b)
20102+4357	This paper	85.05	1886.15	0.4945	448.6	344.00	143.75	117.15	−42.99	3.51	5.40		
191854		$85.02^{+0.27}_{-0.27}$	$1886.22^{+0.27}_{-0.28}$	$0.4889^{+0.0035}_{-0.0035}$	$448.2^{+1.34}_{-1.3}$	$344.07^{+0.82}_{-0.82}$	$143.75^{+0.25}_{-0.26}$	$117.22^{+0.28}_{-0.28}$	$-43.06^{+0.13}_{-0.14}$	$3.65^{+0.37}_{-0.36}$	$5.07^{+0.47}_{-0.49}$		
	ORB6	85.61	1970.27	0.488	449	339.4	142.2	116.4	–	–	–	2	Heintz(1997)
	SB9	85.22 ± 0.12	1970.44 ± 0.18	0.4922 ± 0.0033	–	339 ± 1	–	–	-43.2 ± 0.2	3.97 ± 0.44	5.12 ± 0.47	–	Pourbaix(2000)
20205+4351	This paper	7.9232	1993.1840	0.9060	8.44	42.76	347.7	117.5	1.43	28.0	68.1		
193793		$7.9241^{+0.0037}_{-0.0035}$	$1993.1825^{+0.0036}_{-0.0039}$	$0.9012^{+0.0034}_{-0.0034}$	$8.30^{+0.22}_{-0.23}$	$42.31^{+0.70}_{-0.68}$	$349.1^{+2.5}_{-2.5}$	$119.4^{+3.7}_{-3.4}$	$1.25^{+0.05}_{-0.05}$	$28.3^{+1.8}_{-1.8}$	$68.5^{+1.2}_{-1.1}$		
	ORB6	7.9298 ± 0.0025	1985.2443 ± 0.0082	0.901 ± 0.005	8.99 ± 0.19	48.2 ± 1.9	354.2 ± 0.7	118.9 ± 0.9	–	–	–	3	Monnier(2011)
	SB9	7.9370 ± 0.0036	1985.2225 ± 0.0044	0.881 ± 0.005	–	46.7 ± 1.6	–	–	3.1 ± 1.0	30.5 ± 1.9	82.0 ± 2.3	–	Marchenko(2003)
20527+4607	This paper	31.141	1918.97	0.7505	236.7	321.90	47.72	127.52	−20.30	6.95	7.54		
–		$31.144^{+0.052}_{-0.051}$	$1918.97^{+0.10}_{-0.11}$	$0.7510^{+0.0034}_{-0.0034}$	$236.4^{+2.0}_{-2.0}$	$322.01^{+0.67}_{-0.66}$	$47.74^{+0.53}_{-0.54}$	$127.57^{+0.89}_{-0.86}$	$-20.31^{+0.04}_{-0.04}$	$6.96^{+0.10}_{-0.10}$	$7.54^{+0.10}_{-0.10}$		
	ORB6	30.45	2013.49	0.723	212	351.6	65.9	128.7	–	–	–	3	Docobo(2013)
	SB9	31.4853	1981.2329	0.74	–	320.	–	–	−20.3	6.9	7.5	2	Griffin(1984)
23485+2539	This paper	3.2163	2001.3988	0.6061	40.3	77.75	121.8	86.1	−9.55	16.43	16.35		
223323		$3.2157^{+0.0035}_{-0.0035}$	$2001.3995^{+0.0041}_{-0.0042}$	$0.6060^{+0.0038}_{-0.0038}$	$40.3^{+1.2}_{-1.2}$	$77.79^{+0.60}_{-0.60}$	$121.2^{+1.7}_{-1.7}$	$86.0^{+1.3}_{-1.3}$	$-9.55^{+0.01}_{-0.01}$	$16.43^{+0.12}_{-0.12}$	$16.35^{+0.12}_{-0.12}$		
	ORB6	3.2191 ± 0.0038	2011.0545 ± 0.0085	0.602 ± 0.008	40.8 ± 1.0	78.4 ± 0.6	121.1 ± 1.1	86.0 ± 0.9	–	–	–	3	Horch(2019b)
	SB9	3.2172 ± 0.0036	2004.6134 ± 0.0025	0.604 ± 0.003	–	77.8 ± 0.6	–	–	-9.56 ± 0.06	16.38 ± 0.11	16.40 ± 0.16	–	Griffin(2007)

Even though the astrometric orbits do not always have excellent phase coverage, the combined solution produces very precise orbital parameters. This is most evident in Figure 2.3, which exhibits tight and well-constrained distributions. Judging from our quartile-based uncertainty estimation, we can see that the mass ratio for this sample of objects is determined in the best cases with less than 1 % error, while the uncertainty on the mass sum is around 1 %. The formal error on the best individual component masses that we could determine is $0.01 M_{\odot}$ (see Table 2.4).

In Table 2.4 we present a comparison of the parallax values from Hipparcos and/or Gaia eDR3 with our orbital parallaxes. In the last four columns, we give the mass ratio, the total mass, and the individual masses obtained from our simultaneous fits to the astrometric and RV data, which was done adopting the orbital elements given in Table 2.3. The first line gives the ML values, and the second line gives the quartiles. All mass values were computed allowing the parallax of the system to be a free parameter of the MCMC code, i.e., using the orbital parallax[21], whose ML value and quartiles are given in the fourth column of this table (upper and lower row respectively). Therefore, our mass estimates do include the extra variance from this parameter.

In Figure 2.4 we show a comparison of our orbital parallaxes with those from Hipparcos, Gaia, and the recent study of SB2 binaries by Piccotti et al. (2020). The mean values of the differences $\left\langle \Pi_{\rm orb} - \Pi_{\rm various} \right\rangle$ are 0.0 ± 1.8 mas ($N = 13$ objects), 0.1 ± 1.1 mas ($N = 8$ objects) and -0.9 ± 1.6 mas ($N = 7$ objects), respectively[22], showing that our orbital parallaxes are indeed reliable. It is interesting to note that the rms with respect to Gaia is smaller than that with respect to Hipparcos, which indicates that at least some of the variance on this difference comes from the trigonometric parallaxes themselves and not the orbital parallaxes, as the rms is smaller for the better-quality Gaia parallaxes.

Several objects of our sample show ambiguity regarding their mass ratio; preliminary results using both the ORBIT routine and our MCMC method gave estimates of $m_{\rm B}/m_{\rm A}$ in regions arbitrarily close to 1. Moreover, in most of these cases, swapping the primary and the secondary, i.e., taking observations of the RV of the primary as observations of the secondary, and vice versa, also led to valid solutions. To deal with this ambiguity, we adapted the methodology described in Mendez et al. (2017, 2021) to accept values of $m_{\rm B}/m_{\rm A}$ greater than 1. While both previous studies and the present work rely on a Metropolis-within-Gibbs scheme to generate samples from the posterior distributions, the former rejects samples containing a value of $m_{\rm B}/m_{\rm A}$ outside the interval $(0, 1)$. Instead, the method proposed here swaps RV observations whenever $m_{\rm B}/m_{\rm A}$ is greater than 1 and carries out the minimum least-squares estimation of a, ω, and $V_{\rm CoM}$ -conditional to the rest of the parameters- in a manner akin to that explained in Mendez et al. (2017, Appendix 1). This approach produces a shift of $\pm 180^{\circ}$ in ω as this parameter explicitly depends on the precedence of a binary and secondary, which is corrected in a post-processing step.

[21] Except for target TOK39Aa,Ab=WDS 02128-0224, for which we used a parallax prior; see Section 2.5 and Figure 2.8. In fact, in Table 2.4 we report both solutions for this target: with and without a parallax prior.
[22] In all these calculations we excluded TOK39Aa,Ab; see previous footnote.

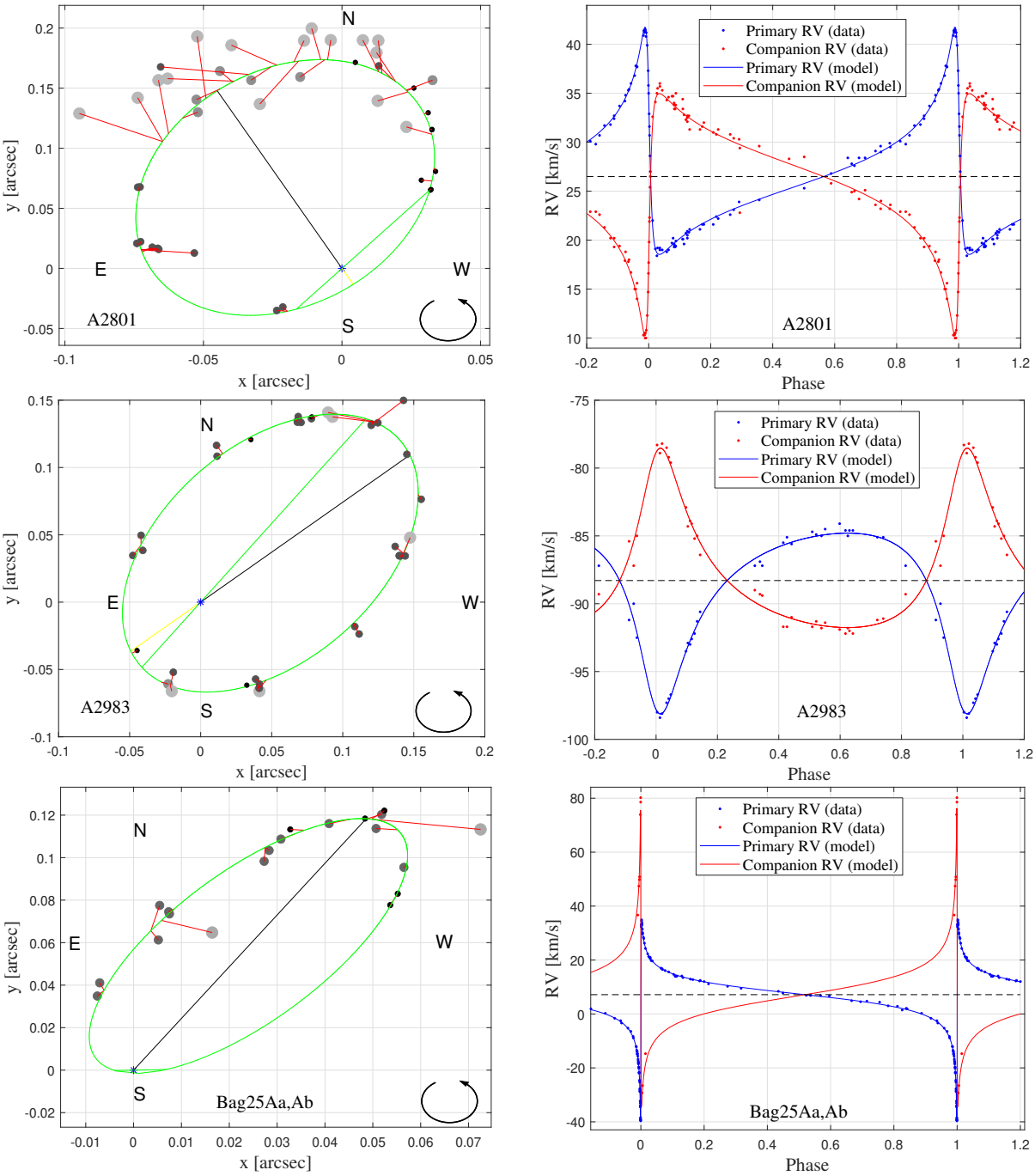

Figure 2.2: ML orbits from simultaneous fits to the astrometric and RV curves for three representative cases. From top to bottom: A2801 (WDS 04107-0452), A2983 (WDS 14492+1013), and Bag25Aa,Ab (WDS 15282-0921). The left panels show the data points and the astrometric orbit. The size and color of the dots indicate the weight (uncertainty) of each observation: large light dots indicate larger errors, and the opposite is true for small dark dots. Smaller dots are from more recent interferometric measurements, including - but not limited to - our own. The green line indicates the line of nodes, while the black line indicates the direction to apoastron. The right panels show the RV curves of both components. The horizontal dashed line indicates the inferred (fitted) systemic velocity reported in Table 2.3.

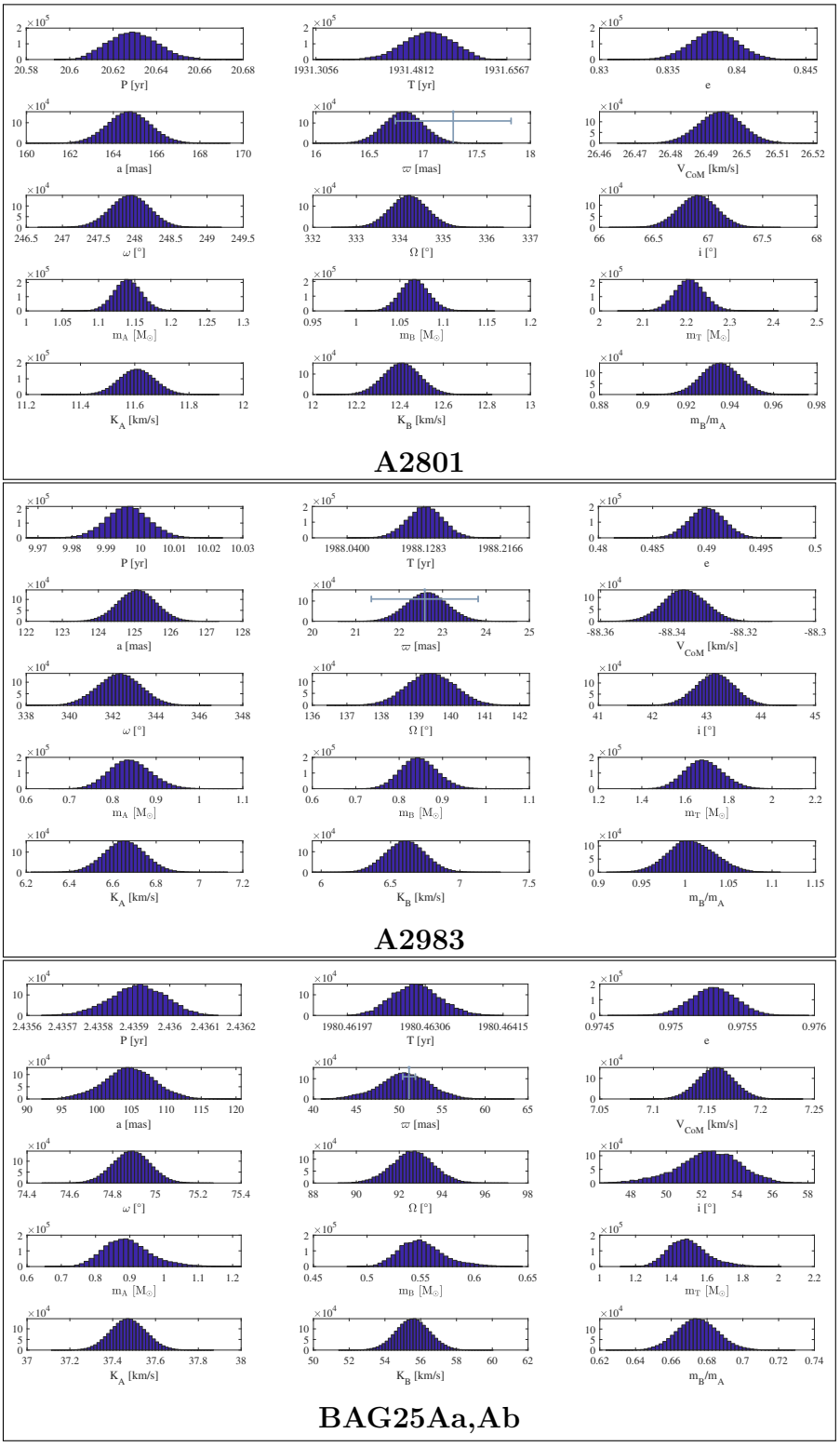

Figure 2.3: Posterior distributions of the classical seven orbital elements; plus the (fitted) orbital parallax, the Gaia DR2 trigonometric parallax and its $\pm 1\sigma$ error, the systemic velocity, the velocity amplitudes for both components, the mass sum, the mass ratio and the individual component masses, for the same objects shown in Figure 2.2. We note that for objects with a mass-ratio close to one (in this case A2983 - middle panel; but see Table 2.4 for other objects), the $m_{\rm B}/m_{\rm A}$ histograms are well-behaved and smooth across that boundary, as explained in the text.

Table 2.4: Parallaxes and Individual Component Masses

WDS name HD number	Hipparcos (mas)	GAIA DR3 (mas)	Orbital (mas)	m_B/m_A	m_T $M_\odot$	m_A $M_\odot$	m_B $M_\odot$
00352−0336	47.05 ± 0.67	–	42.41	0.746	3.54	2.03	1.51
3196			$42.38^{+0.88}_{-0.85}$	$0.749^{+0.034}_{-0.034}$	$3.54^{+0.21}_{-0.21}$	$2.02^{+0.09}_{-0.09}$	$1.52^{+0.13}_{-0.12}$
02128−0224[a]	25.19 ± 1.41	26.54 ± 0.13	23.1	0.968	3.2	1.62	1.57
13612			$24.8^{+7.2}_{-8.1}$	$0.963^{+0.022}_{-0.020}$	$2.7^{+4.9}_{-1.2}$	$1.35^{+2.49}_{-0.62}$	$1.31^{+2.42}_{-0.60}$
02128−0224+prior[a]	25.19 ± 1.41	26.54 ± 0.13	26.03	0.959	2.355	1.20	1.15
13612			$26.29^{+0.21}_{-0.21}$	$0.960^{+0.022}_{-0.020}$	$2.301^{+0.087}_{-0.084}$	$1.17^{+0.05}_{-0.05}$	$1.13^{+0.04}_{-0.04}$
04107−0452	16.09 ± 0.65	17.28 ± 0.54	16.58	0.9386	2.286	1.18	1.11
26441			$16.82^{+0.12}_{-0.12}$	$0.9355^{+0.0059}_{-0.0058}$	$2.207^{+0.023}_{-0.022}$	$1.14^{+0.01}_{-0.01}$	$1.07^{+0.01}_{-0.01}$
04184+2135	18.5 ± 0.5	19.51 ± 0.24	18.15	0.832	3.21	1.76	1.46
27176			$18.11^{+0.39}_{-0.37}$	$0.837^{+0.037}_{-0.038}$	$3.23^{+0.20}_{-0.20}$	$1.76^{+0.08}_{-0.08}$	$1.47^{+0.12}_{-0.12}$
07518−1354	60.59 ± 0.59	–	60.2	1.001	1.93	0.97	0.97
64096			$60.6^{+1.6}_{-1.5}$	$1.002^{+0.053}_{-0.050}$	$1.90^{+0.15}_{-0.14}$	$0.95^{+0.10}_{-0.09}$	$0.95^{+0.06}_{-0.05}$
11560+3520	13.86 ± 0.58	14.73 ± 0.37	17.4	0.839	2.14	1.16	0.98
103613			$17.1^{+1.6}_{-1.9}$	$0.841^{+0.026}_{-0.025}$	$2.25^{+0.83}_{-0.48}$	$1.22^{+0.45}_{-0.26}$	$1.03^{+0.38}_{-0.22}$
14492+1013	22.6 ± 1.2	–	22.69	1.007	1.679	0.84	0.84
130669			$22.64^{+0.31}_{-0.31}$	$1.007^{+0.019}_{-0.017}$	$1.684^{+0.060}_{-0.057}$	$0.84^{+0.03}_{-0.03}$	$0.84^{+0.03}_{-0.03}$
15282−0921	48.6 ± 1.3	–	50.3	0.6731	1.5024	0.90	0.60
137763			$50.7^{+2.0}_{-1.9}$	$0.6745^{+0.0077}_{-0.0076}$	$1.486^{+0.073}_{-0.068}$	$0.89^{+0.05}_{-0.04}$	$0.60^{+0.03}_{-0.03}$
16584+3943	8.8 ± 0.68	8.97 ± 0.05	9.325	0.879	2.059	1.10	0.96
153527			$9.313^{+0.096}_{-0.099}$	$0.879^{+0.016}_{-0.016}$	$2.065^{+0.038}_{-0.036}$	$1.10^{+0.02}_{-0.02}$	$0.97^{+0.02}_{-0.02}$
18384−0312	20.85 ± 0.91	–	20.69	0.9546	2.351	1.20	1.15
172088			$20.70^{+0.12}_{-0.12}$	$0.9539^{+0.0057}_{-0.0056}$	$2.349^{+0.024}_{-0.023}$	$1.20^{+0.01}_{-0.01}$	$1.15^{+0.01}_{-0.01}$
20102+4357	19.48 ± 0.54	19.30 ± 0.13	18.04	0.65	2.12	1.29	0.84
191854			$18.39^{+0.99}_{-0.89}$	$0.72^{+0.13}_{-0.11}$	$2.00^{+0.32}_{-0.29}$	$1.16^{+0.22}_{-0.20}$	$0.84^{+0.14}_{-0.13}$
20205+4351	0.25 ± 0.42	0.538 ± 0.024	0.691	0.411	29.0	20.5	8.4
193793			$0.648^{+0.040}_{-0.044}$	$0.413^{+0.027}_{-0.027}$	$33.6^{+4.7}_{-3.5}$	$23.7^{+3.2}_{-2.4}$	$9.9^{+1.6}_{-1.3}$
20527+4607	19.0 ± 1.0	18.07 ± 0.56	18.75	0.922	2.073	1.08	1.00
–			$18.71^{+0.40}_{-0.41}$	$0.923^{+0.020}_{-0.020}$	$2.079^{+0.090}_{-0.083}$	$1.08^{+0.05}_{-0.04}$	$1.00^{+0.04}_{-0.04}$
23485+2539	14.51 ± 0.47	14.42 ± 0.03	14.28	1.005	2.172	1.08	1.09
223323			$14.25^{+0.45}_{-0.45}$	$1.005^{+0.014}_{-0.014}$	$2.176^{+0.026}_{-0.026}$	$1.09^{+0.01}_{-0.01}$	$1.09^{+0.01}_{-0.01}$

[a] The first solution is computing an orbital parallax. The second solution is imposing the GAIA eDR3 parallax as a (Gaussian) prior to the solution. See also Figure 2.8 and Section 2.5

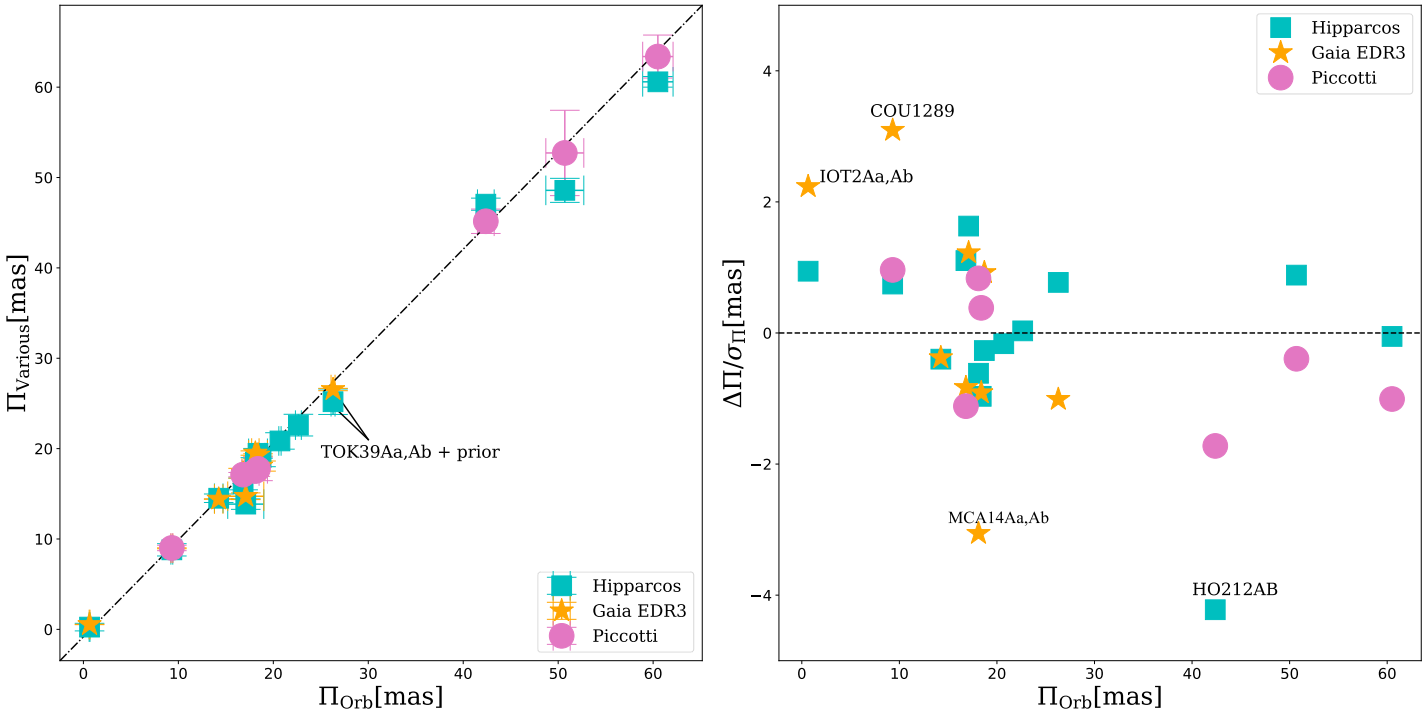

Figure 2.4: Comparison of trigonometric and orbital parallaxes for our sample of SB2s. The left panel shows a comparison of our orbital parallax $\Pi_{\rm Orb}$, with the Hipparcos parallax (from the re-reduction by van Leeuwen (2010)), the Gaia eDR3 parallax and the orbital parallaxes from Piccotti et al. (2020). The correlation is good and tight. The dotted-dashed line is a one-to-one relationship shown for reference. In the right panel, we plot the deviation of $(\Pi_{\rm Orb} - \Pi_{\rm Various})\,/\sigma_\Pi$, where σ_Π includes our uncertainty and those quoted for Hipparcos, Gaia and Piccotti in Table 2.4. The four most discrepant cases, identified in the plot, are further discussed in Section 2.5.

2.4. HR diagram

In Figure 2.5 we present an observational HR diagram for the six visual systems with available V and $(V-I)$ colors for each component. To obtain the $(V-I)$ colors, we used the V magnitudes given in Table 2.1 and the I magnitudes derived as explained in Section 2.2.1. To determine M_V, we used the published trigonometric parallaxes given in Table 2.4. We note that, due to the log factor, there is no significant difference if we instead use the orbital parallax. Also, at this scale, the formal error in absolute magnitude due to photometric and parallax uncertainties is negligible (of course, this does not consider possible systematic effects or biases on the parallaxes, which could be larger than the formal uncertainties). All of these systems lie at a distance of less than 65 pc; hence, we did not apply extinction or reddening correction to the apparent magnitudes and colors.

For reference, in the HR diagram we have superimposed a zero-age main sequence (ZAMS) from Schmidt-Kaler (1982) (gold solid line, kindly provided by G. Carraro[23]). In order to asses the current uncertainties in stellar models, we have also superimposed isochrones from the

[23] Personal communication

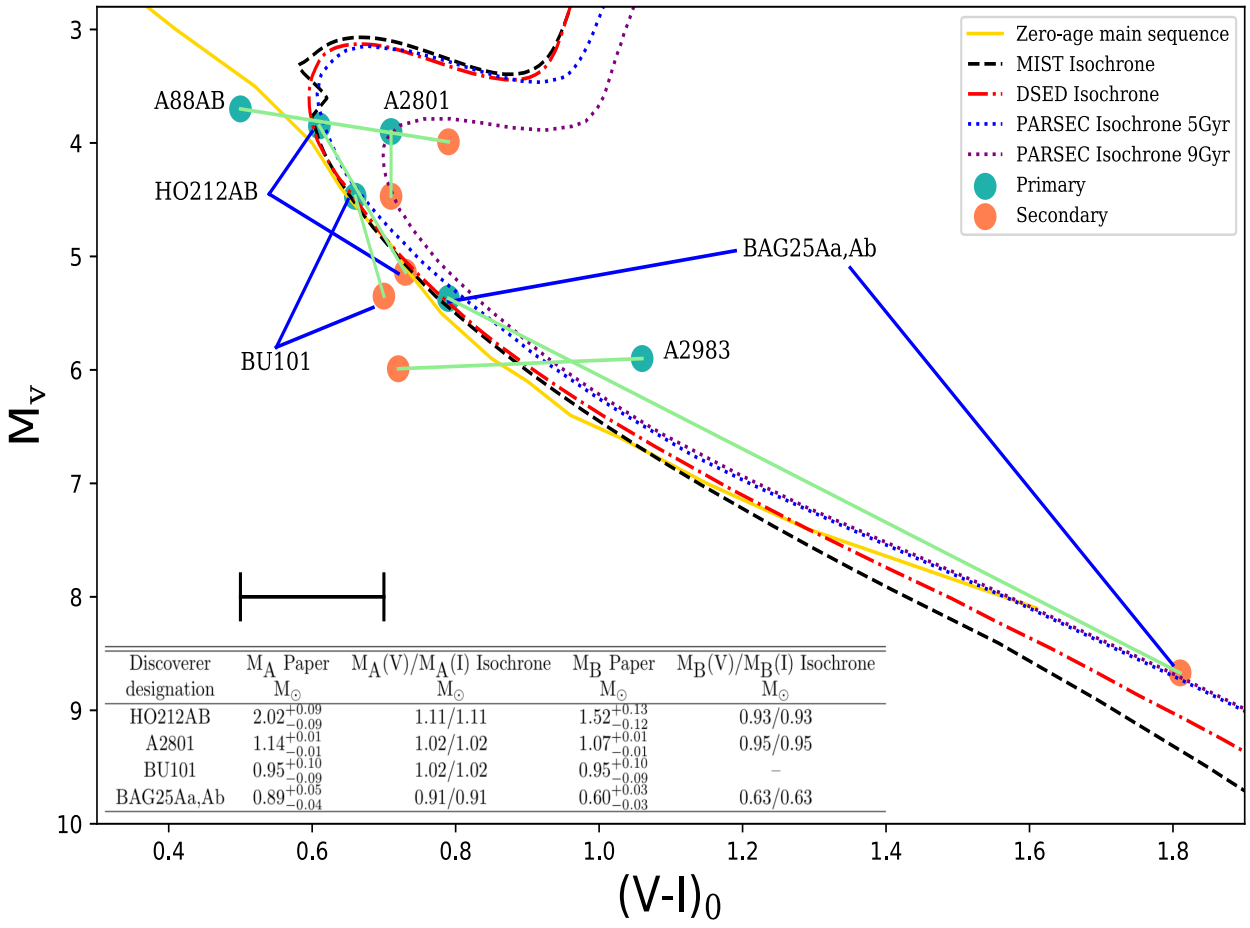

Discoverer designation	M_A Paper $M_\odot$	$M_A(V)/M_A(I)$ Isochrone $M_\odot$	M_B Paper $M_\odot$	$M_B(V)/M_B(I)$ Isochrone $M_\odot$
HO212AB	$2.02^{+0.09}_{-0.09}$	1.11/1.11	$1.52^{+0.13}_{-0.12}$	0.93/0.93
A2801	$1.14^{+0.01}_{-0.01}$	1.02/1.02	$1.07^{+0.01}_{-0.01}$	0.95/0.95
BU101	$0.95^{+0.10}_{-0.09}$	1.02/1.02	$0.95^{+0.10}_{-0.09}$	–
BAG25Aa,Ab	$0.89^{+0.05}_{-0.04}$	0.91/0.91	$0.60^{+0.03}_{-0.03}$	0.63/0.63

Figure 2.5: HR diagram for our sample of SB2 systems with available photometry. Green dots depict primary components and orange dots the secondaries. Each pair has been linked with a line and the discoverer designation is noted. The bar at (0.6,8.0) shows the estimated error of the photometry, as discussed in Section 2.2. For reference, we have plotted an empirical Zero-age main sequence, three solar-metallicity ($Z_\odot = 0.0152$) 5 Gyr old theoretical isochrones and a 9 Gyr isochrone. In the inserted table we show a comparison of our estimated masses and the mass predicted by the theoretical models. See text for details and comments on individual systems.

Dartmouth Stellar Evolution Database (DSED[24]) - as described in Dotter et al. (2008), the Padova and Trieste Stellar Evolution Code (PARSEC[25]) - as described in Bressan et al. (2012) and the MESA Isochrones & Stellar Tracks code (MIST[26]) - as described in Dotter (2016). While there is an overall good agreement between all of these isochrones, the nonzero width of the main- sequence locus for the same age and metallicity shows the impact of using slightly different input physics in the models.

For the four systems that fall close to the isochrones, implying that their photometry is reliable, we have deduced their mass using the M_V and M_I versus mass relationships obtainable from the isochrones, in order to make a comparison with our dynamical masses. To this end,

[24] Available at http://stellar.dartmouth.edu/models/isolf_new.html
[25] Available at http://stev.oapd.inaf.it/cgi-bin/cmd_3.4
[26] Available at http://waps.cfa.harvard.edu/MIST/interp_isos.html

we used the PARSEC 5 Gyr solar-metallicity isochrone, except in the case of A2801 which is better fitted by the PARSEC 9 Gyr isochrone. The comparison is shown in the table inserted in Figure 2.5. This exercise is obviously not meaningful in the case of the three systems that lie far from the isochrones: WDS 07518−1354=BU101, WDS 14492+1013=A2983 and WDS 18384−0312=A88AB. For these, we can do a reverse process; that is, starting from the dynamical masses, we can compute the predicted photometry they should have. This approach assumes that the published photometry is erroneous, our masses are reliable, and the theoretical predictions are accurate. The results of this exercise are shown in Figure 2.6. In the table inserted in this figure, we give the resulting "corrected" photometry. We believe that these discrepancies are not related to metallicity. Even though, of the three offending cases, there is published metallicity only for A2983 (with [Fe/H4] = −0.03 according to SIMBAD), we base our conclusion on the fact that the main sequence of the PARSEC theoretical isochrones with lower metallicity cannot simultaneously fit the location on the H-R diagram of the primary and secondary in any of the cases. Further discussions are presented in the next section on a case-by-case basis.

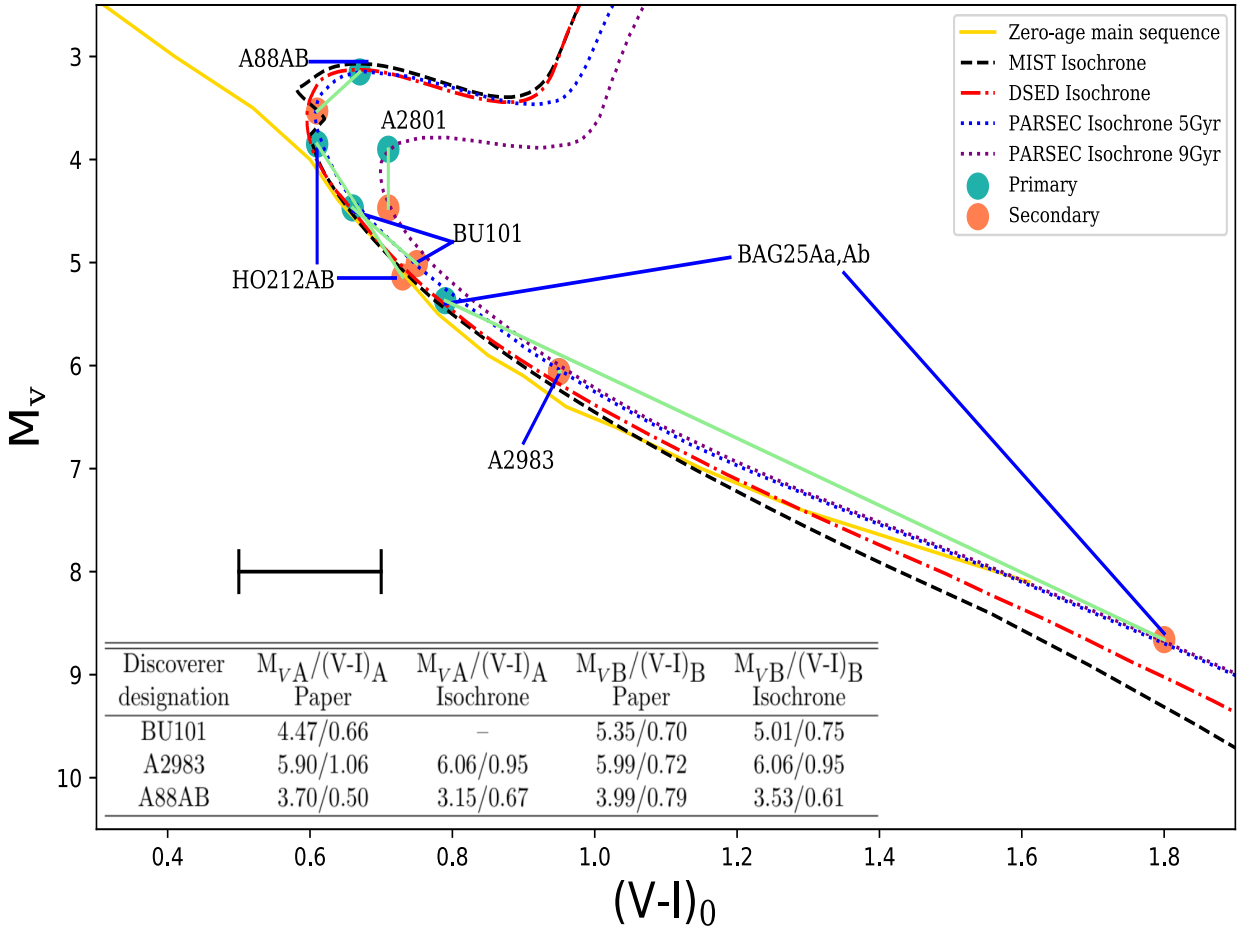

Discoverer designation	$M_VA/(V-I)_A$ Paper	$M_VA/(V-I)_A$ Isochrone	$M_VB/(V-I)_B$ Paper	$M_VB/(V-I)_B$ Isochrone
BU101	4.47/0.66	–	5.35/0.70	5.01/0.75
A2983	5.90/1.06	6.06/0.95	5.99/0.72	6.06/0.95
A88AB	3.70/0.50	3.15/0.67	3.99/0.79	3.53/0.61

Figure 2.6: Same as Figure 2.5, for objects with dubious photometry. Having corrected their photometry using the procedure explained in the text we depict their putative location on the HR diagram. The table inserted in the figure gives their measured and "corrected" photometry.

2.5. Discussion of individual objects

Based on Figures 2.5 and 2.6 in the previous section and our orbital fitting results from Section 2.3, in what follows, we present comments on individual systems.

We note that seven of our systems, identified below, are included in a recent paper by Piccotti et al. (2020), who compiled a list of SB2s with published astrometric orbits in order to determine the orbital parallaxes. This group, however, did not recompute orbits; using the published orbital elements, they derived orbital parallaxes assuming that the (independent) fits to the astrometric orbit and the RV were consistent. This differs substantially from our approach in that we have computed orbital elements in a dynamically self-consistent way by performing a simultaneous fit to all of the available data.

WDS 00352−0336=HO212AB: Ours is the first combined orbit for this SB2 system in which the primary is an SB1 system (not studied here). Since the last published orbit in 2005, we have added 25 new HRCam@SOAR interferometric measurements, the most recent ones on 2018.56 and 2019.95. Our orbital parallax (42.4 ± 0.9 mas) is slightly smaller than that reported by Piccotti et al.(Piccotti et al. (2020); 45.2 ± 1.4 mas), but they are consistent within 2σ. Our result is, however, significantly smaller than the Hipparcos parallax at the 5σ level, not very comfortable considering that both the astrometric orbit and RV curves are quite well sampled and all of the orbital elements have small formal uncertainties. We note that a parallax from Gaia is not available yet.

As shown in Figure 2.4, this is actually our most extreme outlier in terms of the difference between the orbital and trigonometric parallax. In SB9, the orbit for this system is currently considered preliminary, and it was derived by keeping the period and eccentricity, which were presumably assumed from the visual orbit, fixed. In the present work, these parameters were well determined. Based on the location of both components on the H-R diagram, their photometry seems reliable. However, judging from the theoretical isochrones, their inferred masses should be significantly smaller (see table inserted in Figure 2.5). If we scale down the individual masses reported on Table 2.4 to the Hipparcos parallax instead of our orbital parallax, the individual masses become 1.49 and 1.11 $M_{\odot}$, respectively, closer to the values inferred from the isochrones but still too large. The spectral type (F7V-F8V) for the primary implies a mass between 1.23 to 1.29 $M_{\odot}$, while for the secondary (G4V; see Table 2.1) it should be 1.06 $M_{\odot}$ (see Table 18 in Abushattal et al. (2020)). These numbers are still slightly larger than the masses implied by the isochrones but more in line with the larger Hipparcos parallax than our orbital parallax. Even if we disregard the mass implied by the spectral type of the primary, we note that in general, there is a good correspondence between the different sources of the photometry for this binary, as can be seen in Tables 2.1 and 2.2.

We conclude that the implied masses from the isochrone shown in Figure 2.5 are probably reliable; thus, at present, we have no explanation for the large difference between our dynamical and the isochrone masses.

WDS 02128−0224=TOK39Aa,Ab: This object is not listed in Orb6, so ours is the first astrometric orbit and also the first combined orbit. Phase coverage is excellent in RV, but astrometrically, it is rather poor; less than 50 % of the orbit has been sampled, which results in a somewhat uncertain inclination of the orbit. See Table 2.3 and the top panel of Figure 2.8. As a consequence, the orbital parallax is not well determined, and the individual component masses exhibit a very large uncertainty. However, we can use the Gaia parallax as

a prior in our solution (see Table 2.4), which leads to better- defined orbital parameters and well-constrained masses. The main impact of using this prior in the solution is a significant reduction in the uncertainty of the semi-major axis, which varied from $13.98^{+0.75}_{-0.64}$ mas to $14.12^{+0.15}_{-0.15}$ mas. This being a first orbit, we show the fits to this system in Figure 2.7, while in Figure 2.8 we show the PDFs without (top panel) and with (bottom panel) the use of a parallax prior. Examining the values on Table 2.4 and the PDFs, it is interesting to note that despite the fact that there is a significant reduction in the interquartile ranges when using a parallax prior, the ML and midquartiles are not that different between these two solutions; i.e., the best estimates seem to be somewhat resilient to uncertainties in the orbital fitting. Nevertheless, we expect to improve the astrometric orbit in the next few years; the most recent epochs are from our programs with HRCam@SOAR in 2020.82 and 2020.92 and ZORRO@GS[27] in 2020.83. Unfortunately, all of our latest observations cover the same sector of the orbit (see Figure 2.7). As a final note, the F8V spectral type for the primary implies a mass of 1.23 ± 0.05 $M_\odot$ (Abushattal et al. (2020), Table 18), within 1σ of our dynamical mass (with prior), as shown in Table 2.4.

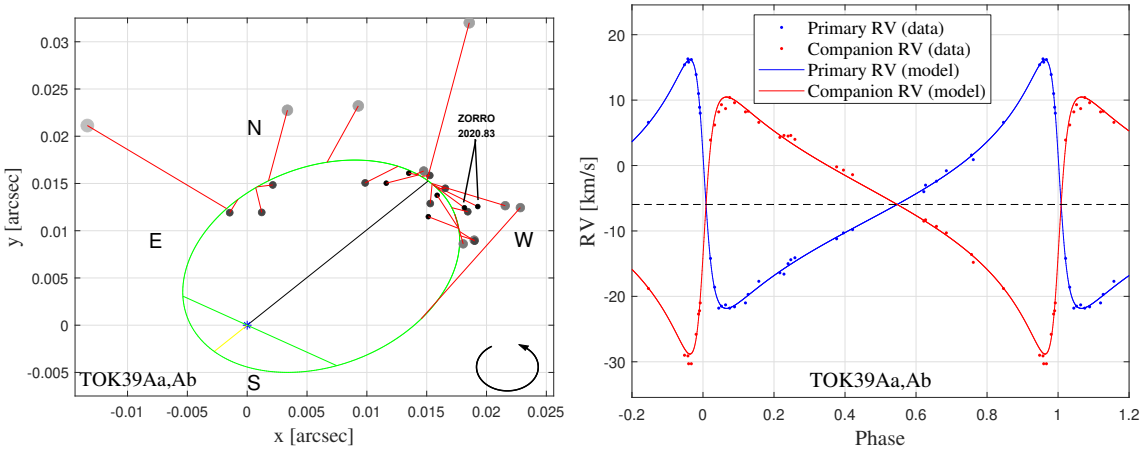

Figure 2.7: ML orbit for TOK39Aa,Ab. Symbols as in Figure 2.2. Shown is the solution without a prior. As explained in the text, if a parallax prior is used the resulting plot is quite similar. The currently incomplete orbital coverage justifies the use of a high-precision Gaia parallax prior, which improved significantly the precision of our estimate of the individual component masses (see Figure 2.8).

WDS 04107−0452=A2801: The latest astrometric orbit available for this system is from Tokovinin (2017). We have added two new measurements made on 2016.96 and 2018.97 with HRCam@SOAR and obtained an orbital parallax of 16.58 ± 0.12 mas. This object is also included in Piccotti et al. (2020)'s study, which obtained an orbital parallax of 17.12 ± 0.24 mas, while a previous study from Docobo et al. (2017) gives 16.18 ± 0.23 mas. This latter value is more in line with our result.

Our derived individual component masses are quite consistent with those from Docobo et al. (2017) and Piccotti, but somewhat larger than those implied by the isochrones (see table inserted in Figure 2.5). If we scale our masses to the Gaia parallax instead of our

[27] For a description of the ZORRO instrument and its reduction pipeline, please see Howell et al. (2011), Horch et al. (2011), and Scott et al. (2018).

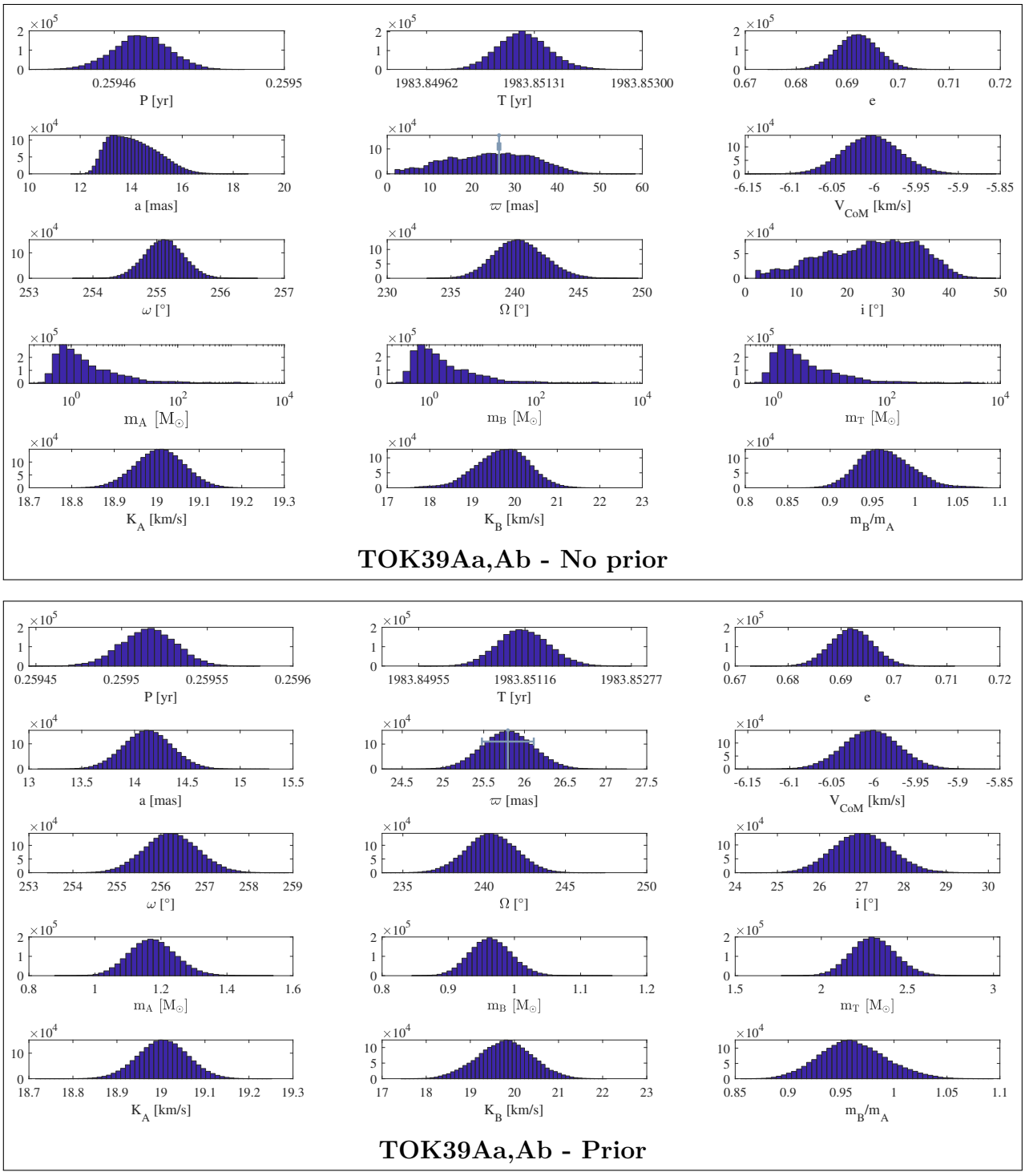

Figure 2.8: PDFs for TOK39Aa,Ab. The top panel shows the solutions obtained without a parallax prior, and the lower panel those obtained with a parallax prior. Note that in the upper panel the mass scale is logarithmic, while in the lower panel it is linear. Even in the no-prior scenario the interquartile range and the ML value for the parallax is commensurate with the Gaia eDR3 value.

orbital parallax, the individual component masses turn out to be 1.10 and 0.98 $M_\odot$ respectively, quite close to those from the isochrones. However, the spectral type of the primary (G0IV–G5IV) implies a mass between 1.26 to 1.20 $M_\odot$ (see Table 19 in Abushattal et al. (2020)), closer to the masses derived from our orbital parallax. The photometry suggests that the primary is leaving the main sequence; in our H-R diagrams, the isochrone that best fits both components is the PARSEC 9 Gyr (see Figure 2.5). This is consistent with the luminosity class IV given for the primary in SIMBAD (see Table 2.1).

WDS 04184+2135=MCA14Aa,Ab: This is a re-analysis of an orbit already studied by Torres et al. (1997), who derived a combined spectroscopic and astrometric solution yielding an orbital parallax of 17.92 ± 0.58 mas, and masses of 1.80 ± 0.13 $M_\odot$ and 1.46 ± 0.18 $M_\odot$ for the primary and secondary, respectively. More recently, Pourbaix (2000) also obtained a combined solution for this resolved SB2, yielding orbital parallaxes and component masses similar to those derived by Torres and collaborators. After these studies, five new astrometric observations of this system were secured between 1997.14 and 2005.86 using 4 m facilities with adaptive optics and speckle imaging, and we included them in our reanalysis. Our derived orbital parallax is slightly larger, at 18.16 ± 0.39 mas, but our individual masses are basically the same as those from Torres et al. (1997). We note that the Gaia eDR3 trigonometric parallax is larger than ours by almost 3σ (see Figure 2.4). Piccotti et al. (2020) give an orbital parallax of 17.55 ± 0.59 mas, even more discrepant with the Gaia eDR3 value, but their derived masses are not so discrepant from ours: 1.87 ± 0.58 and 1.52 ± 0.19 $M_\odot$. Our formal errors are, however, significantly smaller (see Table 2.4). Given the spectral type of the primary (F0V), Abushattal et al. (2020) predicted a mass of 1.64 ± 0.05 $M_\odot$ for it, which differs by less than 1σ of our dynamical mass.

WDS 07518−1354=BU101: We have included this well-studied equal-mass binary as a benchmark to compare literature values with our results. The result reported in SB9 comes from a combined astrometric and spectroscopic orbit by Pourbaix (2000). The visual orbit was subsequently revised by Tokovinin (2012a) using newer astrometric observations made with HRCam@SOAR. Our solution incorporates more recent measurements made with the same setup[28], 2019.95 being our last epoch. Our orbital parameters are in agreement with those from Tokovinin, albeit with smaller formal uncertainties on account of the incorporation of new data. Given its photometry, the mass of the primary is in very good agreement with the prediction from the isochrones (see table inserted in Figure 2.5), but the secondary is off, which casts some doubts on the photometry of the latter. In Figure 2.6, which includes the photometry in the inserted table, we show the location that the secondary should have had given its empirical mass and isochrones. The difference between the measured and expected magnitudes in V is 0.34 mag, which is quite large, but in color, the difference is smaller, 0.05 mag. Also note that the V-band photometry for this target does not exhibit such a large variance according to Tables 2.1 and 2.2. Our individual masses seem more consistent with a G7V-G8V spectral type (according to Abushattal et al. (2020), their Table 18), rather than the earlier types given in WDS (G0V) and SIMBAD (G1V), which imply larger masses. However, given our 10 % mass uncertainty, the earlier types are consistent within 1σ of our mass interquartile range (see Table 2.4). We finally note that Piccotti et al. (2020) reported

[28] Actually, this binary is observed frequently as an "astrometric standard" because it is used to calibrate the plate-scale and orientation of HRCam; see Section 2.3.

an orbital parallax of 64.4 ± 2.4 mas, which is within 1.5σ of our value of 60.2 ± 1.5 mas, and the same happens with the individual component masses. Perhaps the most intriguing aspect of this binary is that, despite the fact that both components have the same mass (within the errors), their photometry seems to indicate different locations for them on the H-R diagram, which should not be the case if they are coeval. Note, e.g., the good correspondence between ΔV and the Δy value given in Table 2.1, which shows that they do not seem to have the same luminosity.

WDS 11560+3520=CHR258: Ours is the first combined orbit for the external pair of this triple hierarchical system. The formal uncertainty of the orbital parallax (1.9 mas) is significantly worse than the uncertainties of the trigonometric parallaxes from Hipparcos (0.58 mas) and Gaia eDR3 (0.37 mas). This is most likely due to the poor orbital coverage; only three astrometric points are available, but they are well distributed in the orbit. An alternative solution, using a fixed parallax at the eDR3 value, leads to larger individual component masses of 1.84 and 1.53 $M_\odot$, in accordance with the smaller system's parallax. The spectral type (F5), however, implies a mass of 1.39 ± 0.05 $M_\odot$ (Abushattal et al. (2020)), in agreement with our value of $1.22^{+0.45}_{-0.26}$ $M_\odot$, thus somewhat validating our larger orbital parallax. This is an interesting system that deserves further astrometric observations of the external pair for better orbital coverage. The phase coverage on the RV curve is already quite good.

WDS 14492+1013=A2983: The latest visual orbit included in Orb6 is that from Docobo et al. (2018a), but more recently, Al-Tawalbeh et al. (2021) revised this solution and obtained a system mass of 1.61 ± 0.26 $M_\odot$, and an orbital parallax of 21.81 ± 0.8 mas. These results lie within 1σ of our derived values, but our combined solution yields much smaller formal uncertainties, due in part to our combined solution and also to the addition of three new HRCam+SOAR measurements in 2018.16, 2019.14, and 2019.54. The mass implied by the spectral type of the primary (K2V) is 0.80 ± 0.03 $M_\odot$ (Abushattal et al. (2020)), in very good agreement with our dynamical mass. Griffin (2015) reported $m_{\rm A} \sin^3 i = 0.308 \pm 0.012$ and $m_{\rm B} \sin^3 i = 0.306 \pm 0.011$ $M_\odot$ for this object, which for our value of the inclination (see Table 2.3) implies masses of 0.898 and 0.892 $M_\odot$, consistent at the 1σ level with our determination shown in Table 2.4. As can be seen in Figure 2.5, the measured photometry, however, seems at odds with its location on the H-R diagram, in particular regarding the large $\Delta I = 0.43 \pm 0.12$ mag given in Table 2.1. In Figure 2.6 we show the location it should have on the H-R diagram on account of its mass; because it is an equal-mass binary, the primary and secondary are located on the same point of the isochrone.

WDS 15282−0921=BAG25Aa,Ab: This is the first combined orbit for this highly eccentric SB2 inner pair of a triple system. Piccotti et al. (2020) gives masses of 0.84 ± 0.30 and 0.58 ± 90.21 $M_\odot$ and an orbital parallax of 52.7 ± 4.7 mas. Our orbital parallax is smaller and more in line with the Hipparcos parallax (no Gaia parallax for this object yet), with formal errors a factor of 2 smaller in orbital parallax and a factor of 6 improvement in the individual masses. This is mostly due to the fact that, since the last published orbit in Orb6 from Tokovinin (2016), our survey has added seven high-precision observations from HRCam@SOAR, the latest being on 2019.14. The photometry seems reliable; all measurements in Tables 2.1 and 2.2 agree within the uncertainties. As shown in the table inserted on Figure 2.5, our orbital masses agree very well with the theoretical masses for both the

primary and secondary. Based on the spectral type (G9V) of the primary, Abushattal et al. (2020) predicted a mass of 0.93 ± 0.04 $M_\odot$, consistent with our reported value of $0.89^{+0.05}_{-0.04}$ $M_\odot$.

WDS 16584+3943=COU1289: Ours is the first combined orbit for this system. Piccotti et al. (2020) obtained an orbital parallax of 9.00 ± 0.30 mas, slightly smaller than ours (but within 1σ) , and more in line with the Gaia eDR3 value. Their individual masses are also within 1σ with ours, but our formal errors are much smaller. No new observations were incorporated into our solution, just the data used in the original visual orbit by Docobo & Ling (2013), and the spectroscopic orbit from Griffin (2003). The differences in uncertainty with respect to the Piccotti result are likely a consequence of the better performance of the self-consistent simultaneous combined fit. Given the small errors of both the Gaia parallax and our orbital parallax, the difference of 0.36 mas seems uncomfortably large (see Figure 2.4). Note that the RV curve covers the range 0.9-1.1 in phase with no data at intermediate phases, while almost the opposite happens in the case of the astrometric curve, which may be the culprit for a somewhat uncertain orbital parallax. If we assume the primary is a G0V, its M_V is +4.40 (Abushattal et al. (2020), their Table 18), which for the Gaia parallax (see Table 2.4) implies a primary $V = 9.64$. If we assume a nearly equal-mass system, consistent with our results given in Table 2.4, and with $\Delta V = 0$ reported by WDS, then the system's magnitude would be $V = 8.88$, which is significantly fainter than the magnitude predicted by WDS (7.65 mag) and also fainter than the Hipparcos measurement (8.09 mag). Incidentally, ASAS-SN reports $V = 8.52 \pm 0.094$, but this value is uncertain due to the bright limit at $V = 10$ of this survey. We have no explanation for this discrepancy on the photometry.

WDS 18384−0312=A88AB: This is the first combined orbit. It has a very tight fit with good orbital and phase coverage. Our results are in agreement with those from Malkov et al. (2012a) who obtained a dynamical mass for the pair of 2.42 ± 0.32 $M_\odot$. On the other hand, Griffin (2013b) obtained $m_{\rm A} \sin^3 i = 0.690 \pm 0.013$ and $m_{\rm B} \sin^3 i = 0.660 \pm 0.012$ $M_\odot$ from the RV alone, which, for our value of the inclination (see Table 2.3) implies masses of 1.75 and 1.15 $M_\odot$. The mass for the primary is significantly larger than ours (1.20 $M_\odot$), whereas the mass of the secondary is totally consistent with our result. Given the spectral type of the primary, F8V–F9V, the implied mass (Abushattal et al. (2020)) is 1.23-1.20 $M_\odot$, which coincides well with our value.

We note that since the last visual orbit published for this binary in 2013, eight new interferometric observations have been made: two on 2014.76 by Horch et al. (2015a) with the 4.3m Discovery Channel Telescope and six by us with HRCam@SOAR program, between 2015.50 and 2019.61.

As result, both the RV curve and the astrometric orbit are now very well sampled, and our orbital parameters and derived masses are tight. There is no Gaia parallax yet for this target, but our orbital parallax coincides within 1σ with the Hipparcos parallax. As was the case for A2983, the measured photometry seems at odds with its location on the H-R diagram (see Figure 2.5). As before, in Figure 2.6, we show the location it should have on the H-R diagram given its mass, together with the photometry in the inserted table. If we assume a typical age for disk stars of 5 Gyr, this location implies that it may be a slightly evolved system.

WDS 20102+4357=STT400: A first combined orbit was published by Pourbaix (2000). In our solution, we have included 12 new interferometric observations carried out in the

period 2000.20–2013.83 by various authors, which improved the orbital coverage. We note that the orbit is not yet complete because of the period, which is nearly 85 years. At this point, the combined solution is limited mostly by the small phase coverage in the RV curve. Piccotti et al. (2020) gave 17.8 ± 1.3 mas for the orbital parallax and masses of 1.24 ± 0.38 and 0.96 ± 0.26 $M_\odot$, similar to our values. There are spectral types for both the primary (G3V–G4V) and secondary (G8V), indicating a mass of 1.07-1.06±0.04 $M_\odot$ (Abushattal et al. (2020)), that compare well with our values within our rather large mass uncertainties of 0.1-0.2 $M_\odot$ for this system.

WDS 20205+4351=IOT2Aa,Ab: We selected this interesting target because of its small, and hence uncertain, trigonometric parallax (even for Gaia). On the other hand, in principle, our orbital parallaxes are distance-independent. The O-type + WR pair has been studied by Monnier et al. (2011), who derived masses of 35.9 ± 1.3 and 14.9 ± 0.5 $M_\odot$, for a distance of 1.76 ± 0.03 kpc, i.e., a parallax of 0.57 ± 0.01 mas. The latest Gaia eDR3 parallax is 0.538 ± 0.069 mas (see Table 2.4), consistent within 1.5σ with the Monnier et al. (2011) value. Our estimated orbital parallax is larger than the previous values, implying smaller component masses of 20.5 ± 3.2 and 8.4 ± 1.6 $M_\odot$. The precision on our orbital parallax is, however, a factor of two worse than that from Gaia (see Figure 2.4), probably due to the combination of the rather poor orbital coverage with the noisy RV of the early-type stars involved[29]. Scaling our parallax to that of Monnier et al. (2011) would imply masses of 36.5 and 15.0 $M_\odot$, more in line with their results. Unfortunately, our attempt to use this system as a test case for the orbital parallaxes is not conclusive, not due to a fundamental limitation of our methodology but rather to the limited coverage and the quality of the observational data.

WDS 20527+4607=A750: Ours is the first combined orbit. The visual orbit only encompasses about 50 % of the orbit, but the combined solution looks solid, with small uncertainties. Our orbital parallax coincides within 1σ with the Gaia eDR3 result, while the individual component masses have a 4 % uncertainty. We have obtained 1.08 ± 0.05 $M_\odot$ for the mass of the primary, which coincides reasonably well with that predicted by Abushattal et al. (2020) from the G8V spectral type of the primary (0.96 ± 0.04 $M_\odot$).

WDS 23485+2539=DSG8: Ours is the first fully self-consistent orbit. Horch et al. (2019b) provided orbital elements by fitting the RV curve independently from the visual orbit obtained using Tokovinin's ORBIT code (see Table 5 on Horch et al. (2019b)). They obtained an orbital parallax 14.3 ± 0.4 mas, similar to our value, and likewise with the masses that have very small uncertainties. At ∼F5V, the WDS spectral types of the primary and secondary imply a large mass of 1.35$M_\odot$, (Abushattal et al. (2020)). SIMBAD gives a spectral type of F2IV–V, indicating even larger masses. This discrepancy is probably due to the low metallicity of the system ([Fe/H]=−0.46) which makes the spectral type of the system seem earlier than it really is.

[29] See the RV fits on http://www.das.uchile.cl/~rmendez/B_Research/JAA-RAM-SB2/

2.6. Conclusions

We have done a thorough search of the Sixth Catalog of Orbits of Visual Binary Stars (Orb6, Mason et al. (2001)) and the 9th Catalog of Spectroscopic Binary Orbits (SB9, Pourbaix et al. (2004)) looking for double-line spectroscopic binaries lacking a published combined visual and spectroscopic orbit. We found eight systems which met this condition: WDS00352−0336=HO212AB, WDS02128−0224=TOK39Aa,Ab, WDS11560+3520=CHR258, WDS15282−0921=BAG25Aa,Ab, WDS16584+3943=COU1289, WDS18384−0312=A88AB, WDS20527+4607=A750, and WDS23485+2539=DSG8. One of these pairs, TOK39Aa,Ab, also did not have a visual orbit.

Using an MCMC code developed by our group, we carried out dynamically self-consistent simultaneous fits to the data, obtaining orbital elements, individual component masses, and orbital parallaxes. A comparison of our orbital parallaxes with trigonometric parallaxes from Hipparcos and Gaia shows a generally good agreement.

We also computed joint solutions for six comparison binaries: WDS04107-0452=A2801, WDS 04184+2135=MCA14Aa,Ab, WDS07518−1354=BU101, WDS14492+1013=A2983, WDS20102+4357= STT400, and WDS20205+4351=IOT2Aa,Ab. Even in these cases, we could improve the previous orbits by adding recent data from our speckle survey of binaries being carried out with HRCam@SOAR and ZORRO@GS.

The mass ratios could be determined in the best cases with less than 1 % uncertainty, while the uncertainty on the mass sum is about 1 %. The formal uncertainty of the best individual component masses that we could determine is $0.01 M_{\odot}$. We have placed those objects that have individual component photometry on an H-R diagram to compare their location in relation to various theoretical isochrones and an empirical ZAMS. We also provide a detailed discussion of our results on an object-by-object basis.

Chapter 3

Mass ratio of single-line spectroscopic binaries with visual orbits using Bayesian inference and suitable priors

3.1. Introduction

Spectroscopic binaries are powerful astrophysical laboratories. Combining precise astrometric and RV measurements for these systems it is possible to obtain a fairly complete characterization of their orbital and basic astrophysical parameters. Among them, two groups are distinguished: double-line spectroscopic binaries, in whose spectra the spectral lines of both components are distinguished, and single-line spectroscopic binaries, for which only the lines of the primary component are easily recognized.

$SB2$ are certainly the most interesting systems because in their case a joint treatment of the atrometric and RV data allows to determine directly the individual component masses (Anguita-Aguero et al. (2022)), as well as a parallax -free distance- allowing an independent assessment of Gaia's trigonometric parallaxes (Pourbaix (2000), Mason (2015)).

Unfortunately, for $SB1s$ -which are the majority (67 %) of the systems included in the 9th Catalog of Spectroscopic Binary Orbits[30], Pourbaix et al. (2004), SB9, only the mass function can be obtained directly[31] (Struve & Huang (1958)). For this reason, in the past this latter group has not been fully exploited.

Now, thanks to a newly developed Bayesian methodology based on the MCMC algorithm, No-U-Turn Sampler (NUTS, Videla et al. (2022)) to address the orbital parameters inference problem in $SB1$ systems, including an estimation of the individual component masses, this situation is rapidly changing. This scheme also provides a precise characterization of the uncertainty of the estimates of the orbital parameters, in the form of joint posterior probability distribution function.

In this approach, the lack of an RV curve for the secondary star is managed incorporating suitable prior distributions for two critical parameters of the system; namely its trigonometric parallax (from an external source), and the mass of the primary component, estimated from its Spectral Type (hereafter SpTy). This methodology has been thoroughly tested on several benchmark $SB2$ systems by Videla et al. (2022), who provide an exhaustive analysis of the

[30] Updated regularly, and available at https://sb9.astro.ulb.ac.be/.

[31] The mass function is defined by $f(M) = \frac{(m_2 \sin i)^3}{(m_1+m_2)^2}$, where m_1 and m_2 are the mass of the primary and secondary stars respectively

results obtained by comparing the PDFs from different observational sources and priors. In that paper we were able to show that this Bayesian approach allows a much richer and complete understanding of the associated uncertainties in the study of binary systems in general.

Here we apply this methodology to twenty two $SB1$ systems, nine of which (HIP # 29860, 36497, 38414, 40167, 54061, 76031, 93017, 96302, and 116259) up to now did not have a published self-consistent spectroscopic/astrometric joint orbital solution.

3.2. The *SB1* sample

To select the sample for the present work, we started by doing a cross-match between Orb6 and SB9.

Orb6 is the most comprehensive catalog of binary systems with published orbital elements, while SB9 contains RV amplitudes for all binary systems for which it has been possible to fit a RV curve. Having identified those systems confirmed as $SB1$ in SB9, we pinpointed the binaries for which a combined astrometric/RV study of the orbit was not available in the literature by means of the notes and comments given in Orb6 and SB9, or which merit further study given new available data. This lead to an initial working list of thirty six binary systems.

For the systems selected as indicated above, we retrieved their RV data from SB9, or from references provided therein; and the astrometric data from the US Naval Observatory Fourth Catalog of Interferometric Measurements of Binary Stars[32] and from historical astrometry included in the Washington Double Star Catalog effort (Mason et al. (2001), kindly provided to us by Dr.Brian Mason from the US Naval Observatory).

Finally, we included recent results obtained with the HRCam Speckle camera on the SOAR 4.1m telescope at Cerro Pachón[33], as part of our monitoring of Southern binaries described in Mendez et al. (2017). We note that some of these measurements have been secured after the publication of their last orbit, which allows for an improvement of the orbital solutions. We have also supplemented the published RV with our own recent observations secured with the FEROS Echelle (Kaufer et al., 1999) high-resolution spectrograph on the 2.2m MPG telescope[34], and the FIDEOS Echelle (Vanzi et al., 2018) on the 1m telescope[35], both operating at the ESO/La Silla Observatory, Chile. FEROS and FIDEOS spectra were reduced using the CERES pipeline (Brahm et al., 2017). In a couple of cases we also found high-precision RV archival data for our binaries obtained during the planet-monitoring program being carried out with HARPS (Mayor et al., 2003) on the 3.6m telescope at ESO/La Silla[36]. This added valuable and highly precise points to the RV curve.

Examination of the information collected showed that only thirty four of the systems in our starting list had sufficient data to warrant further analysis. Out of this final working list, twelve $SB1$ systems were presented and studied in Videla et al. (2022), while the remaining twenty-two are included in the present paper. We must emphasize that, as a result of our selection process, our final sample is very heterogeneous and it should not be considered

[32] The latest version, called int4, is available at https://www.usno.navy.mil/USNO/astrometry/optical-IR-prod/wds/int4/fourth-catalog-of-interferometric-measurements-of-binary-stars
[33] For up-to-date details of the instrument see http://www.ctio.noao.edu/~atokovin/speckle/
[34] See https://www.eso.org/sci/facilities/lasilla/instruments/feros.html
[35] See https://www.eso.org/public/teles-instr/lasilla/1metre/fideos/
[36] See https://www.eso.org/sci/facilities/lasilla/instruments/harps.html

complete or representative of $SB1$ systems in any astrophysical sense. From this point of view, the main contribution of this paper is the addition of new orbits and mass ratios for this type of binaries, nine of which do not have a published joint estimation of their orbital parameters (to the best of our knowledge, ours is therefore the first combined orbit).

Table 3.1 presents basic properties available in the literature for the sample studied in this work. The first two columns present the Hipparcos number and the discovery designation code assigned in the WDS Catalog. The following columns present the trigonometric parallax adopted as prior, the RUWE (Reduced Unit Weight Error - an indication of the reliability of the parallax) parameter as given in the Gaia catalogue, the SpTy adopted for the primary component (from SIMBAD, Wenger et al. (2000), WDS, or our own estimate - as explained below), and the mass of the primary component implied by the SpTy.

The masses have been derived from the mass versus SpTy and mass versus luminosity class calibrations, provided by Abushattal et al. (2020) or, if not available there, from Straizys & Kuriliene (1981). The dispersion in mass comes from assuming a SpTy uncertainty of $\pm$ one sub-type, which is customary in spectral classification. As it can be seen from this table, and mentioned above, our $SB1s$ represent an heterogeneous group of binaries, with masses in the range between $0.4M_{\odot}$ to slightly above $6M_{\odot}$, located at distances between 7 to 263 pc. Also, as we shall see in the following Sections, the data quality and orbital phase coverage available for the sample is quite varied.

Regarding the trigonometric parallaxes used as priors, and indicated in the third column of Table 3.1, we note that for unresolved binary systems (separations smaller than about 0.7 arcsec) and multiple systems, the Gaia solution can be compromised by acceleration and/or unresolved companions because the current astrometric reductions assume single stars. The RUWE parameter given in the fourth column of this table highlights excessive astrometric noise, helping to identify suspicious astrometry (mainly those with RUWE > 2.0; see, e.g., Tokovinin (2022)). Accordingly, as can be seen in this table, most (but not all) of the systems studied here indeed have a high RUWE. This is an important issue that must be considered when analyzing the results for individual objects, and the consistency between the different solutions.

To assign the SpTy to the primary components, listed in column five of Table 3.1, we consulted SIMBAD, the WDS catalog itself, and the Catalogue of Stellar Spectral Classifications by Skiff (2014), which provides a compilation of spectral classifications determined from spectral data alone (i.e., no narrow-band photometry), and which is updated regularly in VizieR (catalog B/mk/mktypes, currently containing more than 90.000 stars).

A comparison of the data from these three sources revealed that some objects in our sample have somewhat ambiguous SpTy. In order to resolve these ambiguities, we computed the absolute magnitude of the primary component using the trigonometric parallax of the system listed in Table 3.1 and their apparent magnitudes given in the WDS catalogue. This absolute magnitude was then compared with the absolute magnitude expected from the listed SpTy, using the calibrations provided by Abushattal et al. (2020)). The SpTy closest to the computed absolute magnitude was finally adopted. We note that some ambiguities in the SpTy persisted after these calculations (see Section 3.4).

Table 3.1: Trigonometric parallax, SpTy (primary component) and mass (primary component) of the $SB1$ stellar systems presented in this paper. See text for details.

HIP #	Discovery Designation	ϖ^a [mas]	RUWE^a	SpTy^b	$m_1{}^c$ [$M_\odot$]
3850	PES1	53.053 ± 0.028	0.9325	G9V^f	0.93 ± 0.04
5336	WCK1Aa,Ab	130.29 ± 0.44	6.9658	G5V	1.05 ± 0.04
17491	BAG8AB	40.33 ± 0.25	11.5927	K0V	0.89 ± 0.04
28691	MCA24	3.82 ± 0.25	2.5179	B8III	4.26 ± 1.15
29860	CAT1Aa,Ab	51.62 ± 0.12	1.9793	F9V/G0V^f	1.175 ± 0.025
36497	TOK392Da,Db	21.19 ± 0.18	5.8032	F8V	1.23 ± 0.05
38414	TOK195	8.98 ± 0.23	6.0363	K1/2II^f	6.09 ± 0.07^g
39261	MCA33	10.24 ± 0.22	5.8681	A2V/A3V^f	2.32 ± 0.08
40167	HUT1Ca,Cb	40.89 ± 0.15	1.3840	F8V	1.23 ± 0.05
43109	SP1AB	26.437 ± 0.098	1.4190	G1III	1.02 ± 0.20
54061	BU1077AB	26.54 ± 0.48^d	–	G9III	1.93 ± 0.26
55642	STF1536AB	$41.93 \pm 0.43^{e,h}$	–	F4IV	1.380 ± 0.035
67620	WSI77	53.88 ± 0.34^e	–	G5V	1.05 ± 0.04
75695	JEF1	29.17 ± 0.76^d	7.2964	A5V	2.00 ± 0.06
76031	TOK48	19.67 ± 0.89^d	–	G0V	1.15 ± 0.04
78727	STF1998AB	35.89 ± 0.23^i	1.2934	F5IV	1.350 ± 0.025
93017	BU648AB	67.14 ± 0.12	2.7280	F9V/G0V^f	1.175 ± 0.025
96302	WRH32	5.37 ± 0.10	1.5265	G8III	1.87 ± 0.26
103655	KUI103	66.554 ± 0.072	5.2017	M2V	0.43 ± 0.02
111685	HDS3211AB	51.2 ± 1.6^d	31.988	M0V	0.54 ± 0.02
111974	HO296AB	29.59 ± 0.68^d	–	G4V	1.06 ± 0.04
116259	HDS3356	29.23 ± 0.15	8.0906	G0V	1.15 ± 0.04

[a] From GAIA DR3 except when noted
[b] From SIMBAD, WDS or from our own estimate, see text for details
[c] From Abushattal et al. (2020) except when noted
[d] From HIPPARCOS
[e] From GAIA DR2
[f] Adopted the mean spectral type
[g] From Straizys & Kuriliene (1981)
[h] Average of Gaia DR2 parallaxes for AB and C components
[i] Average of Gaia DR3 parallaxes for AB and C components

3.3. Orbital elements and mass ratios

To determine the orbital parameters, we followed the scheme presented in detail in Videla et al. (2022). In summary, for each object, we are able to compute four orbital solutions, namely: one using no priors as in classical works, denoted as $SB1$ solution; one using the trigonometric parallax as a prior, denoted $SB1 + p(\varpi)$ solution; one using the mass of the primary as a prior, denoted $SB1 + p(m_1|\theta)$ solution; and finally, a combined solution using parallax and mass as priors simultaneously, denoted $SB1 + p(\varpi) + p(m_1|\theta)$. These solutions are presented in Table 3.2. For reference, in the first two lines of each entry we also present the orbital parameters given in Orb6 and SB9.

For each of our solutions, we provide the orbital elements obtained from the Maximum A-Posteriori estimation (MAP), which gives the most probable sample of the PDF, as well as the upper and lower values that encompass the 95 % credible interval around the MAP solution (denoted HDPI, for High Density Posterior Interval and which encompasses the mode).

Of course, as explained in detail in Videla et al. (2022), only solutions that include a prior can lead to an estimation of the orbital parallax and the mass ratio, which are presented in the last columns of Table 3.2. We must note that the inferred parallaxes reported in this table cannot be properly called orbital parallaxes in the classical sense (as in the case of $SB2$ systems), because, while they have been derived self-consistently from the model and data, they are only resolvable by the incorporation of the priors. Nevertheless, throughout this paper we will still refer to these as orbital parallaxes, to differentiate them from the trigonometric parallax adopted as prior. A plot of our MAP (pseudo) orbital parallaxes (from Table 3.2) versus the adopted prior parallax from Table 3.1 is shown in Figure 3.1, which exhibits a general good agreement between them, with a global rms of 0.97 mas over our 22 objects. In the right panel on Figure 3.1 the residuals have been normalized by the overall parallax uncertainty, which includes the uncertainty in the adopted parallax added in quadrature to the uncertainty of our estimated parallax.

A look at the results on Table 3.2 shows that our values for the orbital elements in general coincide quite well with those from previous studies. In particular, it is well known that periapsis can only be well-determined by RV measurements as long as the distinction between primary and secondary is unambiguous (which is difficult, e.g., for equal-mass binaries); and the table shows our values are indeed quite close to those from SB9, but with smaller uncertainties in our case[37].

On the other hand, the longitude of the ascending node can be well determined from astrometric observations alone, but it is ambiguous in the case of equal-brightness binaries; and, additionally, it is subject to an ambiguity of $\pm 180°$, in which case the ω value is also affected by the same ambiguity (see Equation (28) in Appendix B.2 of Mendez et al. (2017)).

This is clearly seen on HIP 28691: subtracting 180° from Ω and ω on Orb6 gives SB9's and our values and on HIP 43109 and HIP 54061 where, now, adding 180° from Ω and ω on Orb6 gives SB9's and our values. Apart from these two cases, from the table we see that there is good correspondence between our values for Ω and those from Orb6 (but again with smaller formal uncertainties in our case, with a few exceptions). In terms of the other orbital elements, despite the fact that the sample is very heterogeneous, e.g., with periods ranging from 1.7 yr (HIP 76031) to 189 yrs (HIP 55642) and with semi-major axis from 25 mas

[37] Two notable cases where we maintain the ω value from Orb6, at odds with that reported from SB9 have indeed a $q \sim 1$, namely HIP 78727 and HIP 111974.

(HIP 96302) to 1.9 arcsec (HIP 55642) our solutions are, again, similar to those of previous studies, with the notable exception of HIP 29860, where a large difference is seen between our solution and previous studies. This case is further described below, and in Figures 3.9 and 3.10. More specific notes and comments on individual objects are given below, in Section 3.4.

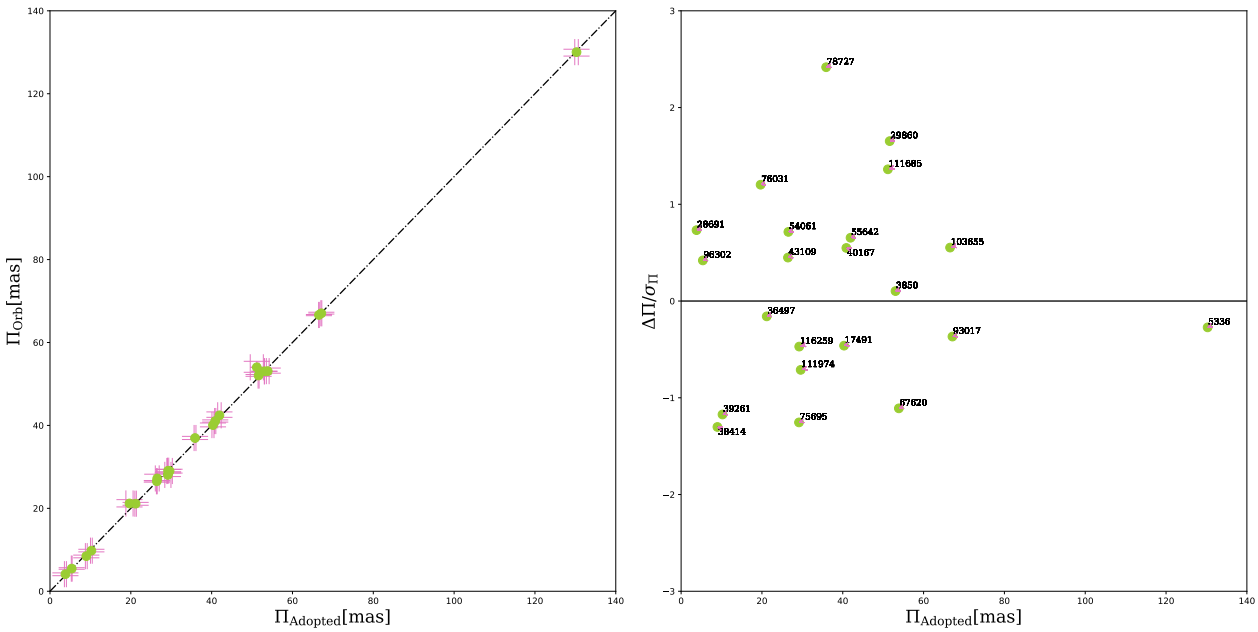

Figure 3.1: (pseudo) Orbital parallaxes from this work, versus the adopted prior parallax (left panel). In the right panel we show the residuals in the sense $\Pi_{\rm Orb} - \Pi_{\rm Adopted}$ normalized by the parallax uncertainty of each target (see text for details). The labels indicate the HIP number.

Table 3.2: MAP estimates and 95 % HDPIs derived from the marginal PDFs of the orbital parameters for the four orbital solutions, based on our astrometric data, discussed in the first paragraph of Section 3.3. m_1 and ϖ are the priors used for the mass of the primary component and the trigonometric parallax, respectively. In the first two lines (of six entries) for each $SB1$ system, we report the values provided by Orb6 and SB9, preserving the significant figures included in those catalogs as an indication of their precision (continued on next page)

HIP #	System	P [yr]	T [yr]	e	a [arcsec]	ω [°]	Ω [°]	i [°]	V_0 [km/s]	ϖ [mas]	f/ϖ^a [pc]	m_1 [$M_\odot$]	q
3850	Orb6	33.08 ± 0.70	1997.066 ± 0.0143	0.732 ± 0.0023	0.5199 ± 0.0512	266.90 ± 0.47	89.9 ± 1.4	46.3 ± 1.1	—	—	—	—	—
	SB9	31.74 ± 3.0626	2028.7857 ± 3.068	0.723 ± 0.013	—	-94.2 ± 1.6	—	—	$9.93 \pm Fixed$	—	—	—	—
	$SB1$	$41.235^{48.786}_{36.471}$	$2032.630^{2035.724}_{2030.426}$	$0.456^{0.524}_{0.363}$	$0.426^{0.451}_{0.410}$	$331.331^{344.740}_{318.163}$	$17.371^{32.777}_{2.360}$	$4.529^{15.426}_{0.380}$	$10.325^{10.574}_{10.162}$	—	$24.804^{173.460}_{3.693}$	—	—
	$SB1 + p(\varpi)$	$31.754^{35.091}_{29.581}$	$2029.636^{2032.741}_{2027.474}$	$0.758^{0.774}_{0.737}$	$0.543^{0.624}_{0.483}$	$263.688^{267.484}_{262.780}$	$94.955^{103.084}_{84.513}$	$50.298^{58.591}_{43.456}$	$9.918^{9.962}_{9.880}$	$53.057^{53.106}_{52.999}$	$1.155^{1.327}_{1.001}$	$1.001^{1.251}_{0.777}$	$0.065^{0.076}_{0.056}$
	$SB1 + p(m_1\|\theta)$	$39.291^{49.103}_{36.457}$	$2031.769^{2035.702}_{2030.320}$	$0.480^{0.525}_{0.349}$	$0.421^{0.456}_{0.410}$	$326.008^{344.392}_{318.748}$	$22.870^{29.713}_{0.017}$	$7.705^{19.077}_{4.913}$	$10.262^{10.600}_{10.171}$	$31.556^{34.916}_{27.870}$	$12.609^{17.658}_{6.263}$	$0.926^{1.003}_{0.848}$	$0.661^{1.000}_{0.296}$
	$SB1 + p(\varpi) + p(m_1\|\theta)$	$31.305^{32.926}_{29.895}$	$2029.210^{2030.483}_{2028.028}$	$0.753^{0.762}_{0.742}$	$0.528^{0.555}_{0.503}$	$263.981^{266.640}_{263.004}$	$93.501^{96.745}_{86.936}$	$48.460^{51.757}_{45.311}$	$9.926^{9.951}_{9.908}$	$53.059^{53.107}_{52.996}$	$1.189^{1.297}_{1.115}$	$0.941^{1.012}_{0.864}$	$0.067^{0.074}_{0.063}$
5336	Orb6	21.568 ± 0.015	1997.2235 ± 0.0067	0.5885 ± 0.0011	0.9985 ± 0.0013	330.37 ± 0.18	223.868 ± 0.064	110.671 ± 0.064	—	—	—	—	—
	SB9	21.4 ± 0.11	1975.901 ± 0.1	0.53 ± 0.02	—	150.0 ± 3.4	—	—	-97.35 ± 0.04	—	—	—	—
	$SB1$	$21.289^{21.317}_{21.250}$	$1997.358^{1997.434}_{1997.279}$	$0.558^{0.565}_{0.551}$	$1.029^{1.035}_{1.023}$	$151.763^{153.274}_{150.371}$	$45.581^{46.037}_{45.202}$	$107.723^{107.953}_{107.483}$	$-97.413^{-97.287}_{-97.526}$	—	$1.322^{1.436}_{1.233}$	—	—
	$SB1 + p(\varpi)$	$21.290^{21.319}_{21.251}$	$1997.360^{1997.433}_{1997.278}$	$0.558^{0.565}_{0.552}$	$1.028^{1.035}_{1.023}$	$151.854^{153.306}_{150.354}$	$45.604^{46.053}_{45.202}$	$107.723^{107.941}_{107.472}$	$-97.371^{-97.281}_{-97.519}$	$130.343^{131.162}_{129.468}$	$1.371^{1.445}_{1.246}$	$0.889^{0.927}_{0.868}$	$0.218^{0.232}_{0.193}$
	$SB1 + p(m_1\|\theta)$	$21.280^{21.316}_{21.251}$	$1997.347^{1997.429}_{1997.276}$	$0.558^{0.565}_{0.552}$	$1.029^{1.035}_{1.023}$	$151.683^{153.196}_{150.304}$	$45.599^{46.031}_{45.201}$	$107.745^{107.948}_{107.474}$	$-97.397^{-97.286}_{-97.520}$	$124.211^{127.363}_{121.247}$	$1.360^{1.444}_{1.239}$	$1.043^{1.123}_{0.966}$	$0.203^{0.218}_{0.182}$
	$SB1 + p(\varpi) + p(m_1\|\theta)$	$21.282^{21.312}_{21.246}$	$1997.335^{1997.417}_{1997.261}$	$0.558^{0.565}_{0.551}$	$1.032^{1.037}_{1.025}$	$151.388^{152.982}_{150.040}$	$45.502^{45.973}_{45.125}$	$107.667^{107.889}_{107.411}$	$-97.454^{-97.301}_{-97.542}$	$130.034^{130.732}_{129.081}$	$1.271^{1.412}_{1.210}$	$0.921^{0.946}_{0.889}$	$0.198^{0.224}_{0.186}$
17491	Orb6	13.877 ± 0.016	1992.092 ± 0.016	0.2764 ± 0.003	0.2574 ± 0.0046	74.85 ± 0.25	281.1 ± 1.0	101.37 ± 0.12	—	—	—	—	—
	SB9	14.021 ± 0.123	1992.039 ± 0.070	0.275 ± 0.010	—	72.30 ± 2.16	—	—	22.238 ± 0.044	—	—	—	—
	$SB1$	$13.762^{13.897}_{13.658}$	$1992.017^{1992.111}_{1991.916}$	$0.263^{0.280}_{0.247}$	$0.254^{0.258}_{0.249}$	$72.003^{74.567}_{69.482}$	$281.083^{281.991}_{279.943}$	$101.987^{102.718}_{101.148}$	$22.312^{22.390}_{22.183}$	—	$10.330^{10.708}_{9.979}$	—	—
	$SB1 + p(\varpi)$	$13.767^{13.897}_{13.656}$	$1992.012^{1992.108}_{1991.910}$	$0.265^{0.281}_{0.248}$	$0.253^{0.258}_{0.249}$	$71.985^{74.497}_{69.425}$	$280.834^{281.952}_{279.916}$	$102.018^{102.723}_{101.168}$	$22.288^{22.384}_{22.175}$	$40.215^{40.800}_{39.819}$	$10.296^{10.750}_{10.019}$	$0.773^{0.827}_{0.698}$	$0.707^{0.764}_{0.672}$
	$SB1 + p(m_1\|\theta)$	$13.801^{13.897}_{13.653}$	$1992.020^{1992.113}_{1991.918}$	$0.264^{0.280}_{0.247}$	$0.253^{0.258}_{0.249}$	$72.409^{74.630}_{69.625}$	$281.113^{281.932}_{279.850}$	$101.778^{102.680}_{101.141}$	$22.306^{22.387}_{22.179}$	$38.620^{39.907}_{37.553}$	$10.395^{10.728}_{10.001}$	$0.884^{0.965}_{0.809}$	$0.671^{0.707}_{0.633}$
	$SB1 + p(\varpi) + p(m_1\|\theta)$	$13.721^{13.879}_{13.638}$	$1992.035^{1992.126}_{1991.933}$	$0.274^{0.286}_{0.254}$	$0.257^{0.260}_{0.252}$	$72.234^{74.703}_{69.683}$	$280.936^{281.963}_{279.929}$	$101.624^{102.474}_{100.973}$	$22.267^{22.384}_{22.173}$	$40.081^{40.591}_{39.651}$	$10.117^{10.461}_{9.833}$	$0.828^{0.869}_{0.766}$	$0.682^{0.724}_{0.652}$
28691	Orb6	13.061 ± 0.03	2006.52 ± 0.16	0.808 ± 0.045	0.0555 ± 0.0022	291.5 ± 9.2	224.4 ± 3.3	111.8 ± 7.8	—	—	—	—	—
	SB9	12.98 ± 0.014	1980.807 ± 0.015	0.7407 ± 0.0042	—	125.30 ± 0.71	—	—	12.607 ± 0.052	—	—	—	—
	$SB1$	$13.012^{13.040}_{12.975}$	$1928.728^{1928.917}_{1928.590}$	$0.739^{0.747}_{0.730}$	$0.046^{0.048}_{0.044}$	$125.335^{126.837}_{124.013}$	$51.094^{55.451}_{47.951}$	$116.340^{122.285}_{110.006}$	$12.607^{12.710}_{12.491}$	—	$86.624^{94.033}_{79.458}$	—	—
	$SB1 + p(\varpi)$	$13.006^{13.040}_{12.977}$	$1928.760^{1928.906}_{1928.588}$	$0.737^{0.747}_{0.730}$	$0.046^{0.048}_{0.044}$	$125.758^{126.881}_{123.964}$	$52.315^{55.542}_{48.112}$	$116.431^{122.709}_{110.387}$	$12.580^{12.708}_{12.489}$	$3.867^{4.316}_{3.333}$	$86.960^{94.938}_{79.925}$	$6.543^{10.555}_{3.917}$	$0.507^{0.623}_{0.391}$
	$SB1 + p(m_1\|\theta)$	$13.009^{13.041}_{12.976}$	$1928.749^{1928.916}_{1928.593}$	$0.737^{0.747}_{0.730}$	$0.046^{0.048}_{0.044}$	$125.603^{126.919}_{124.043}$	$52.137^{55.530}_{48.022}$	$116.018^{122.700}_{110.283}$	$12.632^{12.708}_{12.491}$	$4.246^{5.528}_{3.853}$	$86.694^{94.788}_{79.729}$	$4.727^{5.790}_{1.497}$	$0.582^{0.901}_{0.493}$
	$SB1 + p(\varpi) + p(m_1\|\theta)$	$13.013^{13.043}_{12.979}$	$1928.727^{1928.905}_{1928.584}$	$0.738^{0.748}_{0.730}$	$0.046^{0.047}_{0.044}$	$125.530^{126.928}_{124.055}$	$51.655^{54.833}_{47.300}$	$116.000^{123.755}_{111.186}$	$12.606^{12.706}_{12.487}$	$4.122^{4.433}_{3.756}$	$85.971^{96.688}_{81.065}$	$5.334^{6.887}_{3.785}$	$0.549^{0.665}_{0.477}$
29860	Orb6	35.52	1998.057	0.809	0.648	76.0	166.8	41.3	—	—	—	—	—
	SB9	34.20 ± 0.234	1998.050 ± 0.0013	0.8045 ± 0.0009	—	75.21 ± 0.15	—	—	$-10.035 \pm Fixed$	—	—	—	—
	$SB1$	$43.460^{43.599}_{43.291}$	$1998.081^{1998.082}_{1998.080}$	$0.832^{0.833}_{0.832}$	$0.812^{0.816}_{0.805}$	$78.987^{79.100}_{78.865}$	$175.300^{175.519}_{174.989}$	$55.033^{55.359}_{54.595}$	$9.560^{9.564}_{9.555}$	—	$5.197^{5.258}_{5.150}$	—	—
	$SB1 + p(\varpi)$	$43.423^{43.590}_{43.284}$	$1998.081^{1998.082}_{1998.080}$	$0.832^{0.833}_{0.832}$	$0.810^{0.816}_{0.805}$	$78.957^{79.097}_{78.871}$	$175.284^{175.519}_{174.994}$	$54.944^{55.340}_{54.568}$	$9.558^{9.564}_{9.555}$	$51.674^{51.858}_{51.375}$	$5.209^{5.263}_{5.153}$	$1.492^{1.541}_{1.460}$	$0.368^{0.373}_{0.362}$
	$SB1 + p(m_1\|\theta)$	$43.430^{43.588}_{43.287}$	$1998.081^{1998.082}_{1998.080}$	$0.832^{0.833}_{0.832}$	$0.810^{0.816}_{0.805}$	$78.981^{79.101}_{78.870}$	$175.239^{175.514}_{175.004}$	$54.951^{55.359}_{54.619}$	$9.559^{9.564}_{9.555}$	$55.356^{56.245}_{54.733}$	$5.210^{5.256}_{5.150}$	$1.182^{1.222}_{1.124}$	$0.405^{0.414}_{0.399}$
	$SB1 + p(\varpi) + p(m_1\|\theta)$	$43.337^{43.491}_{43.190}$	$1998.080^{1998.082}_{1998.079}$	$0.832^{0.832}_{0.832}$	$0.797^{0.802}_{0.792}$	$78.879^{79.008}_{78.778}$	$174.749^{174.962}_{174.475}$	$54.046^{54.367}_{53.674}$	$9.556^{9.561}_{9.552}$	$52.035^{52.285}_{51.843}$	$5.347^{5.399}_{5.299}$	$1.380^{1.407}_{1.349}$	$0.386^{0.391}_{0.381}$
36497	Orb6	7.621	2019.554	0.692	0.102	271.8	183.6	40.4	—	—	—	—	—
	SB9	7.415 ± 0.090	1981.605 ± 0.078	0.716 ± 0.098	—	263.19 ± 5.24	—	—	-2.379 ± 0.094	—	—	—	—
	$SB1$	$7.645^{7.675}_{7.607}$	$1981.398^{1981.495}_{1981.321}$	$0.643^{0.666}_{0.616}$	$0.093^{0.096}_{0.089}$	$265.146^{271.781}_{257.952}$	$192.723^{201.801}_{183.966}$	$32.491^{37.315}_{26.094}$	$-2.496^{-2.282}_{-2.648}$	—	$16.175^{20.638}_{13.290}$	—	—
	$SB1 + p(\varpi)$	$7.641^{7.675}_{7.604}$	$1981.406^{1981.497}_{1981.316}$	$0.642^{0.664}_{0.615}$	$0.092^{0.096}_{0.089}$	$264.965^{272.062}_{257.607}$	$192.611^{202.298}_{183.832}$	$31.683^{36.548}_{25.101}$	$-2.455^{-2.284}_{-2.658}$	$21.172^{21.531}_{20.827}$	$16.823^{21.304}_{13.633}$	$0.913^{1.113}_{0.666}$	$0.553^{0.812}_{0.398}$
	$SB1 + p(m_1\|\theta)$	$7.644^{7.677}_{7.607}$	$1981.408^{1981.495}_{1981.319}$	$0.639^{0.664}_{0.614}$	$0.092^{0.096}_{0.088}$	$264.960^{271.764}_{257.353}$	$192.895^{201.661}_{183.302}$	$30.794^{36.855}_{25.422}$	$-2.500^{-2.286}_{-2.659}$	$19.281^{20.734}_{18.047}$	$17.167^{21.408}_{13.716}$	$1.244^{1.324}_{1.131}$	$0.495^{0.641}_{0.395}$
	$SB1 + p(\varpi) + p(m_1\|\theta)$	$7.632^{7.671}_{7.593}$	$1981.442^{1981.516}_{1981.358}$	$0.667^{0.684}_{0.649}$	$0.097^{0.099}_{0.095}$	$269.173^{274.364}_{263.164}$	$188.173^{196.820}_{179.813}$	$37.459^{39.810}_{34.716}$	$-2.426^{-2.258}_{-2.628}$	$21.123^{21.437}_{20.742}$	$13.386^{14.964}_{12.482}$	$1.200^{1.280}_{1.090}$	$0.394^{0.454}_{0.357}$
38414	Orb6	7.388 ± 0.657	2012.067 ± 0.206	0.380 ± 0.000	0.0624 ± 0.0071	170.0 ± 0.0	90.3 ± 6.8	86.2 ± 7.0	—	—	—	—	—
	SB9	6.9925	1905.51	0.38	—	170.	—	—	25.4	—	—	—	—
	$SB1$	$7.164^{7.224}_{7.114}$	$1984.310^{1984.537}_{1984.013}$	$0.553^{0.607}_{0.514}$	$0.055^{0.058}_{0.052}$	$204.818^{206.700}_{201.670}$	$89.931^{91.375}_{87.866}$	$75.422^{79.633}_{70.695}$	$7.337^{11.816}_{3.593}$	—	$185.367^{199.997}_{169.270}$	—	—
	$SB1 + p(\varpi)$	$7.586^{7.621}_{7.540}$	$1982.410^{1982.601}_{1982.273}$	$0.662^{0.724}_{0.625}$	$0.050^{0.052}_{0.047}$	$196.810^{201.030}_{192.150}$	$90.324^{92.329}_{88.135}$	$69.065^{74.513}_{61.549}$	$28.029^{29.008}_{26.712}$	$8.881^{9.413}_{8.520}$	$47.008^{57.014}_{41.607}$	$1.754^{1.995}_{1.212}$	$0.717^{1.000}_{0.615}$
	$SB1 + p(m_1\|\theta)$	$7.540^{7.606}_{7.441}$	$1982.637^{1983.057}_{1982.338}$	$0.672^{0.720}_{0.603}$	$0.050^{0.052}_{0.047}$	$198.631^{203.585}_{193.964}$	$89.770^{91.707}_{87.448}$	$68.068^{75.024}_{61.720}$	$26.403^{28.469}_{23.047}$	$6.011^{6.328}_{5.487}$	$64.513^{89.141}_{46.083}$	$6.058^{6.232}_{5.960}$	$0.632^{1.000}_{0.416}$
	$SB1 + p(\varpi) + p(m_1\|\theta)$	$6.130^{6.161}_{6.097}$	$1981.852^{1982.007}_{1981.756}$	$0.497^{0.540}_{0.477}$	$0.058^{0.059}_{0.055}$	$157.473^{163.057}_{154.046}$	$95.118^{97.683}_{92.935}$	$79.683^{82.481}_{75.663}$	$26.411^{27.129}_{25.879}$	$8.464^{8.722}_{8.066}$	$33.337^{37.271}_{30.043}$	$6.058^{6.208}_{5.933}$	$0.393^{0.444}_{0.345}$
39261	Orb6	6.6504 ± 0.0089	2001.2281 ± 0.025	0.706 ± 0.024	0.055 ± 0.018	8.3 ± 1.8	118.3 ± 20.1	55.4 ± 2.9	—	—	—	—	—
	SB9	6.6312 ± 0.0066	1934.781 ± 0.0392	0.718 ± 0.012	—	5.22 ± 1.64	—	—	-2.10 ± 0.14	—	—	—	—
	$SB1$	$6.626^{6.646}_{6.598}$	$1981.187^{1981.205}_{1981.171}$	$0.777^{0.795}_{0.753}$	$0.052^{0.054}_{0.050}$	$13.176^{16.252}_{10.426}$	$113.564^{116.311}_{110.904}$	$47.889^{56.542}_{39.145}$	$-1.781^{-1.552}_{-2.026}$	—	$45.872^{53.677}_{38.446}$	—	—
	$SB1 + p(\varpi)$	$6.629^{6.648}_{6.601}$	$1981.189^{1981.204}_{1981.171}$	$0.777^{0.794}_{0.754}$	$0.053^{0.054}_{0.051}$	$13.929^{16.182}_{10.397}$	$113.970^{116.396}_{111.158}$	$51.126^{55.723}_{43.281}$	$-1.763^{-1.541}_{-2.022}$	$10.128^{10.643}_{9.799}$	$42.696^{49.059}_{39.686}$	$1.800^{2.041}_{1.355}$	$0.762^{0.999}_{0.699}$
	$SB1 + p(m_1\|\theta)$	$6.627^{6.647}_{6.599}$	$1981.195^{1981.204}_{1981.170}$	$0.769^{0.795}_{0.752}$	$0.053^{0.054}_{0.050}$	$14.193^{15.980}_{10.157}$	$113.275^{116.235}_{110.844}$	$50.481^{55.789}_{39.031}$	$-1.721^{-1.552}_{-2.025}$	$9.534^{9.783}_{8.769}$	$42.654^{53.832}_{38.986}$	$2.300^{2.459}_{2.144}$	$0.685^{0.919}_{0.611}$
	$SB1 + p(\varpi) + p(m_1\|\theta)$	$6.635^{6.651}_{6.603}$	$1981.192^{1981.210}_{1981.174}$	$0.767^{0.784}_{0.744}$	$0.054^{0.055}_{0.052}$	$14.515^{17.334}_{11.403}$	$114.370^{116.627}_{111.651}$	$53.433^{58.896}_{47.021}$	$-1.761^{-1.509}_{-1.983}$	$9.790^{10.126}_{9.500}$	$40.589^{44.553}_{36.887}$	$2.265^{2.398}_{2.097}$	$0.659^{0.750}_{0.580}$

[a] The parameter f/ϖ, with units of pc, introduced in Videla et al. (2022), condenses the pair of parameters ϖ, q, since they are not determinable due to the absence of radial velocities for the secondary component as in the case of $SB2$ systems.

Table 3.3: Table 3.2 (contd.). MAP estimates and 95 % HDPIs derived from the marginal PDFs of the orbital parameters for the four orbital solutions, based on our astrometric data, discussed in the first paragraph of Section 3.3. m_1 and ϖ are the priors used for the mass of the primary component and the trigonometric parallax, respectively. In the first two lines (of six entries) for each $SB1$ system, we report the values provided by Orb6 and SB9, preserving the significant figures included in those catalogs as an indication of their precision (continued on next page)

HIP #	System	P [yr]	T [yr]	e	a [arcsec]	ω [°]	Ω [°]	i [°]	V_0 [km/s]	ϖ [mas]	f/ϖ [pc]	m_1 [$M_\odot$]	q
40167	Orb6	17.263 ± 0.032	1997.743 ± 0.160	0.180 ± 0.013	0.3592 ± 0.0058	287.3 ± 3.6	81.0 ± 1.9	150.0	—	—	—	—	—
	SB9	17.2539 ± 0.1615	1981.248 ± 0.3697	0.119 ± 0.018	—	307.0 ± 8.0	—	—	-7.93 ± 0.08	—	—	—	—
	$SB1$	$17.204^{17.220}_{17.185}$	$1983.188^{1983.357}_{1983.074}$	$0.103^{0.107}_{0.099}$	$0.379^{0.381}_{0.377}$	$343.309^{346.585}_{341.375}$	$68.351^{69.318}_{67.230}$	$143.574^{144.206}_{142.781}$	$-7.956^{-7.812}_{-8.039}$	—	$10.940^{11.377}_{10.398}$	—	—
	$SB1 + p(\varpi)$	$17.198^{17.220}_{17.185}$	$1983.212^{1983.357}_{1983.068}$	$0.103^{0.107}_{0.100}$	$0.379^{0.381}_{0.377}$	$343.552^{346.498}_{341.213}$	$68.340^{69.299}_{67.207}$	$143.455^{144.237}_{142.810}$	$-7.906^{-7.814}_{-8.036}$	$40.874^{41.163}_{40.598}$	$10.812^{11.395}_{10.422}$	$1.502^{1.568}_{1.412}$	$0.792^{0.869}_{0.739}$
	$SB1 + p(m_1\|\theta)$	$17.206^{17.219}_{17.185}$	$1983.247^{1983.358}_{1983.072}$	$0.104^{0.107}_{0.100}$	$0.380^{0.381}_{0.377}$	$344.352^{346.483}_{341.281}$	$67.951^{69.303}_{67.171}$	$143.282^{144.251}_{142.816}$	$-7.930^{-7.812}_{-8.030}$	$42.992^{44.095}_{42.000}$	$10.845^{11.366}_{10.400}$	$1.241^{1.323}_{1.127}$	$0.873^{0.948}_{0.820}$
	$SB1 + p(\varpi) + p(m_1\|\theta)$	$17.200^{17.219}_{17.185}$	$1983.159^{1983.308}_{1983.016}$	$0.101^{0.104}_{0.098}$	$0.377^{0.379}_{0.375}$	$342.733^{345.510}_{340.264}$	$68.620^{69.538}_{67.432}$	$144.097^{144.749}_{143.392}$	$-7.903^{-7.821}_{-8.040}$	$41.054^{41.332}_{40.802}$	$11.317^{11.859}_{11.012}$	$1.404^{1.455}_{1.334}$	$0.868^{0.949}_{0.827}$
43109	Orb6	15.0507 ± 0.0064	1991.247 ± 0.005	0.6558 ± 0.0018	0.2547 ± 0.0009	266.10 ± 0.27	107.99 ± 0.35	50.01 ± 0.27	—	—	—	—	—
	SB9	15.04	1915.93	0.61	—	86.8	—	—	36.4	—	—	—	—
	$SB1$	$15.073^{15.084}_{15.063}$	$1900.819^{1900.878}_{1900.742}$	$0.656^{0.661}_{0.651}$	$0.253^{0.255}_{0.250}$	$85.086^{85.742}_{84.537}$	$288.913^{289.668}_{287.911}$	$49.960^{50.614}_{49.281}$	$35.613^{35.745}_{35.454}$	—	$16.337^{16.904}_{15.848}$	—	—
	$SB1 + p(\varpi)$	$15.072^{15.085}_{15.064}$	$1900.823^{1900.879}_{1900.740}$	$0.655^{0.661}_{0.651}$	$0.252^{0.255}_{0.250}$	$85.234^{85.742}_{84.593}$	$288.685^{289.637}_{287.984}$	$49.844^{50.538}_{49.242}$	$35.567^{35.739}_{35.450}$	$26.418^{26.637}_{26.245}$	$16.480^{16.901}_{15.849}$	$2.166^{2.300}_{2.053}$	$0.771^{0.810}_{0.721}$
	$SB1 + p(m_1\|\theta)$	$15.076^{15.084}_{15.063}$	$1900.801^{1900.889}_{1900.749}$	$0.657^{0.662}_{0.651}$	$0.253^{0.255}_{0.250}$	$85.158^{85.693}_{84.492}$	$288.851^{289.763}_{288.036}$	$50.005^{50.710}_{49.400}$	$35.633^{35.778}_{35.492}$	$30.191^{31.468}_{28.975}$	$16.289^{16.769}_{15.738}$	$1.315^{1.500}_{1.155}$	$0.968^{1.000}_{0.913}$
	$SB1 + p(\varpi) + p(m_1\|\theta)$	$15.074^{15.087}_{15.066}$	$1900.812^{1900.867}_{1900.732}$	$0.654^{0.658}_{0.648}$	$0.252^{0.253}_{0.249}$	$85.265^{85.760}_{84.577}$	$288.568^{289.542}_{287.856}$	$49.655^{50.112}_{48.838}$	$35.526^{35.674}_{35.390}$	$26.535^{26.707}_{26.318}$	$16.667^{17.253}_{16.236}$	$2.094^{2.188}_{1.965}$	$0.793^{0.845}_{0.755}$
54061	Orb6	44.448 ± 0.11	2002.170 ± 0.094	0.4392 ± 0.004	0.590 ± 0.026	232.8 ± 7.9	9.3 ± 8.2	159.9 ± 3.5	—	—	—	—	—
	SB9	43.9992	1909.90	0.35	—	174.	—	—	-8.7	—	—	—	—
	$SB1$	$44.088^{44.452}_{43.914}$	$1914.123^{1914.496}_{1913.418}$	$0.433^{0.437}_{0.430}$	$0.594^{0.598}_{0.592}$	$53.716^{61.244}_{43.766}$	$187.957^{195.301}_{178.369}$	$165.364^{168.578}_{163.889}$	$-9.710^{-9.449}_{-9.964}$	—	$12.895^{18.327}_{8.960}$	—	—
	$SB1 + p(\varpi)$	$44.170^{44.447}_{43.912}$	$1913.957^{1914.492}_{1913.418}$	$0.433^{0.437}_{0.430}$	$0.595^{0.598}_{0.592}$	$52.500^{61.605}_{44.253}$	$186.795^{195.392}_{178.573}$	$165.438^{168.434}_{163.851}$	$-9.715^{-9.455}_{-9.961}$	$26.666^{27.485}_{25.595}$	$12.193^{18.433}_{10.194}$	$3.837^{4.366}_{2.803}$	$0.482^{0.937}_{0.352}$
	$SB1 + p(m_1\|\theta)$	$44.132^{44.438}_{43.898}$	$1914.044^{1914.511}_{1913.429}$	$0.433^{0.437}_{0.429}$	$0.595^{0.598}_{0.592}$	$55.901^{61.426}_{43.903}$	$190.032^{195.216}_{178.211}$	$165.754^{168.185}_{163.889}$	$-9.781^{-9.449}_{-9.959}$	$31.916^{35.259}_{29.187}$	$12.929^{16.685}_{9.978}$	$1.952^{2.402}_{1.401}$	$0.703^{0.999}_{0.521}$
	$SB1 + p(\varpi) + p(m_1\|\theta)$	$44.199^{44.477}_{43.946}$	$1913.888^{1914.400}_{1913.334}$	$0.433^{0.437}_{0.430}$	$0.593^{0.597}_{0.591}$	$51.525^{60.446}_{41.935}$	$185.901^{194.695}_{176.651}$	$167.155^{169.404}_{165.236}$	$-9.681^{-9.429}_{-9.951}$	$27.211^{28.234}_{26.620}$	$17.792^{18.731}_{16.002}$	$2.736^{2.966}_{2.431}$	$0.938^{1.000}_{0.801}$
55642	Orb6	184.4572 ± 1.3275	1948.3626 ± 0.2117	0.53689 ± 0.00459	1.91525 ± 0.01550	142.829 ± 0.878	54.376 ± 0.846	127.642 ± 0.598	—	—	—	—	—
	SB9	191.996	1948.465	0.54	—	140.7	—	—	-11.0	—	—	—	—
	$SB1$	$189.516^{190.180}_{188.784}$	$1948.812^{1949.039}_{1948.553}$	$0.551^{0.553}_{0.547}$	$1.926^{1.937}_{1.919}$	$145.134^{145.836}_{144.501}$	$56.052^{56.616}_{55.712}$	$127.234^{127.504}_{126.787}$	$-11.151^{-11.108}_{-11.195}$	—	$10.523^{11.128}_{9.709}$	—	—
	$SB1 + p(\varpi)$	$189.419^{190.168}_{188.762}$	$1948.799^{1949.043}_{1948.553}$	$0.549^{0.553}_{0.547}$	$1.930^{1.937}_{1.918}$	$145.176^{145.864}_{144.537}$	$56.167^{56.606}_{55.709}$	$127.105^{127.501}_{126.791}$	$-11.142^{-11.111}_{-11.198}$	$41.726^{42.987}_{40.920}$	$10.263^{11.216}_{9.798}$	$1.576^{1.689}_{1.355}$	$0.749^{0.883}_{0.681}$
	$SB1 + p(m_1\|\theta)$	$189.317^{190.200}_{188.775}$	$1948.829^{1949.030}_{1948.554}$	$0.549^{0.553}_{0.547}$	$1.927^{1.937}_{1.919}$	$145.311^{145.822}_{144.527}$	$56.277^{56.608}_{55.714}$	$127.153^{127.489}_{126.869}$	$-11.150^{-11.109}_{-11.195}$	$43.111^{43.931}_{42.185}$	$10.348^{11.160}_{9.739}$	$1.379^{1.447}_{1.310}$	$0.805^{0.903}_{0.742}$
	$SB1 + p(\varpi) + p(m_1\|\theta)$	$189.561^{190.192}_{188.747}$	$1948.860^{1949.053}_{1948.582}$	$0.550^{0.553}_{0.547}$	$1.926^{1.936}_{1.917}$	$145.345^{145.906}_{144.631}$	$56.178^{56.612}_{55.729}$	$127.240^{127.536}_{126.837}$	$-11.166^{-11.130}_{-11.207}$	$42.438^{43.259}_{41.949}$	$10.723^{11.360}_{10.113}$	$1.417^{1.461}_{1.336}$	$0.835^{0.921}_{0.768}$
67620	Orb6	10.485 ± 0.06	2009.218 ± 0.028	0.3462 ± 0.0080	0.2827 ± 0.0014	137.5 ± 1.4	171.3 ± 0.3	96.4 ± 0.2	—	—	—	—	—
	SB9	10.4786 ± 0.019	2009.248 ± 0.0329	0.3586 ± 0.0056	—	140.3 ± 1.3	—	—	5.242 ± 0.028	—	—	—	—
	$SB1$	$10.455^{10.470}_{10.441}$	$1998.842^{1998.879}_{1998.811}$	$0.340^{0.346}_{0.336}$	$0.286^{0.289}_{0.282}$	$141.958^{143.040}_{140.932}$	$171.617^{172.308}_{171.021}$	$96.031^{96.710}_{95.495}$	$5.351^{5.380}_{5.319}$	—	$7.175^{7.320}_{7.087}$	—	—
	$SB1 + p(\varpi)$	$10.456^{10.470}_{10.442}$	$1998.843^{1998.876}_{1998.806}$	$0.340^{0.346}_{0.336}$	$0.286^{0.288}_{0.282}$	$141.981^{143.062}_{140.945}$	$171.636^{172.369}_{171.040}$	$96.194^{96.724}_{95.511}$	$5.356^{5.381}_{5.321}$	$53.936^{54.546}_{53.196}$	$7.175^{7.315}_{7.090}$	$0.835^{0.882}_{0.776}$	$0.631^{0.656}_{0.614}$
	$SB1 + p(m_1\|\theta)$	$10.453^{10.470}_{10.442}$	$1998.850^{1998.877}_{1998.808}$	$0.340^{0.346}_{0.336}$	$0.285^{0.289}_{0.282}$	$142.167^{143.030}_{140.904}$	$171.738^{172.311}_{171.021}$	$96.250^{96.691}_{95.506}$	$5.348^{5.380}_{5.320}$	$50.662^{51.705}_{49.249}$	$7.182^{7.319}_{7.090}$	$1.037^{1.127}_{0.970}$	$0.572^{0.593}_{0.552}$
	$SB1 + p(\varpi) + p(m_1\|\theta)$	$10.452^{10.466}_{10.437}$	$1998.842^{1998.875}_{1998.806}$	$0.339^{0.344}_{0.335}$	$0.289^{0.291}_{0.285}$	$141.761^{142.863}_{140.722}$	$171.539^{172.349}_{171.030}$	$96.138^{96.590}_{95.389}$	$5.361^{5.382}_{5.322}$	$53.095^{53.837}_{52.601}$	$7.093^{7.217}_{7.005}$	$0.917^{0.950}_{0.855}$	$0.604^{0.626}_{0.592}$
75695	Orb6	10.5367 ± 0.0014	1980.473 ± 0.0038	0.53971 ± 0.00021	0.204008 ± 0.000034	180.21 ± 0.13	148.041 ± 0.030	111.452 ± 0.014	—	—	—	—	—
	SB9	10.496	1938.197	0.41	—	185.4	—	—	-18.0	—	—	—	—
	$SB1$	$10.550^{10.553}_{10.546}$	$1906.630^{1906.669}_{1906.600}$	$0.524^{0.528}_{0.520}$	$0.207^{0.208}_{0.206}$	$180.651^{181.688}_{179.545}$	$148.315^{148.652}_{147.991}$	$110.874^{111.185}_{110.297}$	$-19.859^{-19.784}_{-19.924}$	—	$16.140^{16.385}_{15.891}$	—	—
	$SB1 + p(\varpi)$	$10.550^{10.553}_{10.546}$	$1906.632^{1906.669}_{1906.601}$	$0.524^{0.528}_{0.520}$	$0.207^{0.208}_{0.206}$	$180.739^{181.726}_{179.566}$	$148.340^{148.645}_{147.983}$	$110.668^{111.174}_{110.275}$	$-19.861^{-19.787}_{-19.929}$	$28.781^{30.648}_{27.769}$	$16.100^{16.380}_{15.879}$	$1.798^{2.032}_{1.380}$	$0.864^{0.984}_{0.809}$
	$SB1 + p(m_1\|\theta)$	$10.549^{10.553}_{10.546}$	$1906.636^{1906.669}_{1906.600}$	$0.524^{0.528}_{0.520}$	$0.207^{0.208}_{0.206}$	$180.604^{181.741}_{179.554}$	$148.313^{148.643}_{147.985}$	$110.763^{111.186}_{110.281}$	$-19.874^{-19.781}_{-19.927}$	$27.937^{28.455}_{27.520}$	$16.147^{16.373}_{15.878}$	$2.009^{2.122}_{1.885}$	$0.822^{0.852}_{0.796}$
	$SB1 + p(\varpi) + p(m_1\|\theta)$	$10.549^{10.553}_{10.546}$	$1906.632^{1906.669}_{1906.601}$	$0.525^{0.528}_{0.520}$	$0.207^{0.208}_{0.206}$	$180.569^{181.784}_{179.606}$	$148.321^{148.646}_{147.980}$	$110.813^{111.141}_{110.257}$	$-19.856^{-19.787}_{-19.930}$	$28.066^{28.550}_{27.663}$	$16.103^{16.360}_{15.860}$	$1.982^{2.083}_{1.858}$	$0.825^{0.857}_{0.800}$
76031	Orb6	1.713 ± 0.002	2016.470 ± 0.010	0.435 ± 0.017	0.0427 ± 0.0010	45.8 ± 2.3	341.9 ± 2.1	150.0	—	—	—	—	—
	SB9	1.6956 ± 0.0038	2006.180 ± 0.0093	0.406 ± 0.014	—	43.2 ± 2.6	—	—	4.55 ± 0.09	—	—	—	—
	$SB1$	$1.697^{1.699}_{1.693}$	$2002.798^{2002.826}_{2002.783}$	$0.461^{0.484}_{0.432}$	$0.039^{0.040}_{0.037}$	$44.804^{51.325}_{40.852}$	$355.676^{360.000}_{352.768}$	$170.163^{176.872}_{161.733}$	$4.614^{4.908}_{4.287}$	—	$65.700^{190.218}_{29.739}$	—	—
	$SB1 + p(\varpi)$	$1.697^{1.700}_{1.693}$	$2002.810^{2002.832}_{2002.790}$	$0.457^{0.493}_{0.440}$	$0.041^{0.042}_{0.039}$	$48.314^{53.893}_{43.471}$	$356.260^{359.999}_{351.875}$	$153.961^{157.493}_{149.958}$	$4.672^{4.916}_{4.316}$	$19.262^{20.873}_{17.461}$	$24.282^{27.585}_{20.957}$	$1.727^{2.316}_{1.239}$	$0.879^{1.000}_{0.708}$
	$SB1 + p(m_1\|\theta)$	$1.696^{1.701}_{1.694}$	$2002.814^{2002.834}_{2002.790}$	$0.474^{0.498}_{0.445}$	$0.040^{0.042}_{0.039}$	$49.302^{54.297}_{43.654}$	$356.416^{360.000}_{351.466}$	$151.234^{153.730}_{148.193}$	$4.650^{4.939}_{4.321}$	$21.785^{23.088}_{20.739}$	$22.151^{23.900}_{19.831}$	$1.149^{1.238}_{1.082}$	$0.933^{1.000}_{0.834}$
	$SB1 + p(\varpi) + p(m_1\|\theta)$	$1.698^{1.701}_{1.694}$	$2002.812^{2002.835}_{2002.790}$	$0.474^{0.498}_{0.445}$	$0.040^{0.041}_{0.038}$	$48.590^{54.227}_{43.531}$	$355.171^{359.998}_{351.179}$	$151.993^{154.062}_{149.757}$	$4.682^{4.931}_{4.313}$	$21.176^{22.100}_{20.337}$	$23.046^{24.422}_{21.487}$	$1.182^{1.249}_{1.101}$	$0.953^{1.000}_{0.884}$
78727	Orb6	45.90 ± 0.60	1997.22 ± 0.02	0.744 ± 0.001	0.654 ± 0.006	163.8 ± 5.0	25.3 ± 4.0	34.5 ± 1.0	—	—	—	—	—
	SB9	44.699	1905.39	0.75	—	343.6	—	—	-29.4	—	—	—	—
	$SB1$	$45.846^{45.909}_{45.817}$	$1859.564^{1859.646}_{1859.365}$	$0.746^{0.748}_{0.745}$	$0.666^{0.668}_{0.665}$	$155.300^{155.971}_{154.465}$	$32.841^{33.587}_{32.270}$	$34.607^{34.955}_{34.227}$	$-32.625^{-31.509}_{-34.038}$	—	$5.750^{9.470}_{1.274}$	—	—
	$SB1 + p(\varpi)$	$45.878^{45.911}_{45.819}$	$1859.467^{1859.648}_{1859.371}$	$0.747^{0.748}_{0.745}$	$0.667^{0.668}_{0.665}$	$155.171^{156.046}_{154.472}$	$32.937^{33.569}_{32.208}$	$34.648^{34.971}_{34.225}$	$-32.608^{-31.259}_{-33.717}$	$35.847^{36.492}_{35.251}$	$5.957^{10.687}_{2.811}$	$2.405^{2.774}_{1.881}$	$0.272^{0.577}_{0.087}$
	$SB1 + p(m_1\|\theta)$	$45.863^{45.911}_{45.818}$	$1859.515^{1859.660}_{1859.378}$	$0.746^{0.748}_{0.745}$	$0.667^{0.668}_{0.665}$	$155.219^{155.973}_{154.435}$	$32.899^{33.600}_{32.251}$	$34.631^{34.972}_{34.229}$	$-32.589^{-31.285}_{-33.775}$	$43.083^{45.295}_{39.385}$	$5.593^{10.350}_{2.347}$	$1.337^{1.398}_{1.303}$	$0.317^{0.680}_{0.109}$
	$SB1 + p(\varpi) + p(m_1\|\theta)$	$45.855^{45.913}_{45.822}$	$1859.543^{1859.638}_{1859.361}$	$0.746^{0.748}_{0.745}$	$0.666^{0.668}_{0.665}$	$155.376^{156.028}_{154.496}$	$32.806^{33.528}_{32.201}$	$34.515^{34.901}_{34.145}$	$-30.595^{-30.139}_{-31.813}$	$36.960^{37.357}_{36.598}$	$13.424^{13.655}_{13.095}$	$1.404^{1.446}_{1.363}$	$0.985^{1.000}_{0.950}$

Table 3.4: Table 3.2 (contd.). MAP estimates and 95 % HDPIs derived from the marginal PDFs of the orbital parameters for the four orbital solutions, based on our astrometric data, discussed in the first paragraph of Section 3.3. m_1 and ϖ are the priors used for the mass of the primary component and the trigonometric parallax, respectively. In the first two lines (of six entries) for each $SB1$ system, we report the values provided by Orb6 and SB9, preserving the significant figures included in those catalogs as an indication of their precision

HIP #	System	P [yr]	T [yr]	e	a [arcsec]	ω [°]	Ω [°]	i [°]	V_0 [km/s]	ϖ [mas]	f/ϖ [pc]	m_1 [$M_\odot$]	q
93017	Orb6	63.2489 ± 3.0169	1972.7274 ± 1.0996	0.21805 ± 0.05240	1.24739 ± 0.01764	288.164 ± 9.910	49.397 ± 0.773	115.743 ± 1.814	—	—	—	—	—
	SB9	$61.391 \pm Fixed$	1972.220	0.25	—	102	—	—	-45.82 ± 0.69	—	—	—	—
	$SB1$	$61.285^{61.447}_{61.136}$	$1910.765^{1910.916}_{1910.601}$	$0.269^{0.273}_{0.266}$	$1.272^{1.275}_{1.270}$	$101.048^{101.432}_{100.639}$	$48.879^{49.040}_{48.659}$	$114.107^{114.237}_{113.980}$	$-45.947^{-45.857}_{-46.060}$	—	$5.825^{6.071}_{5.503}$	—	—
	$SB1 + p(\varpi)$	$61.291^{61.441}_{61.135}$	$1910.759^{1910.914}_{1910.608}$	$0.269^{0.273}_{0.266}$	$1.272^{1.275}_{1.270}$	$101.036^{101.433}_{100.642}$	$48.850^{49.045}_{48.672}$	$114.136^{114.241}_{113.987}$	$-45.961^{-45.858}_{-46.060}$	$67.125^{67.375}_{66.917}$	$5.785^{6.082}_{5.494}$	$1.108^{1.148}_{1.067}$	$0.635^{0.690}_{0.584}$
	$SB1 + p(m_1\|\theta)$	$61.274^{61.441}_{61.140}$	$1910.765^{1910.917}_{1910.615}$	$0.269^{0.273}_{0.266}$	$1.273^{1.275}_{1.270}$	$100.962^{101.452}_{100.667}$	$48.864^{49.032}_{48.658}$	$114.097^{114.243}_{113.985}$	$-45.942^{-45.860}_{-46.063}$	$65.963^{67.013}_{65.072}$	$5.812^{6.068}_{5.507}$	$1.180^{1.223}_{1.125}$	$0.622^{0.661}_{0.577}$
	$SB1 + p(\varpi) + p(m_1\|\theta)$	$61.286^{61.417}_{61.117}$	$1910.743^{1910.932}_{1910.629}$	$0.270^{0.273}_{0.267}$	$1.273^{1.275}_{1.270}$	$100.938^{101.362}_{100.585}$	$48.839^{49.045}_{48.673}$	$114.072^{114.218}_{113.965}$	$-45.969^{-45.891}_{-46.082}$	$67.049^{67.301}_{66.859}$	$5.609^{5.852}_{5.384}$	$1.138^{1.166}_{1.104}$	$0.603^{0.648}_{0.567}$
96302	Orb6	4.56	1985.56	0.82	0.030	45.5	29.3	114.6	—	—	—	—	—
	SB9	4.303 ± 0.0011	1988.771 ± 0.0011	0.7787 ± 0.0018	—	139.6 ± 0.4	—	—	-17.26 ± 0.05	—	—	—	—
	$SB1$	$4.303^{4.306}_{4.301}$	$1919.920^{1919.953}_{1919.873}$	$0.789^{0.794}_{0.784}$	$0.029^{0.031}_{0.026}$	$139.671^{140.614}_{138.660}$	$181.511^{188.989}_{168.698}$	$106.470^{123.167}_{96.584}$	$-17.242^{-17.093}_{-17.375}$	—	$72.573^{88.625}_{64.879}$	—	—
	$SB1 + p(\varpi)$	$4.304^{4.306}_{4.301}$	$1919.910^{1919.952}_{1919.870}$	$0.788^{0.793}_{0.783}$	$0.029^{0.031}_{0.026}$	$139.491^{140.652}_{138.758}$	$179.270^{188.189}_{168.968}$	$107.302^{122.827}_{97.853}$	$-17.272^{-17.085}_{-17.372}$	$5.380^{5.581}_{5.176}$	$71.053^{89.369}_{66.395}$	$5.389^{6.252}_{2.890}$	$0.619^{0.913}_{0.539}$
	$SB1 + p(m_1\|\theta)$	$4.304^{4.306}_{4.301}$	$1919.904^{1919.952}_{1919.870}$	$0.788^{0.793}_{0.784}$	$0.028^{0.031}_{0.027}$	$139.593^{140.623}_{138.722}$	$181.684^{190.523}_{174.361}$	$104.776^{113.757}_{95.343}$	$-17.266^{-17.095}_{-17.374}$	$6.691^{7.516}_{6.175}$	$72.257^{79.134}_{65.111}$	$2.155^{2.423}_{1.775}$	$0.936^{1.000}_{0.893}$
	$SB1 + p(\varpi) + p(m_1\|\theta)$	$4.303^{4.307}_{4.301}$	$1919.922^{1919.952}_{1919.869}$	$0.789^{0.794}_{0.784}$	$0.025^{0.026}_{0.024}$	$140.029^{140.815}_{138.951}$	$173.956^{179.938}_{168.656}$	$116.725^{121.808}_{110.479}$	$-17.195^{-17.083}_{-17.368}$	$5.464^{5.684}_{5.307}$	$89.468^{93.464}_{84.767}$	$2.611^{2.908}_{2.270}$	$0.956^{1.000}_{0.902}$
103655	Orb6	28.90	2007.26	0.656	0.709	116.0	143.5	36.3	—	—	—	—	—
	SB9	29.51 ± 0.66	1976.88 ± 0.046	0.717776 ± 0.014	—	308.961 ± 3.3	—	—	-33.9674 ± 0.095	—	—	—	—
	$SB1$	$29.466^{29.590}_{29.380}$	$1947.812^{1947.976}_{1947.594}$	$0.610^{0.617}_{0.605}$	$0.674^{0.678}_{0.669}$	$326.055^{328.055}_{322.815}$	$110.038^{113.120}_{108.160}$	$33.590^{34.754}_{31.994}$	$-33.698^{-33.524}_{-33.828}$	—	$7.202^{7.688}_{6.729}$	—	—
	$SB1 + p(\varpi)$	$29.488^{29.580}_{29.379}$	$1947.777^{1947.983}_{1947.616}$	$0.612^{0.616}_{0.606}$	$0.673^{0.678}_{0.670}$	$325.884^{328.224}_{323.178}$	$110.249^{112.916}_{108.185}$	$33.621^{34.759}_{32.166}$	$-33.651^{-33.523}_{-33.805}$	$66.536^{66.692}_{66.411}$	$7.099^{7.514}_{6.825}$	$0.629^{0.661}_{0.590}$	$0.895^{1.000}_{0.833}$
	$SB1 + p(m_1\|\theta)$	$29.488^{29.566}_{29.368}$	$1947.764^{1947.971}_{1947.609}$	$0.611^{0.615}_{0.604}$	$0.676^{0.680}_{0.671}$	$325.655^{328.803}_{323.925}$	$110.264^{111.780}_{107.252}$	$34.273^{35.475}_{33.095}$	$-33.600^{-33.452}_{-33.712}$	$73.521^{75.893}_{71.734}$	$6.750^{6.939}_{6.475}$	$0.451^{0.484}_{0.413}$	$0.985^{1.000}_{0.942}$
	$SB1 + p(\varpi) + p(m_1\|\theta)$	$29.557^{29.637}_{29.443}$	$1947.675^{1947.882}_{1947.528}$	$0.615^{0.619}_{0.609}$	$0.668^{0.672}_{0.664}$	$324.365^{327.348}_{322.440}$	$111.956^{113.634}_{109.037}$	$32.325^{33.379}_{31.251}$	$-33.687^{-33.566}_{-33.817}$	$66.642^{66.751}_{66.465}$	$7.464^{7.521}_{7.409}$	$0.580^{0.593}_{0.569}$	$0.990^{1.000}_{0.976}$
111685	Orb6	16.77 ± 0.15	1991.78 ± 0.08	0.256 ± 0.009	0.330 ± 0.003	118.7 ± 2.2	69.0 ± 1.0	55.9 ± 0.6	—	—	—	—	—
	SB9	16.912 ± 0.0712	2008.719 ± 0.0601	0.249 ± 0.007	—	300.1 ± 1.3	—	—	-58.378 ± 0.113	—	—	—	—
	$SB1$	$16.748^{16.886}_{16.674}$	$1991.514^{1991.621}_{1991.347}$	$0.241^{0.251}_{0.227}$	$0.344^{0.347}_{0.340}$	$295.215^{296.834}_{293.082}$	$66.478^{67.583}_{65.561}$	$59.045^{59.804}_{57.954}$	$-58.203^{-57.963}_{-58.410}$	—	$6.977^{7.564}_{6.399}$	—	—
	$SB1 + p(\varpi)$	$16.754^{16.878}_{16.674}$	$1991.493^{1991.609}_{1991.345}$	$0.240^{0.250}_{0.227}$	$0.344^{0.347}_{0.340}$	$295.062^{296.814}_{293.103}$	$66.412^{67.554}_{65.548}$	$58.929^{59.859}_{57.988}$	$-58.148^{-57.956}_{-58.397}$	$51.432^{54.390}_{48.147}$	$6.997^{7.584}_{6.425}$	$0.682^{0.851}_{0.537}$	$0.562^{0.656}_{0.474}$
	$SB1 + p(m_1\|\theta)$	$16.761^{16.883}_{16.672}$	$1991.508^{1991.613}_{1991.340}$	$0.239^{0.251}_{0.228}$	$0.344^{0.347}_{0.340}$	$295.131^{296.878}_{293.108}$	$66.662^{67.624}_{65.591}$	$58.889^{59.859}_{57.953}$	$-58.208^{-57.952}_{-58.400}$	$54.998^{56.327}_{53.385}$	$6.865^{7.567}_{6.440}$	$0.542^{0.577}_{0.500}$	$0.607^{0.692}_{0.554}$
	$SB1 + p(\varpi) + p(m_1\|\theta)$	$16.802^{16.893}_{16.683}$	$1991.478^{1991.614}_{1991.341}$	$0.239^{0.250}_{0.227}$	$0.342^{0.347}_{0.339}$	$295.410^{297.093}_{293.294}$	$66.556^{67.586}_{65.562}$	$58.596^{59.668}_{57.835}$	$-58.182^{-57.952}_{-58.399}$	$54.019^{55.465}_{52.817}$	$7.137^{7.703}_{6.578}$	$0.552^{0.589}_{0.514}$	$0.627^{0.703}_{0.564}$
111974	Orb6	20.829 ± 0.0030	1983.537 ± 0.0033	0.73499 ± 0.00014	0.28798 ± 0.000049	22.31 ± 0.12	251.540 ± 0.076	139.861 ± 0.032	—	—	—	—	—
	SB9	20.930	1983.570	0.72	—	204.2	—	—	-10.5	—	—	—	—
	$SB1$	$20.837^{20.851}_{20.826}$	$1900.181^{1900.226}_{1900.120}$	$0.733^{0.735}_{0.730}$	$0.290^{0.291}_{0.289}$	$22.007^{22.963}_{21.149}$	$251.203^{252.024}_{250.509}$	$139.355^{139.937}_{138.720}$	$-12.191^{-11.989}_{-12.346}$	—	$17.916^{18.324}_{17.449}$	—	—
	$SB1 + p(\varpi)$	$20.837^{20.849}_{20.826}$	$1900.177^{1900.230}_{1900.127}$	$0.732^{0.735}_{0.730}$	$0.290^{0.291}_{0.289}$	$21.893^{22.886}_{21.073}$	$251.118^{251.873}_{250.383}$	$139.178^{139.707}_{138.544}$	$-12.062^{-11.923}_{-12.263}$	$27.986^{28.785}_{27.331}$	$17.604^{18.028}_{17.236}$	$1.300^{1.397}_{1.177}$	$0.971^{1.000}_{0.948}$
	$SB1 + p(m_1\|\theta)$	$20.838^{20.849}_{20.824}$	$1900.175^{1900.236}_{1900.132}$	$0.732^{0.735}_{0.730}$	$0.290^{0.291}_{0.289}$	$21.671^{22.656}_{20.866}$	$250.820^{251.640}_{250.197}$	$138.771^{139.523}_{138.385}$	$-12.006^{-11.801}_{-12.102}$	$28.876^{29.399}_{28.425}$	$17.254^{17.535}_{16.948}$	$1.175^{1.227}_{1.112}$	$0.993^{1.000}_{0.983}$
	$SB1 + p(\varpi) + p(m_1\|\theta)$	$20.836^{20.848}_{20.824}$	$1900.186^{1900.235}_{1900.129}$	$0.732^{0.735}_{0.730}$	$0.290^{0.291}_{0.289}$	$21.812^{22.626}_{20.829}$	$250.946^{251.645}_{250.194}$	$138.945^{139.530}_{138.403}$	$-11.960^{-11.802}_{-12.088}$	$29.005^{29.433}_{28.509}$	$17.210^{17.494}_{16.927}$	$1.158^{1.213}_{1.106}$	$0.997^{1.000}_{0.983}$
116259	Orb6	15.70 ± 0.23	2005.49 ± 0.01	0.536 ± 0.007	0.220 ± 0.002	89.5 ± 0.8	141.5 ± 0.3	75.1 ± 0.4	—	—	—	—	—
	SB9	16.654 ± 0.354	1989.325 ± 0.058	0.521 ± 0.012	—	97.0 ± 2.7	—	—	-3.359 ± 0.098	—	—	—	—
	$SB1$	$16.352^{16.392}_{16.285}$	$1989.136^{1989.180}_{1989.102}$	$0.537^{0.549}_{0.525}$	$0.223^{0.226}_{0.220}$	$87.683^{88.255}_{87.072}$	$141.842^{142.544}_{141.103}$	$74.466^{75.045}_{73.904}$	$-3.309^{-3.224}_{-3.415}$	—	$12.972^{13.303}_{12.452}$	—	—
	$SB1 + p(\varpi)$	$16.340^{16.392}_{16.284}$	$1989.146^{1989.181}_{1989.102}$	$0.542^{0.550}_{0.525}$	$0.223^{0.226}_{0.220}$	$87.779^{88.251}_{87.037}$	$141.865^{142.521}_{141.064}$	$74.587^{75.035}_{73.901}$	$-3.330^{-3.225}_{-3.418}$	$29.154^{29.518}_{28.924}$	$12.848^{13.310}_{12.469}$	$1.051^{1.103}_{0.969}$	$0.599^{0.639}_{0.573}$
	$SB1 + p(m_1\|\theta)$	$16.359^{16.396}_{16.286}$	$1989.136^{1989.179}_{1989.099}$	$0.541^{0.549}_{0.525}$	$0.223^{0.226}_{0.220}$	$87.691^{88.212}_{87.057}$	$142.018^{142.594}_{141.109}$	$74.431^{75.068}_{73.935}$	$-3.298^{-3.221}_{-3.414}$	$28.528^{29.100}_{27.713}$	$12.903^{13.308}_{12.463}$	$1.132^{1.226}_{1.068}$	$0.583^{0.605}_{0.549}$
	$SB1 + p(\varpi) + p(m_1\|\theta)$	$16.349^{16.394}_{16.286}$	$1989.145^{1989.179}_{1989.101}$	$0.543^{0.553}_{0.530}$	$0.225^{0.227}_{0.222}$	$87.745^{88.123}_{86.962}$	$141.788^{142.623}_{141.155}$	$74.775^{75.183}_{74.129}$	$-3.310^{-3.223}_{-3.409}$	$29.076^{29.382}_{28.828}$	$12.672^{13.094}_{12.331}$	$1.093^{1.139}_{1.033}$	$0.583^{0.614}_{0.559}$

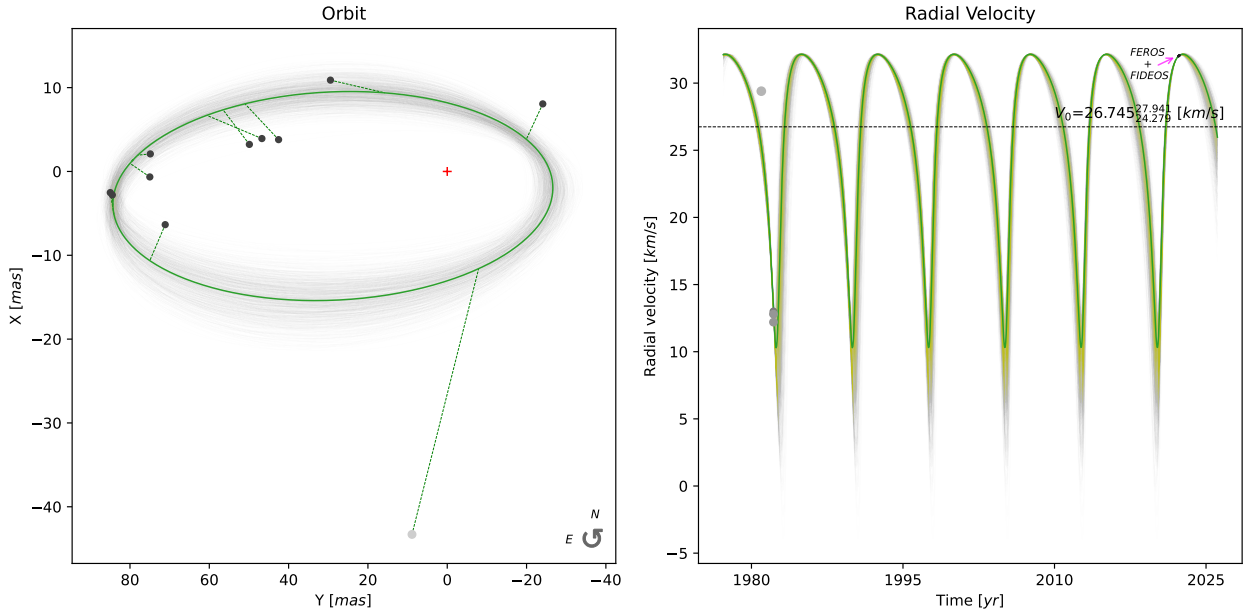

Figure 3.2: Orbit (left panel) and RV curve (right panel) for HIP 38414 based on the MAP values obtained from the $SB1+p(\varpi)+p(m_1|\theta)$ solution given in Table 3.2. The size and color of the dots in both plots depict the weight (uncertainty) of each observation: large clear dots indicate larger errors and the opposite is true for small dark dots. In all astrometric orbits presented, smaller dots are from more recent interferometric measurements, including -but not limited to- our own (although in this particular case, all observations are from SOAR). For this system we have a a phase coverage of about 50 % of the visual orbit. The large deviant point is from SOAR at 2011.9, so gave it a smaller weight in our solution. For the RV curve, we supplemented good quality historical with recent data acquired by us with FEROS and FIDEOS. The dashed horizontal line in the RV curve indicates the estimated systemic velocity, which is included, with its 95 % HDPI range, at the right end of the line.

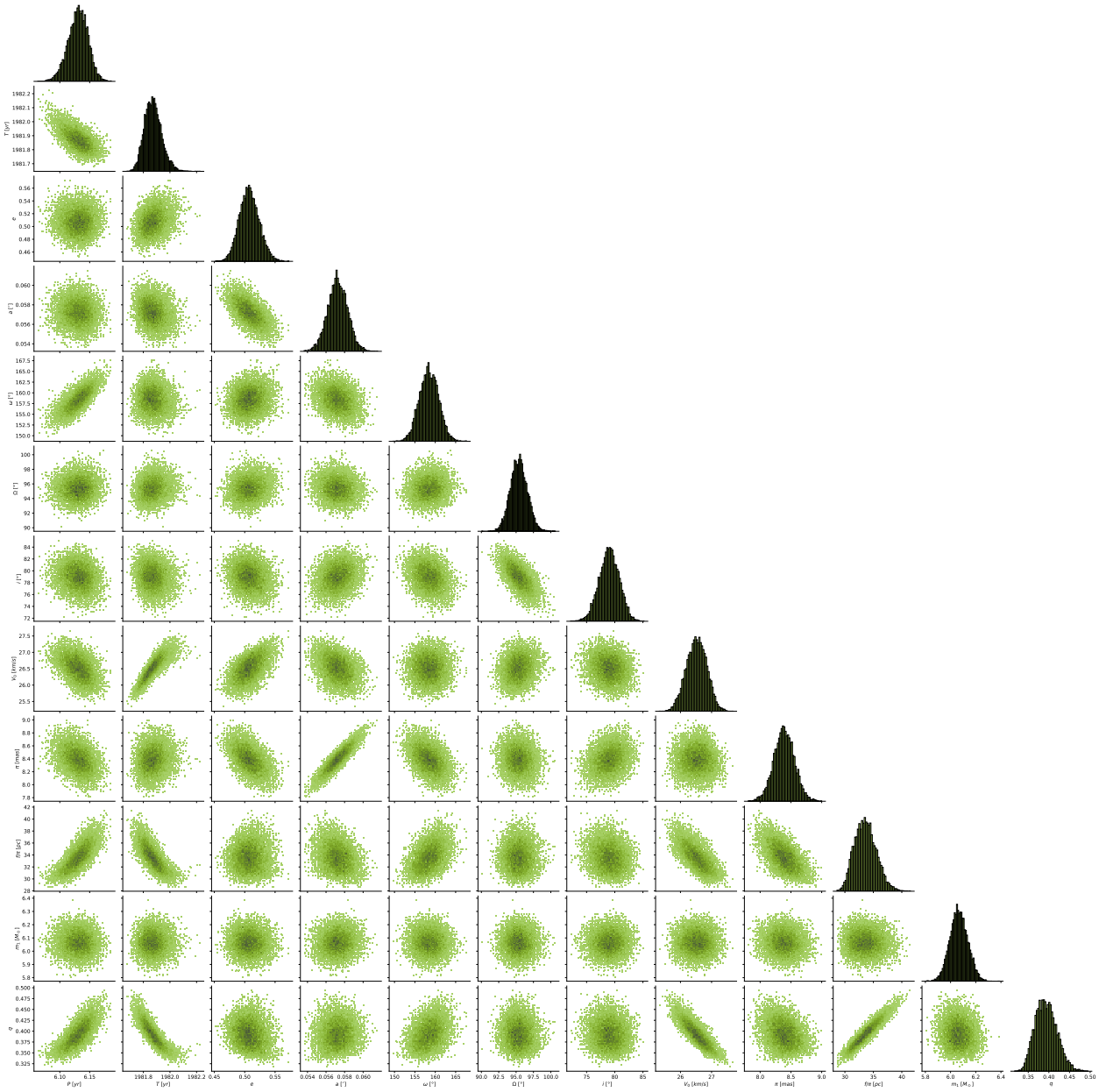

Figure 3.3: Corner plot for HIP 38414. These plots are useful for a qualitative assessment of the quality of the fit, in the sense that better defined orbits, with enough phase coverage, have tight (usually Gaussian-like) PDFs; while less-defined orbits have rather disperse, tangled and/or asymmetrical PDFs with long-tails. Corner plots can also be used to uncover possible correlations between parameters that, if found to be systematic, can eventually be used to reduce the dimensionality of the inference. This is specially useful in problems of high dimensionality. In some cases, we have used these corner plots to check the consistency of our solutions when the SpTy is ambiguous (see the case of HIP 96302, Section 3.4).

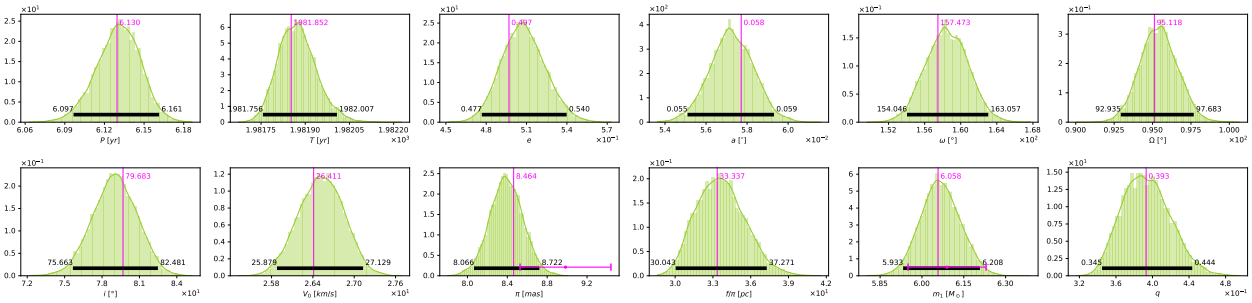

Figure 3.4: Marginal PDFs and MAP estimates (vertical magenta line) for the orbital and physical parameters of the HIP 38414 binary system, for the $SB1 + p(\varpi) + p(m_1|\theta)$ solution. The magenta horizontal error bars ($\pm 2\sigma$) indicate the priors adopted for ϖ and m_1, from Table 3.1.

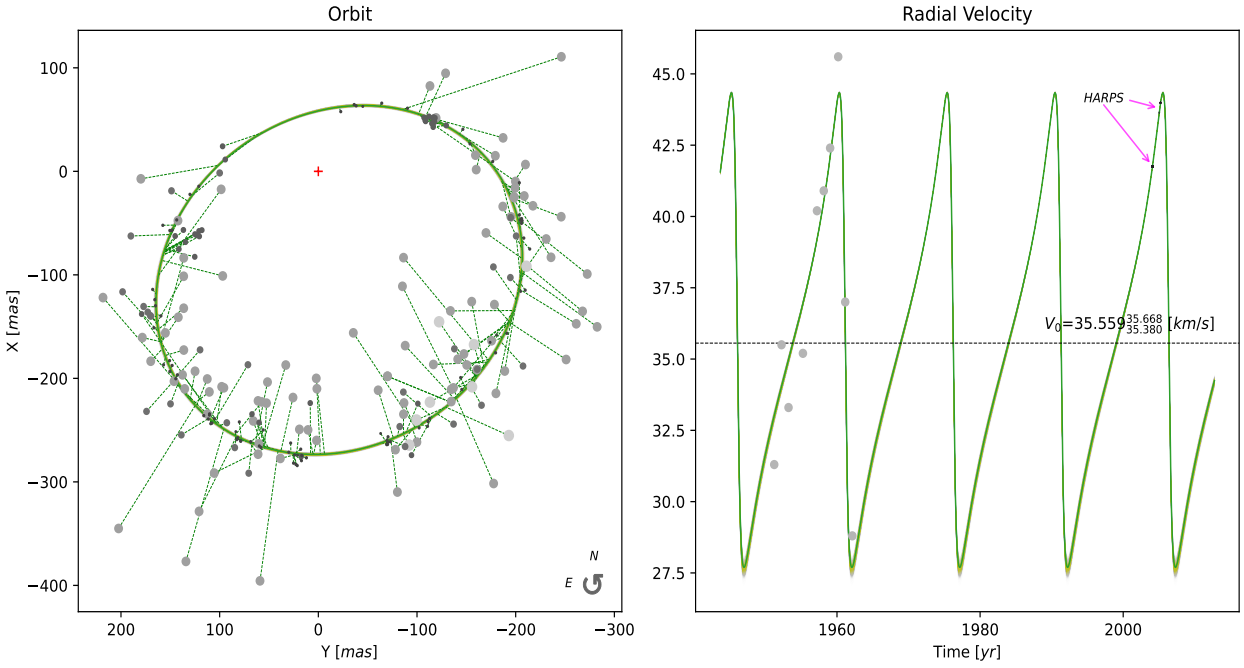

Figure 3.5: Similar to Figure 3.2 but for the HIP 43109 system. In this case we have a good orbital coverage of the visual orbit (save for a small arc near periastron). Data points included are of different quality; some are historical RVs of decent quality, and some are highly precise measurements at three consecutive epochs from HARPS at the ESO/La Silla 3.6m telescope.

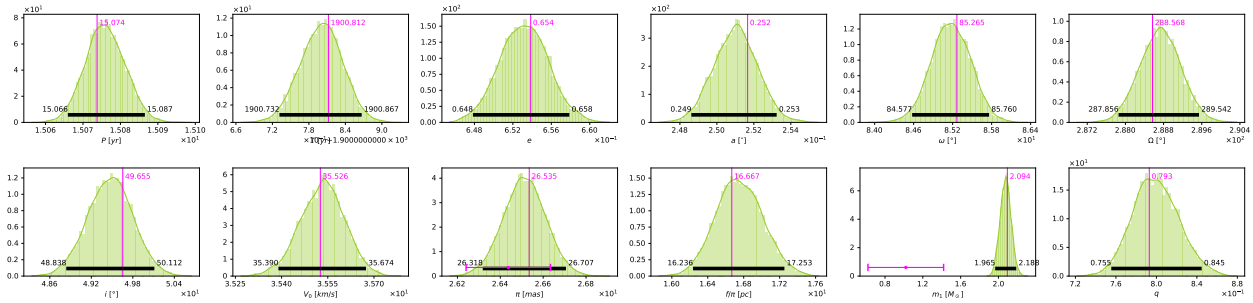

Figure 3.6: Similar to Figure 3.4 but for the HIP 43109 system.

Figures 3.2 to 3.6 show the results for two representative $SB1$ systems studied here: HIP 38414 (TOK195) and HIP 43109 (SP1AB). The corresponding figures for all other $SB1$s presented in this paper can be found at: http://www.das.uchile.cl/~rmendez/B_Research/JAA_RAM_SB1/[38]. In each case we have produced graphical results of our simultaneous fit to the astrometric and RV data (for the $SB1 + p(\varpi) + p(m_1|\theta)$ solution), corner plots, and PDFs for the orbital and physical parameters.

In Videla et al. (2022) a thorough experimental validation of the relative merits of each of the solutions was presented, depending on the prior used (see in particular Sections 3.1.4 and 3.2.4 of that paper). There we conclude that the joint estimation of the orbit and RV curves, subject to the dynamical constraints of the Keplerian motion, allows to share the knowledge provided by both sources of information (trigonometric parallax and SpTy of the primary), reducing the uncertainty of the estimated orbital elements significantly, even if one source of information is highly noisy. Furthermore, we also show that the most robust estimate of the mass ratio is that obtained when both priors ($SB1+p(\varpi)+p(m_1|\theta)$) are used simultaneously. This is true even when there are relatively large differences in the solutions when using different priors, indicative that either the SpTy or the parallax may be somewhat in error or biased.

In Table 3.5 we present a global summary of our mass determination for primaries and secondaries based on the data on Table 3.2 and the respective tables in Videla et al. (2022) (we adopt the combined solution using both priors, for the reasons explained in the previous paragraph). In Table 3.5, the upper (m_2^+) and lower (m_2^-) mass for the secondary have been computed from $q^+ \cdot m_1^+$ and $q^- \cdot m_1^-$ respectively, where the + (or −) indicates the upper (lower) value of the respective quantities from Table 3.2 and its extension (in a way, this is the worst-case scenario for the range of predicted values).

[38] In this site we also have the data used for our orbital solutions (astrometry and RVs) and their adopted errors. Our own Speckle observations are indicated as SOAR, while our RVs are indicated as FEROS or FIDEOS

Table 3.5: Estimated mass of primary and secondary components of the $SB1$ stellar systems presented in this paper, and in Videla et al. (2022), obtained when both priors ($SB1 + p(\varpi) + p(m_1|\theta)$) are used simultaneously. See text for details.

HIP #	Discovery Designation	m_1 [$M_\odot$]	m_2 [$M_\odot$]
171	BU733AB	$0.927^{0.959}_{0.907}$	$0.721^{0.762}_{0.684}$
3504	NOI3Aa,Ab	$5.765^{7.726}_{3.812}$	$4.658^{7.726}_{2.695}$
3850	PES1	$0.941^{1.012}_{0.864}$	$0.063^{0.075}_{0.054}$
5336	WCK1Aa,Ab	$0.921^{0.946}_{0.889}$	$0.182^{0.212}_{0.165}$
6564	BU1163	$1.317^{1.396}_{1.225}$	$1.275^{1.396}_{1.134}$
7918	MCY2	$1.008^{1.035}_{0.981}$	$0.289^{0.302}_{0.279}$
17491	BAG8AB	$0.828^{0.869}_{0.766}$	$0.565^{0.629}_{0.499}$
28691	MCA24	$5.334^{6.887}_{3.785}$	$2.928^{4.580}_{1.805}$
29860	CAT1Aa,Ab	$1.380^{1.407}_{1.349}$	$0.533^{0.550}_{0.514}$
36497	TOK392Da,Db	$1.200^{1.280}_{1.090}$	$0.473^{0.581}_{0.389}$
38414	TOK195	$6.058^{6.208}_{5.933}$	$2.381^{2.756}_{2.047}$
39261	MCA33	$2.265^{2.398}_{2.097}$	$1.493^{1.799}_{1.216}$
40167	HUT1Ca,Cb	$1.404^{1.455}_{1.334}$	$1.219^{1.381}_{1.103}$
43109	SP1AB	$2.094^{2.188}_{1.965}$	$1.661^{1.849}_{1.484}$
54061	BU1077AB	$2.736^{2.966}_{2.431}$	$2.566^{2.966}_{1.947}$
55642	STF1536AB	$1.417^{1.461}_{1.336}$	$1.183^{1.346}_{1.026}$
65982	HDS1895	$0.920^{0.955}_{0.878}$	$0.581^{0.826}_{0.441}$
67620	WSI77	$0.917^{0.950}_{0.855}$	$0.554^{0.595}_{0.506}$
69962	HDS2016AB	$0.752^{0.814}_{0.700}$	$0.401^{0.483}_{0.337}$
75695	JEF1	$1.982^{2.083}_{1.858}$	$1.635^{1.785}_{1.486}$
76031	TOK48	$1.182^{1.249}_{1.101}$	$1.126^{1.249}_{0.973}$
78401	LAB3	$18.090^{29.606}_{8.753}$	$10.709^{22.797}_{3.965}$
78727	STF1998AB	$1.404^{1.446}_{1.363}$	$1.383^{1.446}_{1.295}$
79101	NOI2	$2.350^{2.661}_{2.147}$	$1.699^{2.661}_{1.168}$
81023	DSG7Aa,Ab	$1.019^{1.076}_{0.972}$	$1.013^{1.076}_{0.961}$
93017	BU648AB	$1.138^{1.166}_{1.104}$	$0.686^{0.756}_{0.626}$
96302	WRH32	$2.611^{2.908}_{2.270}$	$2.496^{2.908}_{2.048}$
99675	WRH33Aa,Ab	$9.440^{10.949}_{8.048}$	$6.476^{9.964}_{5.078}$
103655	KUI103	$0.580^{0.593}_{0.569}$	$0.574^{0.593}_{0.555}$
109951	HDS3158	$0.958^{0.990}_{0.934}$	$0.922^{0.990}_{0.802}$
111685	HDS3211AB	$0.552^{0.589}_{0.514}$	$0.346^{0.414}_{0.290}$
111974	HO296AB	$1.158^{1.213}_{1.106}$	$1.155^{1.213}_{1.087}$
115126	MCA74Aa,Ab	$1.195^{1.241}_{1.151}$	$0.754^{0.804}_{0.708}$
116259	HDS3356	$1.093^{1.139}_{1.033}$	$0.637^{0.699}_{0.577}$

3.3.1. A pseudo MLR from *SB1*s

As stressed in Videla et al. (2022), the scheme applied here to $SB1$ systems can only provide informed estimates of the mass-ratio; definitive values for the individual masses of binary components can still only be obtained in the case of $SB2$ systems. It is interesting however to see how our inferred mass-ratio values compare with a well-defined MLR.

In Figure 3.7, a mass-luminosity plot, we show the position of the fifteen luminosity class V systems among our sample, superimposed to the mean fiducial lines given by Unwin et al. (2008) (their Figures 5 and 6). In this plot we have also included another eight luminosity class V systems, studied using the same methodology employed here, by Videla et al. (2022). The results included are those from the solution that provides the lowest uncertainty, which, as mentioned above, is the one that uses both priors (SpTy and trigonometric parallax) simultaneously. As can be seen from this figure, there is an overall good agreement between the location of the primaries and our inferred secondaries from the Bayesian statistical method employed here. We note that we do not pretend to build an MLR using these data; this exercise was meant to demonstrate that it is possible to derive tentative mass ratios for $SB1$ systems that could motivate further studies (e.g., to attempt detection/resolution of the secondary, given the q value and the implied luminosity).

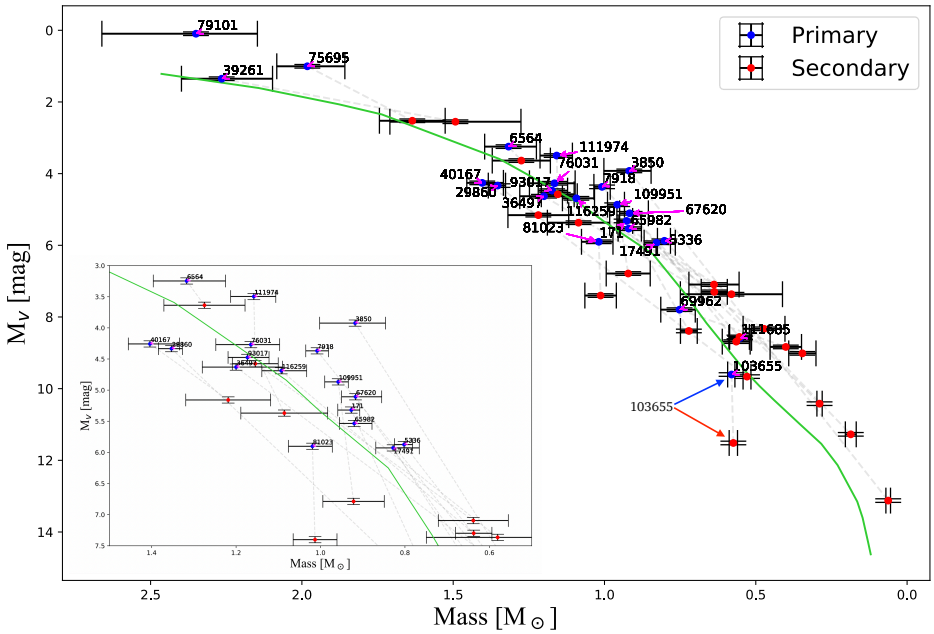

Figure 3.7: Pseudo MLR from the 23 $SB1$ systems of luminosity class V in our sample. The plot inserted shows a zoom in the mass range from 0.5–1.5 $M_\odot$, with M_V from +3.0 – +7.5. Primary components are depicted with a blue dot, and secondaries with a red dot. The components of each binary are joined by a thin dashed line (the most massive object, HIP 7901 - presented in Videla et al. (2022) - does not have photometry for its secondary, hence only the primary star is shown here). The uncertainty on the mass of the primary and secondary are directly based on the values given in the last row of each entry in Table 3.2 (and the corresponding table on Videla et al. (2022)), while we have assumed an uncertainty of ∼0.05 mag in M_V as a representative value, considering the errors in the photometry and distance.

As it can be seen on Figure 3.7, the lateral dispersion (in mass) is reasonable. Indeed, the scatter on mass of our derived secondary masses with respect to a fiducial line is small, amounting to 0.15 $M_{\odot}$ over the twenty two secondaries plotted in Figure 3.7. The mass residuals are shown on Figure 3.8.

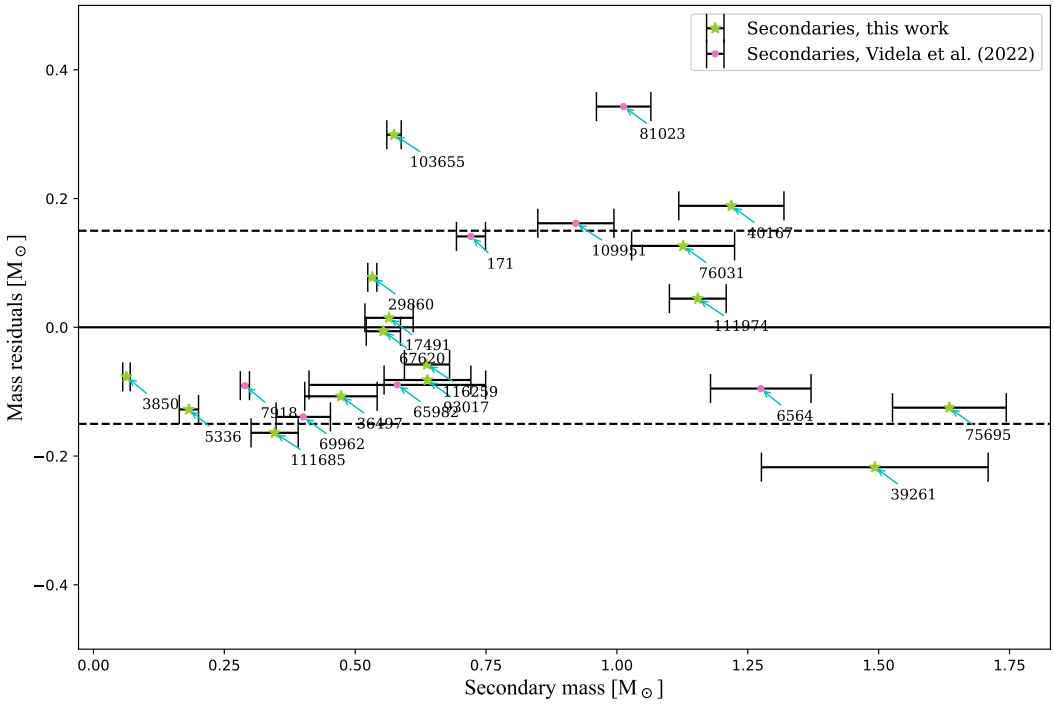

Figure 3.8: Mass residuals for the 22 Class V secondaries of Figure 3.7 (including those from Videla et al. (2022)), in comparison with the expected mass given their luminosity from the fiducial relationships from Abushattal et al. (2020) (their Table 18). The dashed lines indicate the empirical $\pm 1\sigma$ value, while the error on mass in the abscissa comes from the upper and lower values presented in Table 3.2. The labels indicate the HIP number.

3.4. Discussion of individual objects

Based on Tokovinin´s Multiple Star Catalogue (MSC[39], Tokovinin (1997, 2018b)), twelve of our studied binaries are actually in known multiple systems of different multiplicity, these are HIP 28691, 29860, 36497, 40167, 43109, 54061, 55642, 78727, 93017, 103655, 111685, and 111974. However, since we are looking at the inner (or tighter) components of these systems, their multiplicity does not seem to affect our results, based on an inspection of the residuals of our orbital solutions. The sole exception to this rule is HIP 78727, where we do see extant periodic residuals in position angle and separation, indicative of an unaccounted perturber.

[39] Updated version available at http://www.ctio.noirlab.edu/~atokovin/stars/

HIP 3850=PES1: This system has been extensively studied before by Peretti et al. (2019) using spectro-photometry and astrometry, and is a good comparison point for our methodology. The secondary is an L9-type benchmark brown dwarf which leads to the lowest mass-ratio q of our sample (the secondary is the point at the bottom right corner on Figure 3.7).

This system does not have interferometric data, but it has eight high-precision AO observations made with NACO at the ESO/VLT telescope at Cerro Paranal, Chile; covering slightly less than 10 yrs of baseline. The orbital parameters have relatively large errors (specially the Period, with a range from 28–34 yrs), which is a consequence of the small number of observations and the restricted orbit coverage of the available astrometric data. We note that the value of $\omega = -94.2°$ reported in SB9 is not inconsistent with our value of $+264.3°$.

Precise RVs are available from observations made with CORALIE on the Swiss/ESO 1.3m telescope at La Silla, Chile (Sahlmann et al. (2011)), but they cover only 10.3 yrs of the orbit. The SpTy published in WDS is G9V, and G8/K0V in SIMBAD, so we adopted G9V. It is interesting to note that Peretti et al. (2019) derive a primary mass of $0.856 \pm 0.014\ M_{\odot}$ and a secondary mass of $70.2 \pm 1.6\ M_{\rm Jup}$ from spectro-photometric data, giving a mass ratio of $q = 0.0783 \pm 0.022$, while our best solution (last line on the first row of Table 3.2) gives an inferred value of $q = 0.067$, i.e., less than 1σ of their reported value. This gives a strong support to the adequacy of our methodology. Although its semi-major axis is at the (lower) edge of resolution by Gaia (0.53 arcsec), the large magnitude difference between primary and secondary (9.2 mag) leads to a small RUWE of 0.93, while the Hipparcos and Gaia parallaxes are equal within less than 1σ (considering the Hipparcos uncertainty). Our systemic RV $V_0 = 9.926 \pm 0.025$ kms^{-1} compares well with the value reported by Gaia[40] of 9.71 ± 0.12 kms^{-1}.

HIP 5336=WCK1Aa,Ab: This is the system with the second lowest-q. There is abundant historical and recent astrometric data covering most of the orbit (including high-resolution imaging secured with the Hubble Space Telescope, spanning almost two decades), as well as good precision RV data. While SB9 indicates that a combined spectroscopic+visual solution has already been obtained by Agati et al. (2015), the authors do not list all the orbital elements of their orbit (see second line on second row on Table 3.2). On the contrary, our combined MCMC solution seems quite robust, with low formal uncertainties. Bond et al. (2020) have performed a more recent and detailed spectro-photometric and astrometric study of this system, obtaining $0.7440 \pm 0.0122\ M_{\odot}$ for the G5V primary and $0.1728 \pm 0.0035\ M_{\odot}$ for the dM companion, implying a $q = 0.2335 \pm 0.0061$, which compares quite well with our inferred value of $q = 0.198 \pm 0.026$ considering our uncertainty. Our inferred mass for the primary ($0.921 \pm 0.032\ M_{\odot}$) is smaller than that expected for a G5V used as prior ($1.05 \pm 0.04\ M_{\odot}$; see Table 3.1, and the PDF on the web page), and it is more consistent with a G9V. Incidentally, the apparent magnitude for the primary from WDS and the parallax do imply an SpTy of G9-K0V. This object has a very large proper-motion, $(\mu_{\alpha}\cos\delta, \mu_{\delta}) = (3468.25 \pm 0.35, -1564.94 \pm 0.37)$ mas, and a large negative systemic velocity $V_0 = -97.5$ kms^{-1} (see 10th column on Table 3.2), indicative of Halo-like kinematics (the RV given by Gaia is -97.09 ± 0.25 kms^{-1}). Indeed, its measured metallicity indicates [Fe/H] ~ -0.75, the lowest measured value in our sample. Despite the large magnitude difference between primary and secondary (5.4 mag), it has a large RUWE (7.0). There is a large dif-

[40] The RVs in the Gaia catalog result from the average on a variable time window (depending on the number of scans through the source), and covers up to 34 months of observations, Katz et al. (2022).

ference between the HIPPARCOS and Gaia parallaxes (more than 2 mas), probably because it is nearly resolved by Gaia (semi-major axis of 1.0 arcsec), being the nearest object in our sample, at 7.7 pc. There is a difference of 180° between ω and Ω determined by us, and the corresponding values obtained from the astrometry alone (from Orb6). This is a well known ambiguity that can only be resolved by RV data.

HIP 17491=BAG8AB: This object has a pretty good interferometric coverage of the orbit, except near periastron, and high-precision RV observations covering more than one period that were obtained with CORAVEL on the Danish/ESO 1.5m telescope. As a prior for the SpTy, we adopted K0V, from SIMBAD, which is quite close to that given on WDS (G9.5V), and which seemed more adequate given the (Gaia) parallax. There is however a rather large discrepancy between the HIPPARCOS and Gaia DR3 parallaxes (38.63 ± 0.79 *vs.* 40.33 ± 0.25 mas respectively). Our MAP parallax obtained from the combined solution is quite similar to that of Gaia (40.08 mas; see 11th column on last line of third row in Table 3.2), despite the fact that the RUWE for this objects is the second largest of our sample (see Table 3.1). This in principle indicates that the Gaia parallax could be biased, but it may be that the possible bias is being alleviated by the large brightness contrast: the primary has $V = 7.9$ while the secondary has $V = 10.7$, and hence the photocenter is almost coincident with the primary itself. A combined orbit is also reported by Balega et al. (2002), but it is not included on SB9 (only on Orb) and hence no systemic velocity from this combined fit is available. Our value of 22.31 ± 0.13 kms^{-1} is not incompatible with the Gaia at 26.44 ± 0.61 kms^{-1}, considering the amplitude of the velocity curve (see our web page with figures). Based on the Balega et al. (2002) study, Malkov et al. (2012b) report a $q = 0.723 \pm 0.074$ which is within 1σ of our value ($q = 0.682$).

HIP 28691=MCA24: This is a triple system with an inner binary AaAb, but our analysis refers to the AB system alone (i.e., we used the center-of-mass velocity of the AaAb pair, and the astrometry for AB). It is difficult to observe because the orbit is seen nearly edge-on, and has a small semi-major axis ($a = 53$ mas) and a large eccentricity ($e = 0.74$). There is no data on the vicinity of periastron, and the astrometric data (including six recent data points, epochs 2015.9 to 2019.1, from our Speckle survey) covers only a small fraction of the orbit. This is compensated, in part, by abundant spectroscopic observations that cover several periods. In WDS its SpTy is listed as an B8III, but in SIMBAD, B8V is indicated. Based on the available photometry and trigonometric parallax, we find the primary to be more consistent with a B8III and at a distance of about 262 pc (in agreement with the analysis by Fekel & Scarfe (1986)). This is the most distant system, and the second most massive of our sample. A combined spectroscopic/astrometric solution has already been obtained by Scarfe et al. (2000) but our new data adds a handful of points that merits a revision of their solution. Independently, Tokovinin et al. (2020) published a purely astrometric orbit (listed in the Orb6 line of the corresponding entry in our Table 3.2). As it can be seen from that table, our values for the combined solution in particular for P and a are both slightly smaller than those from Tokovinin et al. (2020), and with slightly larger errors; about halfway from the SB9 values (at least for P). Our MAP parallax is found to be 4.1 mas, close to the Gaia parallax of 3.8 mas, and within 1σ of their uncertainties. In contrast, the Hipparcos parallax for this system is reported to be 4.54 ± 0.29 mas, which is probably biased. The same correction on ω and Ω as for HIP 5336 is seen in this system (see Table 3.2).

HIP 29860=CAT1Aa,Ab: This is the first fully combined orbit for the AaAb sub-system (WDS name CAT*1) of this apparently septuple system. It has the largest eccentricity ($e = 0.83$) of the objects in our sample. Less than half the orbit is covered, mostly by our own Speckle data secured between 2008 and 2020. Old, low-precision RV data, has been supplement with recent data from our FIDEOS and FEROS monitoring program (with formal uncertainties on the order of 0.01 kms^{-1}), which has greatly helped to pin-down the period. Our first attempts to fit the orbit with our astrometric + RV data failed miserably because the RVs published on SB9 were completely off-scale. A careful look at the source of those RVs on Katoh et al. (2013) shows that some arbitrary zero-point offsets were applied to the old data to conform to their own data. These authors however, were not concerned with the systemic velocity[41]. Specifically, in their Table 3, they indicate offsets of -5.2550 and -14.2000 kms^{-1} applied to data from Vogt et al. (2002) and Beavers & Eitter (1986) respectively, in order for these data to conform to theirs. Because our data indicates that RVs from Katoh et al. (2013) are completely off, we undid these corrections, applying offsets of +14.2000 kms^{-1} to the data from Katoh et al. (2013) (effectively putting the RV scale on the zero point of Beavers & Eitter (1986)), and of +8.945 kms^{-1} to the data from Vogt et al. (2002), while not applying any offset to the data from Beavers & Eitter (1986). These were the historic RVs used for our fits, and available on the data tables in the web page http://www.das.uchile.cl/~rmendez/B_Research/JAA_RAM_SB1/. The final combined fit to this system is shown in Figure 3.10, which shows the excellent correspondence between the (corrected) RVs from Vogt et al. (2002) (epochs 1996 to 2001, near periastron) and Katoh et al. (2013) (epochs 2006 to 2009) with our recent data points from FEROS and FIDEOS. In Figure 3.9 we show the corresponding PDFs. Our systemic velocity, 9.556±0.005 kms^{-1} agrees reasonably well with the Gaia value at 8.70 ± 0.20 kms^{-1} (certainly within the RV curve, see right plot on Figure 3.10), giving us further confidence on our zero-point re-normalization procedure.

In the notes of Orb6, it is indicated that the individual masses are 0.96 ± 0.18 $M_{\odot}$ and 0.67 ± 0.04 $M_{\odot}$ from Catala et al. (2006), derived from ground-based AO observations of the AaAb pair made with the CFH telescope at Mauna-Kea, plus the RVs from Vogt et al. (2002) alone. The CFH observations cover however a very short arc (3 years) considering the orbital period (44 years). They reported a period of 28.8 ± 1.1 yr which is significantly smaller than all values published since then (see Orb6 and SB9 values), including our own fitted value. Their semi-major axis is also smaller, $a = 0.621 \pm 0.019$ arcsec. Our derived primary mass is somewhat larger, at $1.38 M_{\odot}$, leading to a smaller q (0.386 ± 0.005) than that implied by Catala et al. (2006) (0.491 ± 0.064), albeit within 1.6σ of their inferred value and errors. We note that our PDFs indicate that the posterior mass for the primary actually tends to be slightly larger than the input a-priory mass for an F9.5V (1.15 $M_{\odot}$) from Abushattal et al. (2020), while the a-priory and the posterior parallax are, within the errors, commensurable to each other (see Figure 3.9).

[41] Indeed, in the notes on SB9 it says: "No systemic velocity provided in the paper, the value reported and the offset have been supplied by the author directly".

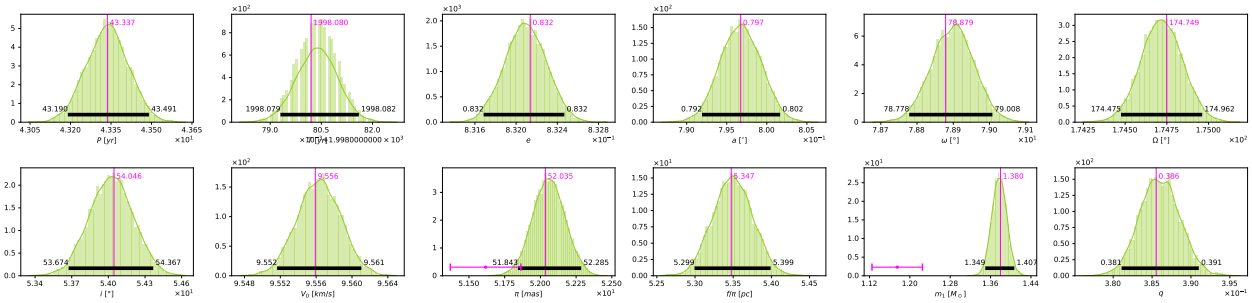

Figure 3.9: Same as Figure 3.4 but for the HIP 29860 binary system.

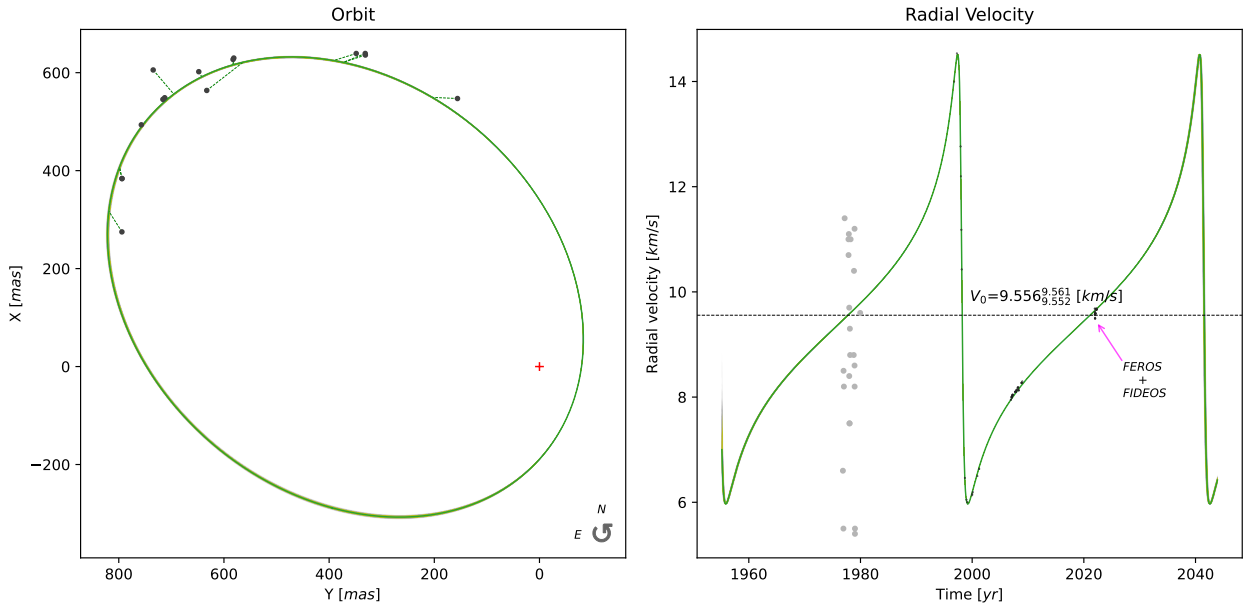

Figure 3.10: Similar to Figure 3.2 but for HIP 29860. For this system, the visual orbit is incomplete, with a severe lack of observations near periastron. Old RV data show a large scatter, while modern data and our own data from FEROS and FIDEOS (obtained in 2021 and 2022 - indicated in the plot), are of much higher quality. This helped to constrain the final orbit which, as indicated in Table 3.2, has a formal uncertainty of 0.3 % in the period, and 0.6 % in the semi-major axis.

HIP 36497=TOK392Da,Db: Ours is the first combined orbit for this $SB1$ binary which is member of a quadruple system. About one-half of the astrometric orbit of the pair is covered by our Speckle data. Previous attempt with the Robo-AO system failed to resolve the binary (Riddle et al. (2015)). There is abundant high-quality RV data secured with CORAVEL, covering almost three full periods. There is no ambiguity in the SpTy (F8V). Despite its elevated RUWE (5.80), the Hipparcos, Gaia, and our own MAP parallaxes agree well. Once again, as it was the case for HIP 17491, the primary has $V = 8.0$ mag while the secondary has $V = 11.7$ mag, so, the photocenter is almost coincident with the primary itself, which could explain the high RUWE. Our systemic velocity of -2.43 ± 0.20 kms^{-1} is compatible with the Gaia value at -2.07 ± 0.43 kms^{-1}.

HIP 38414=TOK195: Ours is the first combined orbit for this relatively short period $SB1$ system at about 110 pc from the Sun. The K1/2II red giant primary component is the most massive primary object (6.1 $M_\odot$) of our sample. The few historic (from the 1980's) RV points taken from Parsons (1983) supplement our own RVs derived from FEROS and FIDEOS observations secured on 2022, which greatly helped our joint solution. The astrometric data covers about one-half of the orbit and is all from our SOAR program. The somewhat elevated residuals are due to the small semi-major axis (62 mas) and the large inclination (almost 80°; see Figure 3.2[42]). While the RUWE value is large (6.0), the difference between the Hipparcos and Gaia parallaxes is small, less than 0.3 mas, within 1σ of the Gaia uncertainty. Our MAP orbital parallax is 8.46 ± 0.40 mas, 0.79 mas smaller than the Gaia parallax, but almost within 1σ considering the Gaia error (see Figure 3.4). Finally, it is noteworthy that, given its parallax and photometry, the absolute magnitude ($M_V = -1.0$) is not consistent with a K1.5II star. According to Straižys & Kuriliene (1981), their Table II, it is about $M_V = -2.5$. We have no explanation for this discrepancy.

HIP 39261=MCA33: About one-half of the astrometric orbit has been covered for this object and there is abundant RV data of variable precision covering more than two revolutions. According to the notes on Orb6, the mass sum for this system reported in the literature spans a wide range; from 4.1 $M_\odot$ (Scholz & Lehmann (1988)), or 3.61 ± 0.38 $M_\odot$ (according to Balega et al. (2004)); to 1.49 ± 0.66 $M_\odot$ (from Carrier et al. (2002)). Our inferred total mass of the system, based on the results of Table 3.2, is 3.73 ± 0.32 $M_\odot$ and is within 1σ of the joint astrometric+spectroscopic solution of Balega et al. (2004)). The PDF for the parallax indicates that our solution has a slightly smaller value than that of Gaia, but within 1.2σ, so our mass estimate does not seem to be affected by the small inferred parallax. The Hipparcos parallax, at 10.13 ± 0.52 mas, agrees well with Gaia (despite the elevated RUWE at 5.9) and with our MAP parallax.

HIP 40167=HUT1Ca,Cb: Ours is the first combined orbit. This $SB1$ system is the CaCb subsystem of a septuple (and, possibly, octuple) system. The coverage of the orbit is good; the last 13 points being from our Speckle survey (2016.9 to 2021.0). The first astrometric measurement is from Hipparcos (1991.25). It also has abundant RV data of reasonable precision covering slightly more than one period. WDS reports a SpTy of M1 (likely referring to the D member; see below), but this does not seem adequate for our object: both, apparent magnitude and distance indicates that the primary (Ca) is a late F (F9; adopted by us). The only paper devoted to this subsystem in particular (see Section 3 in Hutchings et al. (2000)) indicates: "...thus, we conclude from the color differences that C and D have SpTy G0 and M2, respectively, with an uncertainty only on the order of one spectral subtype." Indeed, the photometry for Cb indicates an SpTy of G5-G6V, while the photometry for the D component indicates an M0.

HIP 43109=SP1AB: This $SB1$ binary is the AB pair ($a = 0.25$ arcsec) of a quintuple system. It has a good orbital coverage, including historical data of lower precision and more recent interferometric data (including points in 2001.1, 2014.3, 2018.3, and 2021.2 from our survey), except near periastron. There was no data included in SB9, but we recovered the

[42] Indeed in the notes to Orb6 it says: "The binary is difficult to measure, always close to the diffraction limit (on a 4m telescope), and with a magnitude difference ∼3."

original RV measurements from Adams (1939) and Underhill (1963) which encompass about one full revolution. This system has recently been observed with HARPS (Trifonov et al. (2020)): https://vizier.u-strasbg.fr/viz-bin/VizieR?-source=J/A+A/636/A74 at 2004.1 (214 measurements), 2005.0 (1 measurement) and 2005.2 (seven measurements)[43]. The new RVs, with uncertainties below 0.01 kms^{-1}, greatly helped constrain the overall fit, which is shown in Figure 3.5. While the published SpTy differ, namely F8V in WDS and G1III in SIMBAD, the apparent magnitude and parallax render it more consistent with the primary being a giant G1III with a mass of 1.02 $M_{\odot}$ (adopted as prior). However, the MAP mass for the primary from our combined fits leads to a mass that is a factor of two larger, indicating it is a more massive and younger object (see Figure 3.6). Indeed, according to SIMBAD, it is known to be a fast rotator and variable; both characteristics being indicative of youth. A similar correction on ω and Ω with respect to the Orb6 values as that found for HIP 5336 is seen in this system (see Table 3.3).

HIP 54061=BU1077AB: Ours is the first combined orbit. This giant of SpTy G9III has a good orbital coverage, except for a short arc near periastron where the small separation has precluded so far a definitive resolution. The astrometric data includes historical micrometric observations dating back to 1889, as well as interferometric data as recent as 2017. The RVs, which encompass one full orbit, are from the old work by Spencer Jones & Furner (1937), and have a rather large scatter. Initially, it was thought to have a very small inclination (fixed at 180° in the Hipparcos solution, see Söderhjelm (1999b)), but the inclination is now firmly determined: retrograde, at $167.2 \pm 2.1°$ (see Table 3.3). The PDF for the mass indicates a larger mass (2.7 $M_{\odot}$) than the input a-priory value (1.93 $M_{\odot}$ given its SpTy, see Table 3.1). As it can be seen on Table 3.3 (4th and 5th lines), this could be due to an erroneous parallax. Indeed, this object does not have a published parallax from Gaia, and the Hipparcos value has a rather large uncertainty. A purely astrometric mass sum of high-quality has been obtained by Baines et al. (2018) with the Navy Precision Optical Interferometer, leading to 3.44 ± 0.11 $M_{\odot}$. This value is consistent with our $SB1 + p(m_1|\theta)$ solution, which gives 3.32 ± 0.68 $M_{\odot}$, but very far from our $SB1 + p(\varpi)$ solution, 5.7 ± 1.6 $M_{\odot}$. This is puzzling considering that they adopted the same Hipparcos parallax. Using both priors simultaneously, we obtained a mass sum of 5.32 ± 0.57 $M_{\odot}$, i.e., 3.3σ larger than that derived by Baines et al. (2018). Of course, another possibility is that both WDS and SIMBAD are erroneous in the SpTy for the primary. The parallax and photometry indicate an earlier SpTy of B8-B9III, which according Abushattal et al. (2020) would imply a mass of around 4 $M_{\odot}$, which is indeed close to our $SB1 + p(\varpi)$ solution which gives 3.8 $M_{\odot}$ for the primary (see Table 3.3). The scarcity and relatively low quality of the available RV data suggests that a better coverage of the RV curve with modern spectrographs, should help solve this puzzle. A similar correction on ω and Ω with respect to the Orb6 values as that found for HIP 5336 is seen in this system (see Table 3.3).

HIP 55642=STF1536AB: This is the tighter $SB1$ binary -AB- of a triple system. Abundant astrometry of relatively good quality, and covering the whole orbit, is available for this 184+ yrs period system (it is the system with the longest period in our sample). Two interferometric observations from SOAR, at epochs 2018.3 and 2021.3, are included. No RV

[43] Incidentally, in the notes on SB9 it is indicated: "High-dispersion observations have been continued at Victoria by C.D. Scarfe, and it should be possible soon to give a definitive spectroscopic orbit of this system."

data are given in SB9; only the references (Campbell & Moore (1928a), Harper (1928), Petrie (1949), and Abt & Levy (1976)) from which we have extracted the RV data. To these, we have added 13 extra recent (2021.5 to 2022.3) high-precision RV measurements obtained with FIDEOS, which fit very well in the RV curve. Our adopted prior parallax is the unweighted average from Gaia DR2 (no data for this object on DR3) for the AB and C components (separation of 5.5 arcmin). The SpTy reported is F4IV in WDS and F3V in SIMBAD, but the photometry and parallax indicate that the primary is a sub-giant of type F0. We thus adopted the SpTy reported in WDS. Our systemic velocity of -11.166 ± 0.041 kms^{-1} is in reasonable agreement with the Gaia value at -7.5 ± 2.7 kms^{-1}, specially considering the large formal uncertainty of the Gaia measurement.

HIP 67620=WSI77: Pretty good coverage of the astrometric orbit. All but one data point are from our HRCam observations made with SOAR. Almost 1.5 revolutions are covered by the RV curve, including 24 recent data points from HARPS (Trifonov et al. (2020)), at epochs 2012.2 to 2013.2, which match the orbit very well. The elements given in SB9 are from the spectroscopic-only study by Willmarth et al. (2016), but there is however a previous combined orbit + RV solution from Tokovinin (2012b) (given in the Orb6 line of the corresponding row in Table 3.3), which compares quite well with our values (see his Table 3). The solution from Tokovinin (2012b) implies masses of $m_1 = 0.99\ M_\odot$ and $m_2 = 0.63\ M_\odot$, which are equivalent to our $m_1 = 0.917 \pm 0.048\ M_\odot$ and $m_2 = 0.554 \pm 0.043\ M_\odot$ given on Table 3.3. Our calculated systemic velocity is 5.361 ± 0.039 kms^{-1}. The Gaia value has a huge error (17 ± 23 kms^{-1}) which precludes a proper comparison. The Hipparcos and Gaia DR2 parallax (adopted by us as prior) differ quite substantially, being 53.88 ± 0.34 mas and 51.35 ± 0.4 mas, respectively. Our inferred MAP value is 53.10 ± 0.74 mas, closer to the Hipparcos parallax. There is no parallax on Gaia DR3 for this system (hence no RUWE either).

HIP 75695=JEF1: Pretty good orbital coverage, including periastron. There are data of various quality, including interferometric measurements, the last of which from our SOAR program (two data points on 2019.1). Historical RV data of good quality, spanning one full orbit, is available from 1930 to 1943, and there also is earlier scattered data from 1902 to 1913 (Neubauer (1944)), all of which fit the orbit quite well. While there is a parallax from Gaia DR3 (27.93 ± 0.97 mas, albeit with a large RUWE, 7.3) its formal error is 20 % larger than that of Hipparcos (29.17 ± 0.76 mas), so we opted to use the Hipparcos value as a prior. Interestingly enough, our MAP parallax resulted to be 28.07 ± 0.44 mas (see Table 3.3), within less than 1σ of the Gaia value (see the PDF in the web page). While SIMBAD indicates a type F2V, and WDS A5V, the photometry and parallax is more consistent with an earlier type, so we adopted WDS's type as a prior. The combined orbit solution by Muterspaugh et al. (2010) gives $m_1 = 1.71 \pm 0.18\ M_\odot$ and $m_2 = 1.330 \pm 0.074\ M_\odot$, while we obtain slightly larger masses, $m_1 = 1.98 \pm 0.12\ M_\odot$ and $m_2 = 1.63 \pm 0.12\ M_\odot$ respectively. This is perhaps due to our smaller MAP parallax (they used the Hipparcos value). Of all the objects in our sample, this one has the largest measured metallicity, at [Fe/H] $\sim +1$, however its location in the MLR (indicated in Figure 3.7) coincides with that of the solar-metallicity mean relationship.

HIP 76031=TOK48: Ours is the first combined orbit. The orbital coverage of this tight pair ($P = 1.7$ yrs, the shortest-period system in our sample) is poor, less than half the orbit. All data available is from our SOAR interferometry and covers epochs from 2009.3 to 2021.3 (15 data points). Due to the small separation, data are lacking near periastron, implying a relatively large uncertainty in the inclination ($i = 152.0 \pm 2.2°$). Fortunately, we have RV of good quality covering several periods, which helps to constrain the fit. We adopted as prior the Hipparcos parallax (19.67 ± 0.89 mas; this is the object in our sample with the largest parallax error, after HIP 111685) due to its smaller formal error (no parallax is given on Gaia DR3, while on DR2 it is 23.56 ± 1.2 mas). Our fitted MAP value for the orbital parallax resulted to be 21.18 ± 0.92 mas. Our fitted systemic velocity, 4.68 ± 0.37 kms^{-1}, disagrees slightly with the Gaia value at 6.2 ± 3.8 kms^{-1}, but note the large formal uncertainty of the Gaia measurement. Also, given the short period of the system, the Gaia value is not incompatible with the RV excursion from -2.5 kms^{-1} to about +16 kms^{-1} seen in the RV curve (see figures in web page).

HIP 78727=STF1998AB: This $SB1$ is the inner pair -AB- of a quintuple system. It has a good coverage of the astrometric orbit since 1825, with data of various quality, including a few data points from our survey at epochs 2008, 2017 and 2019. There are no data on SB9, but we recovered old results from Campbell & Moore (1928b) and Chang (1929). Unfortunately they cover less than a period and are of relatively low quality, as result of which our fitted value of V_0 is rather uncertain. In Gaia DR3 there is a double parallax: based on the coordinate, the first one in the catalog is for the C component and the second one is for the A component (RUWE is nearly 1.3 in both cases, not that large). The value in Table 3.3 refers to the unweighted average of both. As for the SpTy, WDS lists the primary as F5IV, while SIMBAD gives F7V, but the parallax and photometry leads us to believe that the primary is a sub-giant, thus we adopted F5IV as prior. Tokovinin (2020) has reported $m_1 = m_2 = 1.53\ M_\odot$, which is similar, but slightly larger than our values of $m_1 = 1.404 \pm 0.042\ M_\odot$ and $m_2 = 1.383 \pm 0.054\ M_\odot$. As mentioned in the introduction to this section, this system exhibits periodic residuals after the MCMC orbital fit, most notably in position angle, with a peak-to-peak amplitude of about 14 degrees (see Figure 3.11 top left panel), and a period comparable to that of the system itself ($\sim$ 50 yr, top right panel). The trends are less evident in separation (middle panel) or radial velocity (lower panel). It is unlikely that this is a perturbation to the Keplerian orbit induced by the C companion, located almost 8 arcsec away (in comparison with the less than 1 arcsec separation of the AB system), and with an estimated period of more than 1,500 yr, according to Tokovinin´s MSC catalogue. The extant residuals may indicate the presence of an as yet unidentified third body in the AB system itself, an aspect that needs to be further investigated.

HIP 93017=BU648AB: Ours is the first combined orbit. At a distance of almost 15 pc, this is the second nearest $SB1$ system in our sample. It is the host of an exoplanet with a 2.8 yrs period. The coverage of the visual orbit is quite complete, including periastron passage, and the data available is in general of good quality. The RVs obtained from the exoplanet campaign (see Duquennoy & Mayor (1991b)) cover only a tiny fraction of the orbit (the period of the binary is 61 yrs), but this has been supplemented with newer data in Abt & Willmarth (2006a), downloaded from Abt & Willmarth (2006b), which covers from 2001.5 to 2004.4 (see data tables on web page). There is good correspondence between our systemic velocity, -45.97 ± 0.11 kms^{-1}, and that reported by Gaia DR3 at -43.00 ± 0.23 kms^{-1}.

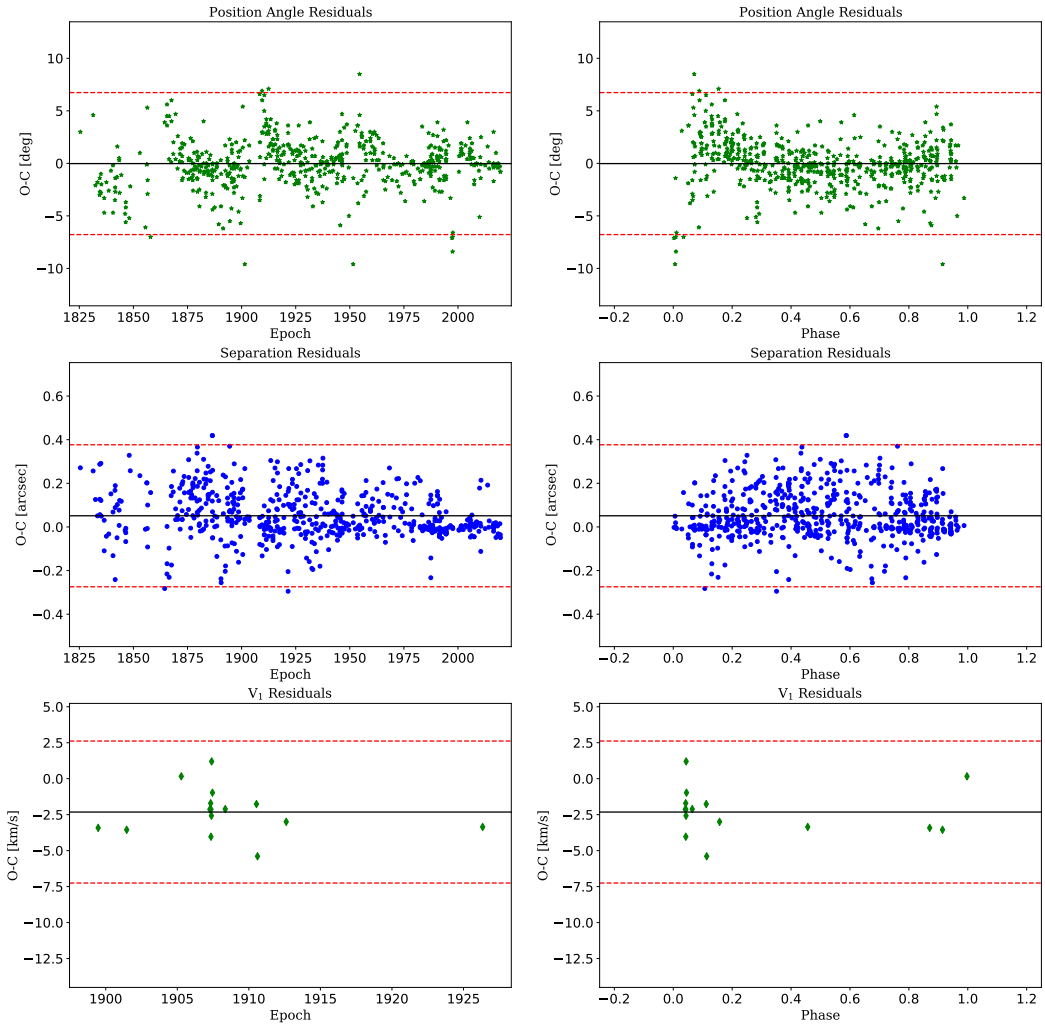

Figure 3.11: Residual O−C plots for HIP 78727 based on our MCMC solution with the orbital parameters indicated in Table 3.3. The dashed lines indicate the 3σ boundaries computed from the overall rms on each panel. There is a clear indication of a significant wobble in position angle, with a period of about 50 yr (top panel), possibly due to an unknown companion to the AB system (see text for details). There are hints of some periodicity in the separation residuals as well (middle panel), but less significant. Scarce radial velocity data precludes us from any conclusion based on the lower panel.

HIP 96302=WRH32: Ours is the first combined orbit. This tight binary (separation of 25 mas) is the most compact system in our sample. At nearly 186 pc, it is the second most distant target in our sample. It has scarce astrometric data covering only one-half of the orbit which excludes periastron (where the separation becomes a few mas). It has plenty of RV observations covering several cycles, including old and new higher-precision data, hence the period is very well determined. There is a large discrepancy in the published values for the SpTy of the primary: A0V in WDS and G8III in SIMBAD. Its photometry and parallax are incompatible with both of these SpTy, predicting either a B6-7V or a B9III; in both cases much more massive than our inferred value (indeed, see the $SB1+p(\varpi)$ solution in Table 3.4). In the end, for our prior, SIMBAD's SpTy was adopted based on the appearance and consistency of our MCMC corner plots for this solution. We note that, with a moderate RUWE of 1.5, the Hipparcos and Gaia values are consistent with each other; 5.37 ± 0.10 mas and 5.84 ± 0.31 mas respectively, while our MAP orbital parallax is 5.46 ± 0.22 mas. The Hipparcos parallax was adopted as prior.

Our inferred mass values are somewhat different than previously published values, with a more massive secondary; Martin et al. (1998) derive 3.344 ± 1.165 $M_\odot$ and 1.586 ± 0.612 $M_\odot$, whereas we obtain 2.61 ± 0.32 $M_\odot$ and 2.50 ± 0.33 $M_\odot$ for m_1 and m_2 respectively. Note the smaller errors of our combined solution. There is good correspondence between our systemic velocity, -17.20 ± 0.17 kms^{-1}, and that reported by Gaia DR3 at -15.8 ± 1.9 kms^{-1}.

HIP 103655=KUI 103: This is a triple hierarchical system AaAb,B (AaAb is not resolved). Our solution refers only the AB system, and we treat it as a binary. While AB is considered as $SB2$ in SB9, it has only two measurements of the secondary component. As a result, our MCMC code was unable to converge to a reasonable binary solution, so we decided to treat it as an $SB1$ until more data is secured for the B companion. It has a coverage of about 3/4 of the astrometric orbit with data of reasonable quality. In RV, the phase coverage of the primary is only about one-half the orbit, near periastron. Pourbaix (2000) has published a combined solution, treating it as an $SB2$, but his solution is highly unreliable, the individual derived masses being 3.0 ± 2.7 $M_\odot$ and 1.00 ± 0.65 $M_\odot$. These masses are however incompatible with the SpTy of the primary being M2V, as indicated by both WDS and SIMBAD. These SpTy are furthermore consistent with the apparent magnitude and distance as derived from Gaia DR3 parallax of 66.554 ± 0.072 mas (which in turn is also consistent with the Hipparcos parallax at 65.4 ± 1.8 mas, despite the large RUWE=5.2). Our derived mass for the primary, 0.580 ± 0.013 $M_\odot$, is somewhat larger than that implied from its SpTy (0.43 $M_\odot$, from Abushattal et al. (2020)). The same is true for the secondary, for which $q = 0.990 \pm 0.014$ $M_\odot$, implying 0.574 ± 0.015 $M_\odot$, while its apparent magnitude and parallax would suggest a SpTy for the secondary of M4-M5, with an implied mass of $0.24 - 0.31$ $M_\odot$. We note however that both, WDS and SIMBAD, suggest an earlier type for the secondary, M0.5V (and corresponding mass of about 0.5 $M_\odot$), in agreement with our result. This solution however poses a problem, because in the MLR, HIP 103655B is located far below the mean relationship (see Figure 3.7), which is because its mass ratio is almost one, but the photometry indicates a $\Delta m \sim 1.9$). We have no explanation for this discrepancy, but, despite these inconsistencies, we can conclude that our solution for this system is more reliable than that presented by Pourbaix (2000).

HIP 111685=HDS3211AB: Not a lot of data is available, but it is well spread in both the orbital and RV phase coverage. There is a large discrepancy between the Hipparcos (51.2 ± 1.6 mas) and Gaia DR3 (46.89 ± 0.56 mas) parallaxes. This latter has a very large RUWE (32), which renders the Gaia solution somewhat questionable. Indeed, our solutions are more reliable and consistent adopting as prior the Hipparcos parallax (despite having the largest parallax uncertainty of our sample), leading to a MAP orbital parallax of 54.0±1.4 mas about 5σ larger than the Gaia value. While SB9 reports a combined solution, full orbital parameters are not provided in this catalog (see Table 3.4).

HIP 111974=HO296AB: Very good coverage of the visual orbit, with abundant and well spread historical data, as well as newer higher precision data. This includes 20 HRCam data points from our survey, between 2014.76 and 2019.86. No RV data is provided in SB9, so we extracted it from Batten et al. (1985). We note that while in that paper RV data for the companion is provided (which would place this system in the $SB2$ class), the authors do not use these data and treat it as an $SB1$ (see their Figure 1), probably because of the low precision of these latter data. No Gaia parallax is available, and we have used the Hipparcos value at 29.59 ± 0.68 mas as prior, leading to a an inferred MAP orbital parallax of 29.01 ± 0.50 mas. We have also treated this system as $SB1$, and it provides an interesting test case of our single-line with priors methodology. Muterspaugh et al. (2010) obtained a combined $SB2$ solution for this system using a selected subsample of the Batten et al. (1985) RVs, leading to masses of 1.171 ± 0.047 $M_\odot$ and 1.075 ± 0.058 $M_\odot$, and an (orbital) distance of 34.43 ± 0.34 pc. This result compares quite well with our values as can bee seen from Table 3.4. In the notes of WDS it says that "the primary is a giant, from isochrone fit" (no reference given), while both SIMBAD and WDS indicate a G4V, which is what we have adopted as prior. However, the parallax and photometry are more consistent with an earlier SpTy, F4-5V ($M_V \sim +3.5$), but certainly not a giant.

HIP 116259=HDS3356: Ours is the first combined orbit. This system has a sparse but reasonable coverage of the visual orbit, except near periastron, and abundant good quality RV data covering the full phase space. It has a large RUWE value (8.1), and the Hipparcos (28.62 ± 0.95 mas) and Gaia DR3 (29.22 ± 0.15 mas) parallaxes differ by 0.6 mas. Our MAP orbital parallax is 29.08 ± 0.31 mas, i.e., within 1σ of the Gaia value. There is good correspondence between our systemic velocity, -3.310 ± 0.099 kms^{-1}, and that reported by Gaia DR3 at -1.30 ± 0.21 kms^{-1}, specially considering that the RV curve has excursions from -10 to +3 kms^{-1} (see plot on web page). It is interesting to note that Latham et al. (2002) obtain a binary mass function of $f(M) = 0.0774 \pm 0.0043$ $M_\odot$ from RV alone, in perfect agreement with our predicted value from Table 3.4 of 0.0776 $M_\odot$.

3.5. Conclusions and final comments

Applying a Bayesian method developed by our group, we have obtained mass ratio estimates for 22 $SB1$s with available astrometric and RV data, using as priors the SpTy of the primary and the trigonometric parallax of the system. For nine previously unstudied systems, we present, for the first time, a combined orbital solution and uncertainty estimates based on a Bayesian approach. We have made an exhaustive comparison of our results with previous studies finding a very good agreement. This includes a comparison of our systemic velocities with Gaia RVs. We have combined the present results with those from a previous study by Videla et al. (2022), for systems of luminosity class V covering a mass range $0.6 \leq M_{\odot} \leq 2.5$ to construct a pseudo MLR based on 23 systems (46 stars). We find good correspondence with previously determined MLRs based on $SB2$ systems, proving the usefulness of our method. Although some inconsistencies have been found, when the next Gaia data releases are available (with an improved treatment of binary systems), the parallaxes will become more reliable and some discrepancies could disappear. An effort is being made by our team to obtain high signal-to-noise low-resolution spectra for these (bright) binaries, so that their SpTy and luminosity class are firmly established. This will open the path to utilize $SB1$s for more refined studies of the MLR, using larger samples.

Chapter 4

Summary and Conclusions

We have done an exhaustive search for binaries that are in both the WDS (Washington Double Star Catalog effort, Mason et al. (2001), kindly provided to us by Dr.Brian Mason from the US Naval Observatory), and the SB9 (9th Catalog of Spectroscopic Binary Orbits, Pourbaix et al. (2004)) catalogues for binaries that do not have a combined joint simultaneous astrometric and spectroscopic orbit. WDS and SB9 are the most authoritative and up-to-date catalogues of visual and spectroscopic binaries, respectively. As a result of this search, we found 36 spectroscopic binaries, 14 double-line and 22 single-line, whose orbits could be studied using astrometric data. For this sample, we have performed combined dynamically self-consistent orbital solutions, leading to individual masses and orbital parallaxes. The published astrometric and spectroscopic data has been supplemented, whenever possible, with our own data from a survey of binaries in the southern hemisphere using the speckle camera HRCam at the SOAR 4.1m telescope, and high-resolution Echelle spectroscopy with FEROS at the 2.2m MPG/ESO telescope. Furthermore, in some cases we could add some data from FIDEOS spectroscopy at the 1.0m at La Silla and the ZORRO Speckle Camera on the Gemini South 8.1m telescope.

Given the nature of the selection criteria, the samples are heterogeneous and cover a wide range in masses ($0.8M_{\odot} \leq m_1 \leq 36M_{\odot}$ and $0.3M_{\odot} \leq m_2 \leq 15M_{\odot}$ for SB2s; m_1 between $0.4M_{\odot}$ to slightly above $6M_{\odot}$ for SB1s), distances (between 15 pc to 1.76 kpc for SB2s and 7 to 263 pc for SB1s), and spectral and luminosity classes (from $WR+O$ to $K2V$ for SB2s and $B8III$ to $M2V$ for SB1s), and do not represent a complete or representative sample of binaries in any way, which prevents us from using them for statistical studies, e.g., on orbital properties.

On the specifics, our work can be summarized as follows:

- We underline the relevance of orbital parallaxes, and construct H-R diagrams to understand the sample's evolutionary status (for SB2).
- We provide a posterior probability distribution functions, computed with an MCMC code, in all derived parameters, as a powerful means to estimate the orbital uncertainties. In the case of SB1s, we use a method that takes into account suitable priors (in particular, the spectral type as proxy to the mass of the primary, and the trigonometric parallax), which allows us to compute a mass ratio.
- We determine mass ratios and mass sums with a typical uncertainty of less than 1 %,

and individual component masses with a formal uncertainty of $0.01 M_{\odot}$ in the best cases.

- We construct a (pseudo) mass-to-luminosity relationship (using SB1s) that correlates well with the shape of the MLR using high-precision masses from SB2 systems.

Finally, the good results obtained for SB1s opens the path to use these type of systems - which are much more numerous in our Galaxy to constrain the MLR using larger samples on a wide range of spectral types. Also, our improved orbits add to the list of well-determined masses and orbital parameters for future studies using the WDS and SB9 catalogues.

Bibliography

Abt, H. A., & Levy, S. G. 1976, Astrophysical Journal, Supplement, 30, 273, doi: 10.1086/190363

Abt, H. A., & Willmarth, D. 2006a, Astrophysical Journal, Supplement, 162, 207, doi: 10.1086/498095

—. 2006b, VizieR Online Data Catalog, J/ApJS/162/207

Abushattal, A. A., Docobo, J. A., & Campo, P. P. 2020, Astronomical Journal, 159, 28, doi: 10.3847/1538-3881/ab580a

Adams, B. 1939, Publications of the ASP, 51, 116, doi: 10.1086/125020

Agati, J. L., Bonneau, D., Jorissen, A., et al. 2015, Astronomy and Astrophysics, 574, A6, doi: 10.1051/0004-6361/201323056

Al-Tawalbeh, Y. M., Hussein, A. M., Taani, A. A., et al. 2021, Astrophysical Bulletin, 76, 71, doi: 10.1134/S199034132101003X

Anguita-Aguero, J., Mendez, R. A., Clavería, R. M., & Costa, E. 2022, Astronomical Journal, 163, 118, doi: 10.3847/1538-3881/ac478c

Anguita-Aguero, J., Mendez, R. A., Videla, M., et al. 2023, arXiv e-prints, arXiv:2309.06394, doi: 10.48550/arXiv.2309.06394

Baines, E. K., Armstrong, J. T., Schmitt, H. R., et al. 2018, Astronomical Journal, 155, 30, doi: 10.3847/1538-3881/aa9d8b

Balega, I. I., Balega, Y. Y., & Malogolovets, E. V. 2004, in The A-Star Puzzle, ed. J. Zverko, J. Ziznovsky, S. J. Adelman, & W. W. Weiss, Vol. 224, 683–685, doi: 10.1017/S1743921305009579

Balega, Y. Y., Tokovinin, A. A., Pluzhnik, E. A., & Weigelt, G. 2002, Astronomy Letters, 28, 773, doi: 10.1134/1.1518715

Batten, A. H., Lu, W., & Scarfe, C. D. 1985, Journal of the RAS of Canada, 79, 167

Beavers, W. I., & Eitter, J. J. 1986, Astrophysical Journal, Supplement, 62, 147, doi: 10.1086/191136

Benedict, G. F., Henry, T. J., Franz, O. G., et al. 2016, Astronomical Journal, 152, 141, doi: 10.3847/0004-6256/152/5/141

Bennett, D. P., Bhattacharya, A., Beaulieu, J.-P., et al. 2020, Astronomical Journal, 159, 68, doi: 10.3847/1538-3881/ab6212

Bond, H. E., Schaefer, G. H., Gilliland, R. L., & VandenBerg, D. A. 2020, Astrophysical Journal, 904, 112, doi: 10.3847/1538-4357/abc172

Boyajian, T. S., McAlister, H. A., van Belle, G., et al. 2012a, Astrophysical Journal, 746, 101, doi: 10.1088/0004-637X/746/1/101

Boyajian, T. S., von Braun, K., van Belle, G., et al. 2012b, Astrophysical Journal, 757, 112, doi: 10.1088/0004-637X/757/2/112

Brahm, R., Jordán, A., & Espinoza, N. 2017, Publications of the ASP, 129, 034002, doi: 10.1088/1538-3873/aa5455

Brandt, T. D. 2021, Astrophysical Journal Supplement Series, 254, 42, doi: 10.3847/1538-4365/abf93c

Bressan, A., Marigo, P., Girardi, L., et al. 2012, Monthly Notices of the Royal Astronomical Society, 427, 127, doi: 10.1111/j.1365-2966.2012.21948.x

Campbell, W. W., & Moore, J. H. 1928a, Pub. Lick Obs., 16

—. 1928b, Pub. Lick Obs., 16, 234

Carrier, F., North, P., Udry, S., & Babel, J. 2002, Astronomy and Astrophysics, 394, 151, doi: 10.1051/0004-6361:20021122

Catala, C., Forveille, T., & Lai, O. 2006, Astronomical Journal, 132, 2318, doi: 10.1086/508374

Chang, Y. C. 1929, Astrophysical Journal, 70, 182, doi: 10.1086/143214

Claveria, R. M., Mendez, R. A., Silva, J. F., & Orchard, M. E. 2019, Publications of the Astronomical Society of the Pacific, 131, 084502, doi: 10.1088/1538-3873/ab22e2

Cournoyer-Cloutier, C., Tran, A., Lewis, S., et al. 2021, Monthly Notices of the Royal Astronomical Society, 501, 4464, doi: 10.1093/mnras/staa3902

Docobo, J. A., & Campo, P. 2013, IAU Comm. 26 Inform. Circular (IAUDS), 180, 2

Docobo, J. A., Campo, P., & Abushattal, A. 2018a, IAU Comm. 26 Inform. Circular (IAUDS), 196, 1

Docobo, J. A., Campo, P. P., Gomez, J., & Horch, E. P. 2018b, Astronomical Journal, 156, 185, doi: 10.3847/1538-3881/aae092

Docobo, J. A., Gomez, J., Campo, P. P., et al. 2019, Monthly Notices of the Royal Astronomical Society, 482, 4096, doi: 10.1093/mnras/sty2704

Docobo, J. A., Griffin, R. F., Campo, P. P., & Abushattal, A. A. 2017, Monthly Notices of the Royal Astronomical Society, 469, 1096, doi: 10.1093/mnras/stx906

Docobo, J. A., & Ling, J. F. 2013, IAU Comm. 26 Inform. Circular (IAUDS), 180, 2

Docobo, J. A., Tamazian, V. S., Campo, P. P., & Piccotti, L. 2018c, Astronomical Journal, 156, 85, doi: 10.3847/1538-3881/aad179

Dotter, A. 2016, Astrophysical Journal Supplement Series, 222, doi: 10.3847/0067-0049/222/1/8

Dotter, A., Chaboyer, B., Jevremović, D., et al. 2008, Astrophysical Journal Supplement Series, 178, 89, doi: 10.1086/589654

Ducati, J. R., Penteado, E. M., & Turcati, R. 2011, Astronomy and Astrophysics, 525, A26, doi: 10.1051/0004-6361/200913895

Duchêne, G. 2010, Astrophysical Journal Letters, 709, L114, doi: 10.1088/2041-8205/709/2/L114

Duchêne, G., & Kraus, A. 2013, Annual Review of Astron and Astrophys, 51, 269, doi: 10.1146/annurev-astro-081710-102602

Duquennoy, A., & Mayor, M. 1991a, Astronomy and Astrophysics, 248, 485

—. 1991b, Astronomy and Astrophysics, 248, 485

Dvorak, R. 1982, Oesterreichische Akademie Wissenschaften Mathematisch naturwissenschaftliche Klasse Sitzungsberichte Abteilung, 191, 423

Eddington, A. S. 1924, Monthly Notices of the Royal Astronomical Society, 84, 308, doi: 10.1093/mnras/84.5.308

El-Badry, K., Rix, H.-W., & Heintz, T. M. 2021, Monthly Notices of the Royal Astronomical Society, 506, 2269, doi: 10.1093/mnras/stab323

Feiden, G. A., & Chaboyer, B. 2012, Astrophysical Journal, 757, 42, doi: 10.1088/0004-637X/757/1/42

Fekel, F. C., & Scarfe, C. D. 1986, Astronomical Journal, 92, 1162, doi: 10.1086/114248

Fontanive, C., & Bardalez Gagliuffi, D. 2021, Frontiers in Astronomy and Space Sciences, 8, 16, doi: 10.3389/fspas.2021.625250

Fuhrmann, K., Chini, R., Kaderhandt, L., & Chen, Z. 2017, Astrophysical Journal, 836, 139, doi: 10.3847/1538-4357/836/1/139

Ghosh, H., DePoy, D. L., Gal-Yam, A., et al. 2004, Astrophysical Journal, 615, 450, doi: 10.1086/423665

Gómez, J., Docobo, J. A., Campo, P. P., et al. 2021, Monthly Notices of the Royal Astronomical Society, doi: 10.1093/mnras/stab2633

Gomez, J., Docobo, J. A., Campo, P. P., & Mendez, R. A. 2016, Astronomical Journal, 152, 216, doi: 10.3847/0004-6256/152/6/216

Gould, A. 2014, Journal of Korean Astronomical Society, 47, 215, doi: 10.5303/JKAS.2014.47.6.215

Griffin, R. F. 1984, The Observatory, 104, 143

—. 2003, The Observatory, 123, 301

—. 2007, The Observatory, 127, 113

—. 2013a, The Observatory, 133, 322

—. 2013b, The Observatory, 133, 269

—. 2015, The Observatory, 135, 193

Griffin, R. F., & Mason, B. D. 2013, IAU Comm. 26 Inform. Circular (IAUDS), 181, 1

Halbwachs, J. L., Mayor, M., & Udry, S. 2018, Astronomy and Astrophysics, 619, 16, doi: 10.1051/0004-6361/201833377

Halbwachs, J. L., Kiefer, F., Lebreton, Y., et al. 2020, Monthly Notices of the Royal Astronomical Society, 496, 1355, doi: 10.1093/mnras/staa1571

Harper, W. 1928, Publication of the Dominion Astrophysical Observatory, 6, 151

Hatzes, A. P., Cochran, W. D., Endl, M., et al. 2003, Astrophysical Journal, 599, 1383, doi: 10.1086/379281

Heintz, W. 1997, Astronomical Journal, 111, 335, doi: 10.1086/313011

Henden, A. A., Welch, D. L., Terrell, D., & Levine, S. E. 2009, in American Astronomical Society Meeting Abstracts, Vol. 214, American Astronomical Society Meeting Abstracts #214, 407.02

Horch, E. P., Gomez, S. C., Sherry, W. H., et al. 2011, Astronomical Journal, 141, 45, doi: 10.1088/0004-6256/141/2/45

Horch, E. P., van Belle, G. T., Davidson, James W., J., et al. 2015a, Astronomical Journal, 150, 151, doi: 10.1088/0004-6256/150/5/151

Horch, E. P., van Altena, W. F., Demarque, P., et al. 2015b, Astronomical Journal, 149, 151, doi: 10.1088/0004-6256/149/5/151

Horch, E. P., Tokovinin, A., Weiss, S. A., et al. 2019a, Astronomical Journal, 157, 56, doi: 10.3847/1538-3881/aaf87e

—. 2019b, Astronomical Journal, 157, 56H, doi: 10.3847/1538-3881/aaf87e

Howell, S. B., Everett, M. E., Sherry, W., Horch, E., & Ciardi, D. R. 2011, Astronomical Journal, 142, 19, doi: 10.1088/0004-6256/142/1/19

Hutchings, J. B., Griffin, R. F., & Ménard, F. 2000, Publications of the ASP, 112, 833, doi: 10.1086/316587

Iben, I. 2012, Stellar Evolution Physics 2 Volume Hardback Set

Jayasinghe, T., Stanek, K. Z., Kochanek, C. S., et al. 2019, Monthly Notices of the Royal Astronomical Society, 485, 961, doi: 10.1093/mnras/stz444

Kahler, H. 1972, Astronomy and Astrophysics, 20, 105

Katoh, N., Itoh, Y., Toyota, E., & Sato, B. 2013, Astronomical Journal, 145, 41, doi: 10.1088/0004-6256/145/2/41

Katz, D., Sartoretti, P., Guerrier, A., et al. 2022, arXiv e-prints, arXiv:2206.05902, doi: 10.48550/arXiv.2206.05902

Kaufer, A., Stahl, O., Tubbesing, S., et al. 1999, The Messenger, 95, 8

Kervella, P., Arenou, F., Mignard, F., & Thévenin, F. 2019, Astronomy and Astrophysics, 623, A72, doi: 10.1051/0004-6361/201834371

Kippenhahn, R., Weigert, A., & Weiss, A. 2012, Stellar Structure and Evolution, doi: 10.1007/978-3-642-30304-3

Kochanek, C. S., Shappee, B. J., Stanek, K. Z., et al. 2017, Publications of the Astronomical Society of the Pacific, 129, 104502, doi: 10.1088/1538-3873/aa80d9

Latham, D. W., Stefanik, R. P., Torres, G., et al. 2002, Astronomical Journal, 124, 1144, doi: 10.1086/341384

Lindegren, L., Mignard, F., Söderhjelm, S., et al. 1997, Astronomy and Astrophysics, 323, L53

Luri, X., Brown, A. G. A., Sarro, L. M., et al. 2018, Astronomy and Astrophysics, 616, A9, doi: 10.1051/0004-6361/201832964

Maíz Apellániz, J. 2017, Astronomy and Astrophysics, 608, L8, doi: 10.1051/0004-6361/201732167

Malkov, O. Y., Tamazian, V. S., Docobo, J. A., & Chulkov, D. A. 2012a, Astronomy and Astrophysics, 546, A69, doi: 10.1051/0004-6361/201219774

—. 2012b, Astronomy and Astrophysics, 546, A69, doi: 10.1051/0004-6361/201219774

Mann, A. W., Dupuy, T., Kraus, A. L., et al. 2019, Astrophysical Journal, 871, 63, doi: 10.3847/1538-4357/aaf3bc

Marchenko, S. V., Moffat, A. F. J., Ballereau, D., et al. 2003, Astrophysical Journal, 596, 1295, doi: 10.1086/378154

Martin, C., Mignard, F., Hartkopf, W. I., & McAlister, H. A. 1998, Astronomy and Astrophysics, Supplement, 133, 149, doi: 10.1051/aas:1998459

Mason, B., Penteado, E., & Hartkopf, W. I. 2005, IAUDS, 156, 1M

Mason, B. D. 2015, in IAU General Assembly, Vol. 29, 2300709

Mason, B. D., Wycoff, G. L., Hartkopf, W. I., Douglass, G. G., & Worley, C. E. 2001, Astronomical Journal, 122, 3466, doi: 10.1086/323920

Massey, P., & Meyer, M. 2001, Stellar Masses, ed. P. Murdin, 1882, doi: 10.1888/0333750888/1882

Matson, R. A., Howell, S. B., Horch, E. P., & Everett, M. E. 2018, Astronomical Journal, 156, 31, doi: 10.3847/1538-3881/aac778

Mayor, M., Pepe, F., Queloz, D., et al. 2003, The Messenger, 114, 20

Mendez, R. A., Clavería, R. M., & Costa, E. 2021, Astronomical Journal, 161, 155, doi: 10.3847/1538-3881/abdb28

Mendez, R. A., Claveria, R. M., Orchard, M. E., & Silva, J. F. 2017, Astronomical Journal, 154, 187, doi: 10.3847/1538-3881/aa8d6f

Mendez, R. A., Tokovinin, A., & Horch, E. 2018, in Revista Mexicana de Astronomia y Astrofisica Conference Series, Vol. 50, Revista Mexicana de Astronomia y Astrofisica Conference Series, 56–57

Monnier, J., Zhao, M., Pedretti, E., et al. 2011, Astrophysical Journal, 742, 6, doi: 10.1088/2041-8205/742/1/L1

Mordasini, C., Alibert, Y., Benz, W., & Naef, D. 2008, in Astronomical Society of the Pacific Conference Series, Vol. 398, Extreme Solar Systems, ed. D. Fischer, F. A. Rasio, S. E. Thorsett, & A. Wolszczan, 235. https://arxiv.org/abs/0710.5667

Muterspaugh, M. W., Hartkopf, W. I., Lane, B. F., et al. 2010, Astronomical Journal, 140, 1623, doi: 10.1088/0004-6256/140/6/1623

Neubauer, F. J. 1944, Astrophysical Journal, 99, 134, doi: 10.1086/144602

Nordström, B., Mayor, M., Andersen, J., et al. 2004, Astronomy and Astrophysics, 418, 989, doi: 10.1051/0004-6361:20035959

Parsons, S. B. 1983, Astrophysical Journal, Supplement, 53, 553, doi: 10.1086/190901

Pegues, J., Czekala, I., Andrews, S. M., et al. 2021, Astrophysical Journal, 908, 42, doi: 10.3847/1538-4357/abd4eb

Peretti, S., Ségransan, D., Lavie, B., et al. 2019, Astronomy and Astrophysics, 631, A107, doi: 10.1051/0004-6361/201732454

Petrie, R. 1949, Publication of the Dominion Astrophysical Observatory, 8, 117

Piccotti, L., Docobo, J. Á., Carini, R., et al. 2020, Monthly Notices of the Royal Astronomical Society, 492, 2709, doi: 10.1093/mnras/stz3616

Pickles, A., & Depagne, É. 2010, Publications of the Astronomical Society of the Pacific, 122, 1437, doi: 10.1086/657947

Pojmanski, G. 1997, Acta Astronomica, 47, 467. https://arxiv.org/abs/astro-ph/9712146

Pourbaix, D. 1994, Astronomy and Astrophysics, 290, 682

Pourbaix, D. 2000, Astronomy and Astrophysics, Supplement, 145, 215, doi: 10.1051/aas:2000237

Pourbaix, D., Tokovinin, A. A., Batten, A. H., et al. 2004, Astronomy and Astrophysics, 424, 727, doi: 10.1051/0004-6361:20041213

Queloz, D., Mayor, M., Weber, L., et al. 2000, Astronomy and Astrophysics, 354, 99

Raghavan, D., McAlister, H. A., Henry, T. J., et al. 2010, Astrophysical Journal Supplement Series, 190, 1, doi: 10.1088/0067-0049/190/1/1

Riddle, R. L., Tokovinin, A., Mason, B. D., et al. 2015, Astrophysical Journal, 799, 4, doi: 10.1088/0004-637X/799/1/4

Riello, M., de Angeli, F., Evans, D. W., et al. 2021, VizieR Online Data Catalog, J/A+A/649/A3

Sahlmann, J., Ségransan, D., Queloz, D., et al. 2011, Astronomy and Astrophysics, 525, A95, doi: 10.1051/0004-6361/201015427

Scarfe, C. D., Barlow, D. J., & Fekel, F. C. 2000, Astronomical Journal, 119, 2415, doi: 10.1086/301366

Schmidt-Kaler, T. 1982, Landolt-Börnstein: Numerical Data and Functional Relationships in Science and Technology - New Series VI, 2, 19

Scholz, G., & Lehmann, H. 1988, Astronomische Nachrichten, 309, 33, doi: 10.1002/asna.2113090107

Scott, N. J., Howell, S. B., Horch, E. P., & Everett, M. E. 2018, Publications of the Astronomical Society of the Pacific, 130, 054502, doi: 10.1088/1538-3873/aab484

Skiff, B. A. 2014, VizieR Online Data Catalog, B/mk

Söderhjelm, S. 1999a, Astronomy and Astrophysics, 341, 121

—. 1999b, Astronomy and Astrophysics, 341, 121

Spencer Jones, H., & Furner, H. H. 1937, Monthly Notices of the RAS, 98, 92, doi: 10.1093/mnras/98.2.92

Straizys, V., & Kuriliene, G. 1981, Astrophysics and Space Science, 80, 353, doi: 10.1007/BF00652936

Straižys, V., & Kuriliene, G. 1981, Astrophysics and Space Science, 80, 353

Struve, O., & Huang, S. S. 1958, Spectroscopic Binaries, ed. S. Flügge (Berlin, Heidelberg:

Springer Berlin Heidelberg), 243–273, doi: 10.1007/978-3-642-45906-1_8

Thebault, P., & Haghighipour, N. 2015, Planet Formation in Binaries, 309–340, doi: 10.1007/978-3-662-45052-9_13

Tokovinin, A. 1992, in Astronomical Society of the Pacific Conference Series, Vol. 32, IAU Colloq. 135: Complementary Approaches to Double and Multiple Star Research, ed. H. A. McAlister & W. I. Hartkopf, 573

Tokovinin, A. 2012a, Astronomical Journal, 144, 20, doi: 10.1088/0004-6256/144/2/56

—. 2012b, Astronomical Journal, 144, 56, doi: 10.1088/0004-6256/144/2/56

—. 2016, Astronomical Journal, 152, 9, doi: 10.3847/0004-6256/152/5/138

—. 2017, Astronomical Journal, 154, doi: 10.3847/1538-3881/aa8459

—. 2018a, Publications of the Astronomical Society of the Pacific, 130, 035002, doi: 10.1088/1538-3873/aaa7d9

—. 2018b, Astrophysical Journal, Supplement, 235, 6, doi: 10.3847/1538-4365/aaa1a5

—. 2020, Astronomical Journal, 159, 265, doi: 10.3847/1538-3881/ab8af1

—. 2022, Astronomical Journal, 163, 161, doi: 10.3847/1538-3881/ac5330

Tokovinin, A., & Cantarutti, R. 2008, Publications of the Astronomical Society of the Pacific, 120, 170, doi: 10.1086/528809

Tokovinin, A., & Latham, D. W. 2017, Astrophysical Journal, 838, 54, doi: 10.3847/1538-4357/aa6331

Tokovinin, A., Mason, B. D., & Hartkopf, W. I. 2010, Astronomical Journal, 139, 743, doi: 10.1088/0004-6256/139/2/743

Tokovinin, A., Mason, B. D., Mendez, R. A., Costa, E., & Horch, E. P. 2020, Astronomical Journal, 160, 7, doi: 10.3847/1538-3881/ab91c1

Tokovinin, A. A. 1997, Astronomy and Astrophysics, Supplement, 124, 75, doi: 10.1051/aas:1997181

Torres, G., Andersen, J., & Giménez, A. 2010, Astronomy and Astrophysics Reviews, 18, 67, doi: 10.1007/s00159-009-0025-1

Torres, G., Stefanik, R. P., & Latham, D. W. 1997, Astrophysical Journal, 474, 256, doi: 10.1086/303465

Trifonov, T., Tal-Or, L., Zechmeister, M., et al. 2020, Astronomy and Astrophysics, 636, A74, doi: 10.1051/0004-6361/201936686

Underhill, A. B. 1963, Publications of the Dominion Astrophysical Observatory Victoria, 12, 159

Unwin, S. C., Shao, M., Tanner, A. M., et al. 2008, Publications of the ASP, 120, 38, doi: 10.1086/525059

van Leeuwen, F. 2010, Space Science Reviews, 151, 209, doi: 10.1007/s11214-009-9606-6

Vanzi, L., Zapata, A., Flores, M., et al. 2018, Monthly Notices of the RAS, 477, 5041, doi: 10.1093/mnras/sty936

Videla, M., Mendez, R. A., Clavería, R. M., Silva, J. F., & Orchard, M. E. 2022, Astronomical

Journal, 163, 220, doi: 10.3847/1538-3881/ac5ab4

Villegas, C., Mendez, R. A., Silva, J. F., & Orchard, M. E. 2021, arXiv e-prints, arXiv:2105.05258. https://arxiv.org/abs/2105.05258

Vogt, S. S., Butler, R. P., Marcy, G. W., et al. 2002, Astrophysical Journal, 568, 352, doi: 10.1086/338768

Wall, J. E., McMillan, S. L. W., Mac Low, M.-M., Klessen, R. S., & Portegies Zwart, S. 2019, Astrophysical Journal, 887, 62, doi: 10.3847/1538-4357/ab4db1

Wand, M. P., & Jones, M. C. 1994, Kernel smoothing (CRC press)

Wenger, M., Ochsenbein, F., Egret, D., et al. 2000, Astronomy and Astrophysics, Supplement, 143, 9, doi: 10.1051/aas:2000332

Willmarth, D. W., Fekel, F. C., Abt, H. A., & Pourbaix, D. 2016, Astronomical Journal, 152, 46, doi: 10.3847/0004-6256/152/2/46

Wyrzykowski, $\mathcal{L}$., & Mandel, I. 2020, Astronomy and Astrophysics, 636, A20, doi: 10.1051/0004-6361/201935842

Ziegler, C., Law, N. M., Baranec, C., et al. 2018a, Astronomical Journal, 156, 259, doi: 10.3847/1538-3881/aad80a

—. 2018b, Astronomical Journal, 156, 259, doi: 10.3847/1538-3881/aad80a